HOKKAIDO UNIVERSITY

Title	Development of Microdevice-based Immunoassay Systems for Point-of-Need Testing
Author(s)	西山, 慶音
Degree Grantor	北海道大学
Degree Name	博士(工学)
Dissertation Number	甲第14471号
Issue Date	2021-03-25
DOI	https://doi.org/10.14943/doctoral.k14471
Doc URL	https://hdl.handle.net/2115/81280
Type	doctoral thesis
File Information	NISHIYAMA_Keine.pdf

Hokkaido University Collection of Scholarly and Academic Papers : HUSCAP

Development of Microdevice-based Immunoassay Systems for Point-of-Need Testing

現場即時検査のための

マイクロデバイスを用いたイムノアッセイシステムの開発



Keine Nishiyama

Graduate School of Chemical Sciences Engineering

Hokkaido University

Title Development of Microdevice-based Immunoassay Systems for Point-of-Need Testing

Author Keine Nishiyama

Degree Doctor of Philosophy (Engineering)

Supervisor Professor Manabu Tokeshi

CONTENTS

CHAPTER 1 General Introduction 1

1.1 Point-of-Need Testing 2

1.2 Immunoassays 3

1.2.1 Heterogeneous Immunoassay 5

1.2.2 Homogeneous Immunoassay 6

1.3 Microdevices for analytical chemistry 8

1.3.1 The "μTAS" Concept 8

1.3.2 Microdevices for Immunoassays 9

1.3.2.1 Immunoassay systems for easy-to-use detection 9

1.3.2.2 Highly sensitive immunoassay systems 12

1.4 Objectives of the Thesis 14

1.5 References 17

CHAPTER 2 Ultrasensitive Detection of Disease Biomarkers Using an Immuno-wall Device with Enzymatic Amplification 29

2.1 Introduction 30

2.2 Experimental 31

2.2.1 Materials and reagents 31

2.2.2 Fabrication of immuno-wall device 32

2.2.3 Assay procedure 34

2.2.4 Fluorescence microscope 35

2.3 Results and Discussion 36

2.3.1 Biomarker detection with fluorescence-labeled antibody 36

2.3.2 Selection of fluorogenic substrates for enzymatic amplification 37

2.3.3 Biomarker detection with the enzyme-labeled antibody, alkaline phosphatase-labeled antibody 42

2.4 Conclusions 46

2.5 References 47

CHAPTER 3 Simple Approach for Fluorescence Signal Amplification Utilizing a Poly(vinyl alcohol)-based Polymer Structure in a Microchannel 53

3.1 Introduction 54

3.2 Experimental 55

3.2.1 Materials 55

3.2.2 AWP-wall in a microchannel 56

3.2.3 Evaluation of AWP-wall in a microchannel as a fluorescence signal amplifier 56

3.2.4 Evaluation of transfer of fluorescent molecules to AWP in a microplate 57

3.2.5 Fluorescence spectrum of DDAO 57

3.2.6 Prediction of octanol-water partition coefficient 58

3.3 Results and discussion 58

3.4. Conclusions 67

3.5 References 69

CHAPTER 4 Non-competitive Fluorescence Polarization Immunoassay Based on a Fab Fragment for Protein Quantification 73

4.1 Introduction 74

4.2 Experimental 76

4.2.1 Chemicals 76

4.2.2 Labeling procedure 76

4.2.3 Assay procedure 77

4.2.4 Fluorescence analysis of human serum 77

4.2.5 Portable FP analyzer 78

4.2.6 Microfluidic device 78

4.3 Theoretical fluorescence polarization value 79

4.4 Results and Discussion 80

4.4.1 Development of non-competitive FPIA based on a Fab fragment 80

4.4.2 Application: diagnosis of inflammation based on CRP level in serum 84

4.5 Conclusions 89

4.6 References 90

CHAPTER 5 Application of non-competitive fluorescence polarization immunoassay for antigen and antibody detection of H5 avian influenza virus 95

5.1 Introduction 96

5.2 Experimental 98

5.2.1 Materials 98

5.2.2 Preparation of purified H5N3 AIV 98

5.2.3 Preparation of F-Fab 99

5.2.4 Preparation of Fluorescein-labeled antigen 99

5.2.5 Anti-AIV sera 100

5.2.6 Potable FP analyzer 100

5.2.7 Measurement procedure of H5N3 AIV 101

5.2.8 Measurement procedure of antibody 101

5.3 Results and Discussion 101

5.3.1 Virus detection 101

5.3.2 Antibody detection 105

5.4 Conclusions 108

5.5 References 109

CHAPTER 6 Conclusion and Future Prospects 113

List of Publications 118

Acknowledgement 123

CHAPTER 1 General Introduction

1.1 Point-of-Need Testing

The terms “point-of-need testing” (PONT) and “point-of-care testing” (POCT) are defined to mean rapid diagnosis that can be performed close to a patient [1]. The PONT concept was introduced in the United States in the late 1980s, and had previously been interpreted to only mean medical diagnosis [2,3]. However, the diagnostic targets and applications of PONT have expanded as molecular biology and sensor technology have developed. The current meaning of PONT has been expanded to include tests that can be performed rapidly outside of the laboratory and is not limited to medical diagnosis. PONT generally require portability, rapidity, ease-of-use, and inexpensiveness, and PONT systems with these characteristics will contribute to improving medical efficiency, quality of life, and to the maintenance of public health. At the present time, the most popular PONT system is the blood glucose sensor for diabetes management [4,5], which enables the patient to monitor glucose levels at home by collecting and analyzing blood themselves. The glucose sensor is a pioneering technology in the PONT field, and many studies into the non-invasive measurement of blood glucose concentrations continue [6-8]. In addition, more infectious disease diagnoses using PONT systems have been reported in recent years [9]. In the resource-poor areas of developing countries, the use of PONT is expected to provide simple diagnostic methods for the detection of viral infection diseases, such as malaria [10], while a lateral flow device has been used for initial influenza diagnosis in developed countries [11]. In addition, the recent COVID-19 epidemic has highlighted the importance of PONT testing for infectious diseases.

PONT systems based on a variety of measurement principles have been developed. Molecular analysis technology for measuring biological samples is the most important basic PONT technology. The glucose sensor, which is a typical example of a PONT system based on a molecular analysis technology, uses an electrochemical method to measure the concentration of glucose molecules in the blood [12]. In addition, wearable electrochemical sensors for the non-invasive measurements of small molecules, such as glucose in sweat, are being actively developed with the growth of IoT technologies and smartphones [13]. Such electrochemical sensors are often used to analyze lactic acid and uric acid in addition to glucose. Moreover, the number of PONT systems that target nucleic acids has increased. Although nucleic acids have previously been analyzed in the

laboratory using polymerase chain reaction methods, it is currently possible to analyze them using small platforms [14–16]. In a similar manner to PONT systems for small molecules and nucleic acids, PONT systems that target proteins are also being actively developed. Among various molecular analysis technologies, immunoassays are regarded to be basic technologies for protein quantification in the PONT field. Numerous immunoassay-based PONT systems have been reported to date [17,18]; however, they are limited in their applications. The diversifying needs of PONT require the development of an immunoassay system that meets the high requirements of miniaturization, inexpensiveness, speed, accuracy, and stability.

This dissertation focuses on PONT systems for the quantification of proteins that are used in various PONT application. The immunoassay was chosen as the basic technology for the PONT system design, with details provided in the following sections.

1.2 Immunoassays

Immunoassays are analytical methods that rely on specific antibody–antigen recognition. The antibody selectively recognizes the antigen and the formed antibody–antigen complex is then quantified by physical or chemical analysis. The greatest advantages of the immunoassay method are its simplicity and high sensitivity. Accordingly, many immunoassay-based test kits and biosensors have been commercialized, with the value of the global immunoassay market expected to reach US$ 27.15 billion by 2023 [19]. The history of immunoassays began with Berson and Yalow in 1959, who reported the first immunoassay technique for the detection of insulin using radioactive iodine as a label (radioimmunoassay) [20]. Various types of immunoassay based on the radioimmunoassay principle were subsequently developed in the 1970s and 1980s [21–24]. In particular, the enzyme-linked immunosorbent assay (ELISA) is an immunoassay technique byword and has been used in various analytical field to date [25,26]. In recent years, the development of genetic engineering technology has facilitated the use of artificially produced antibodies with high affinities in immunoassays. The use of artificial antibodies has enabled precise antibody design and reduced reagent costs. A typical method for artificially

producing an antibody uses phage display technology and biopanning [27,28]. In addition, the use of fusion proteins, in which functional proteins, such as enzymes, are genetically bound to antibodies and expressed, have also been studied [29,30].

The development of immunoassay techniques has also witnessed the diversification of immunoassay analytes, with the most common analytes being macromolecular antigens. In the medical field, immunoassays are commonly used to analyze protein biomarkers [31,32] and pathogens, such as viruses and bacteria [33–36]. It is also possible to analyze antibodies (as analytes) rather than using them as recognition molecules [37,38]. On the other hand, haptens, which are small molecules that bind to proteins and elicit immune responses, are also major immunoassay analytes. For example, immunoassays that target haptens are used to detect mycotoxins and endocrine disruptors in the food-control [39,40] and environmental-conservation [41,42] fields, respectively.

Immunoassays are categorized into two groups: heterogeneous and homogeneous, according to the presence or absence of a bound/free (B/F) separation step (Figure 1.1). Each immunoassay type is described in detail in the following paragraphs. In addition, they can be classified according to the type of labeling molecule and whether or not the reaction is competitive. The appropriate use of these immunoassay methods depends on the purpose and application. In addition, new analytical methods that use immunoassays have been developed through the evolution of related research fields, such as molecular biology and materials engineering.

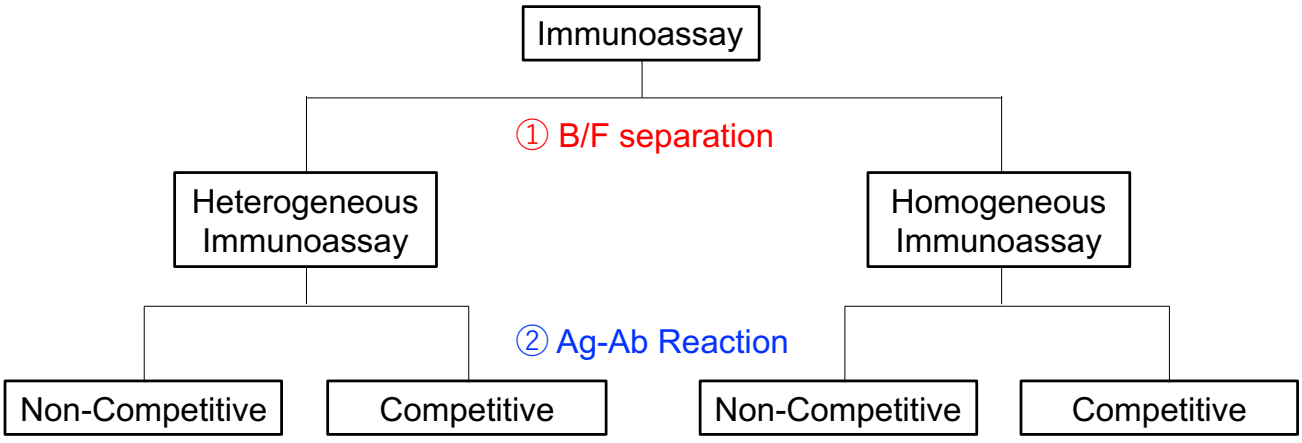


Figure 1.1 Classification of immunoassays. Ag denotes antigen and Ab denotes antibody.

1.2.1 Heterogeneous Immunoassay

A heterogeneous immunoassay relies on the reaction of an analyte with a solid-phase-immobilized antibody, with the analyte–antibody complex (bound) requiring separation from the free analyte/antibody (free). Figure 1.2 shows the mechanism used by a heterogeneous immunoassay, with the "sandwich immunoassay" as an example. The analytical sample containing the target is added to a container, such as a microplate, on which the antibody is immobilized. Following incubation, substances other than the antigen bound to the antibody are removed by washing, after which the labeled antibody is added. The sample is analyzed after washing to remove free labeled antibodies. In most cases, labeling molecules, which include radioisotopes, enzymes, or fluorescent molecules, provide signals. ELISA is the most popular of a number of heterogeneous immunoassays. ELISA relies on enzymes, such as horseradish peroxidase (HRP), alkaline phosphatase (ALP), and β-galactosidase (β-GAL), as labels that react with substrates to produce chromogenic, fluorescent, or luminescent products [43]. ELISA is a highly sensitive analytical method because the enzymatic reaction produces a large amount of product per analyte. Sandwich ELISA, in which two or more antibodies are bound to one molecule of analyte, can be used to analyze macromolecular antigens. The sandwich immunoassay is generally difficult to apply to haptens and competitive ELISA is used instead; however, competitive ELISA is less sensitive than sandwich ELISA. Therefore, ELISA is an appropriate method for the highly sensitive analysis of trace amounts of macromolecular antigens. Some researchers have reported sandwich ELISAs for haptens [44,45]; however, they are not widely used because the required reagents are difficult to prepare. In addition to ELISA, fluoroimmunoassays (FIAs) and chemiluminescence immunoassays (CLIAs) have been widely studied [46,47]. FIAs use fluorescent-molecule-labeled antibodies. Since FIAs do not contain amplification steps, they are less sensitive than ELISA. On the other hand, FIA is simple and requires little time. CLIA uses a substance as an antibody label that catalyzes a chemiluminescent reaction. Despite being a highly sensitive measurement method compared to ELISA and FIA, it generally requires a photomultiplier tube as the detector. CLIA is also easily affected by fluctuations in environmental factors such as temperature, which is a disadvantage.

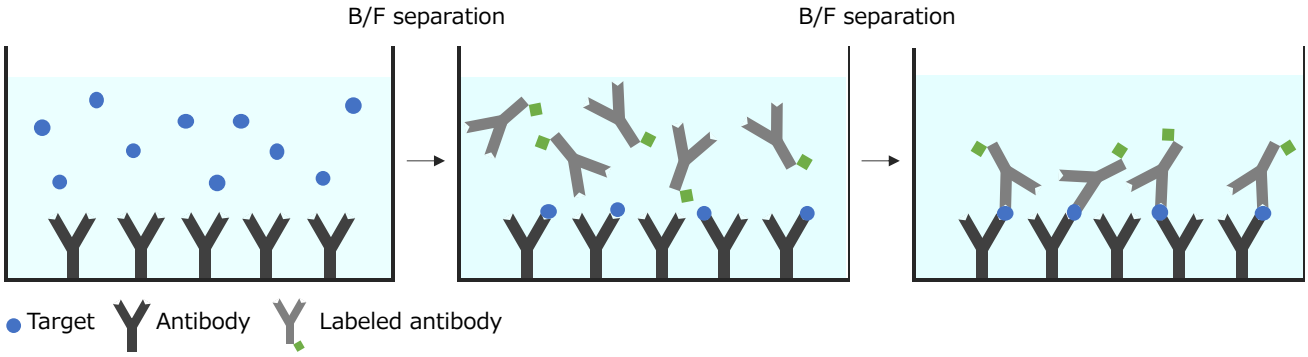


Figure 1.2 The heterogeneous immunoassay principle.

General problems associated with heterogeneous immunoassays include operational complexity and long analysis times. Because B/F separation is used, a washing operation is also necessary, which requires a trained technician. In addition, long incubation times are required for highly sensitive analyses. Commercially available immunoassay kits that use 96-well plates typically require several washing steps and several hours for incubation [48]. In addition, signals are often amplified using enzymatic reactions when more sensitivity is desired, which increases the reaction time and further complicates the analysis procedure.

1.2.2 Homogeneous Immunoassay

A homogeneous immunoassay is a format that does not require B/F separation. Figure 1.3 shows the mechanism of a homogeneous immunoassay, with a competitive method as the example. Targets labeled with enzymes or fluorescent molecules and antibodies are used as reagents, with reactions completed by mixing the labeled target and the antibody in a sample solution containing the target, followed by incubation. No washing step is required, and any change in the state of the labeling substance due to antibody binding to the labeling target is detected. Competitive immunoassays, such as the fluorescence polarization immunoassay (FPIA), the cloned enzyme donor immunoassay (CEDIA), and the enzyme multiplied immunoassay (EMIT), are well-known representative examples [3,49,50]. Enzyme activity increases with increasing amounts of hapten in the

CEDIA and EMIT methods, and fluorescence or a chromogenic substrate is used for detection. FPIA, which was first reported in the 1960s, has many applications reported to date [51,52]. In FPIA, the analyte competes with a fluorescence-labeled analyte (tracer) for binding to the antibody, with detection based on the degree of fluorescence polarization. Simplicity and rapidity are advantages of this assay, which has been used in PONT applications and therapeutic drug monitoring with haptens. In addition, some non-competitive homogeneous immunoassays have also been developed. The luminescent oxygen channeling immunoassay (LOCI) and the open sandwich immunoassay are representative examples; these assays use the proximity effect associated with two antibodies binding to an antigen [53,54].

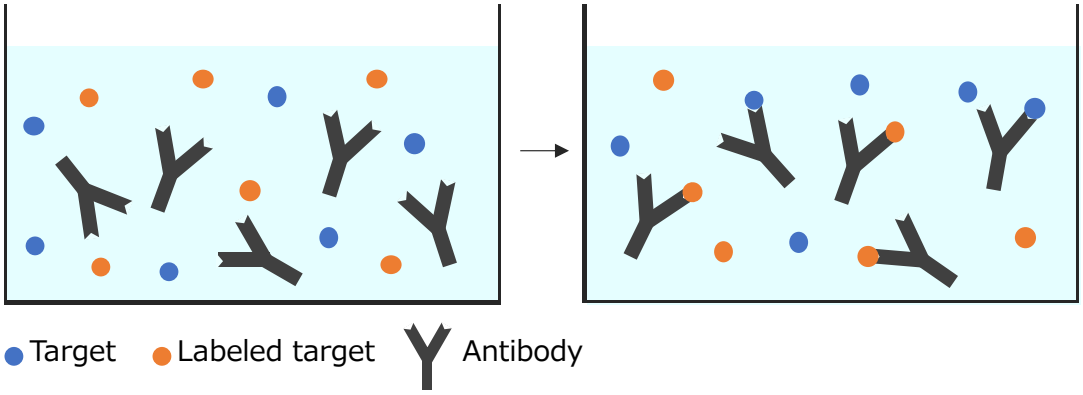


Figure 1.3 The homogeneous immunoassay principle.

The detection sensitivities of homogeneous immunoassays are generally lower than those of heterogeneous immunoassays. In addition, they are easily affected by real sample matrices because no washing is performed. Therefore, these assay types are suitable for analyses that require rapidity and ease of handling, such as bedside and initial diagnoses. Most homogeneous immunoassay targets are small molecules, such as drugs. Therefore, the development of homogeneous immunoassays for large molecules, such as proteins, would lead to their more widespread use.

1.3 Microdevices for analytical chemistry

1.3.1 The "μTAS" Concept

Research into integrating various chemical operations onto plastic or glass chips has developed rapidly since around 1990. The development of material-processing technologies, such as soft lithography, has enabled microfabrication on glass and polymer substrates [55]. Research has led to the downsizing of various chemical operations using microstructured devices that typically have micro-order channels on a substrate and are referred to as "microfluidic devices" or "microdevices. The concept of integrating laboratory functions on a microdevice has been referred to as "Lab-on-a-Chip" [56]. There are various advantages associated with performing chemical reactions in microchannels. Firstly, significantly lower volumes of samples and reagents are used, which is a great advantage when rare biological samples or expensive reagents are involved. Secondly, short diffusion distances and large specific surface areas result in faster chemical reactions in microchannels. These features contribute to reducing the overall experimental time. In addition, multi-functional integration and the parallelization of some chemical reactions can be realized on a small platform. Chemical processes that were previously only performed in the laboratory can now easily be performed anywhere. Due to these advantages, research aided by microdevices has developed in various chemical fields. Among them, the use of microdevices in analytical chemistry was examined early on, with the first chemical analyses using microdevices reported by Terry *et al*. in 1979 [57]. Subsequently, in 1990 Manz *et al.* [58] reported the "micro total analysis system" (μTAS) concept by integrating an analytical system on a microdevice.

μTAS technology enabled the significant downsizing of conventional chemical analysis methods, with miniaturized chromatography systems representing the earliest applications of μTAS [59]. Chromatography systems, such as gas chromatography and HPLC, have been significantly miniaturized to date [60–62]. In addition, the development of analytical techniques based on capillary electrophoresis [63,64] as well as microreactors [65,66] have been actively studied in the early days of μTAS. Moreover, highly sensitive detectors applicable to μTAS, such as thermal lens microscopes, have also been developed [67,68]. The development of

such basic μTAS-related technologies has enabled the construction of sophisticated analysis systems with multiple integrated functions.

1.3.2 Microdevices for Immunoassays

Among the many analysis applications of microfluidic devices, immunoassays based on microdevices have been studied since 2000 [69,70]. Compared with conventional immunoassays that use 96-well microplates, microdevices have successfully led to a significant reduction in sample volume and measurement time. In addition, miniaturized immunoassay systems, including detectors, have been reported [71,72]. Immunoassay systems that use microdevices are roughly classified into those that emphasize analysis speed and simplicity, and those that emphasize analysis sensitivity. Representative immunoassay systems in each category are introduced below.

1.3.2.1 Immunoassay systems for easy-to-use detection

Many immunoassays based on microdevices that enable simple and rapid analyses have been developed. A typical immunoassay system that uses a microdevice for simple detection is shown in Figure 1.4. The most common simple immunoassay platform is the lateral flow immunoassay (LFIA), which usually uses nitrocellulose or cellulose acetate as the substrate. A LFIA device includes labeled and capture antibodies. When the analytical sample is injected into the device, capillary forces move the solution in the uniaxial channel direction. The sample is immunoassayed when it reaches the antibody-immobilized area. The advantage of LFIA is that it readily analyzes a sample through simple injection, and results are generally judged visually with no detection device required. With these merits in mind, this method is used for on-site analysis in the medical [73], food [74], and environmental fields [75]; however, its low sensitivity compared to that of a conventional microplate immunoassay is a disadvantage. In addition, many LFIA devices only provide qualitative results.

Furthermore, the “prozone phenomenon”, in which false negatives are obtained due to competitive inhibition of antigens that do not form complexes with labeled antibodies, is a concern when analytes are present in large excess in the sample [76].

As a device that uses the capillary force of the substrate (such as in an LFIA device), immunoassay systems that uses paper devices have attracted significant amounts of attention in recent years. In 2007, Martinez *et al.* [77] first reported chemical analyses using a paper device patterned with a hydrophobic polymer. Since then, many devices have been reported for use in immunoassay applications. These devices are referred to as “microfluidic paper-based analytical devices” (μPADs), and photolithography, wax patterning, and cutting techniques are commonly used for their fabrication. Antibodies are commonly immobilized on prepared paper devices and used for immunoassaying purposes, and μPADs are often used in combination with competing immunoassays [78–80]. Apilux *et al.* [81] realized a sandwich immunoassay system using a μPAD through complicated fluid control by designing a two-dimensional channel shape. Chen *et al.* [82] developed a three-dimensional origami device and used a μPAD in a sandwich immunoassay application. The advantages of a μPAD include its high portability, inexpensiveness, and ease of disposal after use. Therefore, μPADs are expected to be used in medical diagnosis applications in developing countries. However, in general, the sensitivity and accuracy of a μPAD are often lower than those of a conventional immunoassay using a plate reader. Many studies aimed at improving analytical sensitivity and accuracy have been reported [83]; however, expensive materials, hardware, and software are needed, which offset the advantages of μPAD technology.

Unlike the LFIA and μPAD concepts, simple systems that integrate more complicated immunoassay reactions and pretreatment into one device have also been developed. “Lab-on-a-disc” or the “centrifugal microfluidic platform” is a relatively new platform that realizes this concept [84]; this platform uses disc-shaped devices with microchannels and microchambers. The device is pre-filled with reagents for sample pretreatment and immunoassaying. After introducing the analytical sample into the device, the disc device is rotated by a motor to manipulate the solution and to assay the sample. Basically, analysis is completed by simply introducing the sample into the device and setting it in the detection device; hence, it is a highly convenient analytical

method. In addition, compared to LFIA and μPAD, centrifugal microfluidic platforms are very flexible in terms of immunoassay use. For example, such a platform can be used in combination with ELSIA [85,86], CLIA [87], and FIA [88]; however, a dedicated device with a detector and a built-in motor for rotating the disc device is required, with cost and portability significantly inferior to those of LFIA and μPAD systems. In addition, because many reagents are encapsulated in the disc device, the storage stability of each reagent becomes a problem.

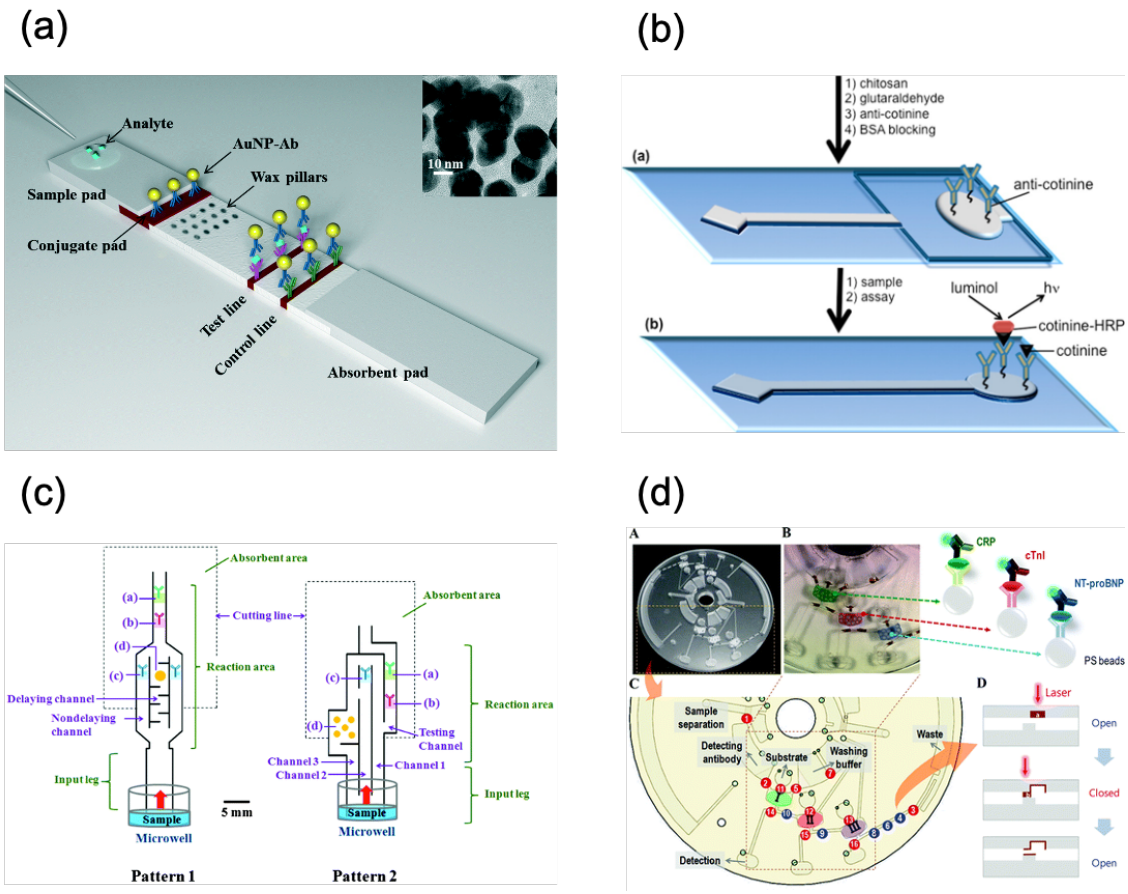


Figure 1.4 Examples of easy-to-use immunoassay systems. (a) A LFIA device. Reprinted with permission from reference [73]. Copyright 2014 The Royal Society of Chemistry. (b) A μPAD device for competitive immunoassaying. Reprinted with permission from reference [78]. Copyright 2013 American Chemical Society (c) A μPAD device for sandwich immunoassaying. Reprinted with permission from reference [81]. Copyright 2013 The Royal Society of Chemistry. (d) A centrifugal microfluidic platform. Reprinted with permission from reference [86]. Copyright 2012 American Chemical Society.

1.3.2.2 Highly sensitive immunoassay systems

Improving the sensitivities of immunoassay systems has been one of the most important themes since immunoassays were first developed. A typical immunoassay system that uses a microdevice for highly sensitive detection is shown in Figure 1.5. CLIA and ELISA are known to be highly sensitive immunoassays and are often used in analysis systems that use microdevices to detect trace amounts of analytes [89–91]. In addition, sample pre-concentration with a microdevice followed by immunoassaying reportedly provides high sensitivities [92,93]. However, CLIA and ELISA have long reaction times and are often complicated to operate. In addition, the combination of pre-concentration and FIA also requires additional operations, which increases the overall number of steps. In order to solve these problems, a new immunoassay concept that takes advantage of microdevices has been developed in recent years.

A highly sensitive immunoassay system that has received significant levels of attention in recent years uses surface-enhanced Raman scattering (SERS). This analytical method takes advantage of the phenomenon in which the scattered Raman light from a molecule is dramatically enhanced by the localized electric field caused by the localized surface plasmon resonance of metal nanoparticles [94]. As a result, the intensity of the Raman scattered light from reporter molecules adsorbed on the surfaces of the metal nanoparticles is dramatically enhanced. However, the details of the SERS mechanism have not yet been fully elucidated [95]. SERS can be used to effectively detect low-sensitivity signals using antibodies immobilized on metal nanoparticle. SERS is often used in combination with a sandwich immunoassay, and microdevice-based SERS immunoassays have also been successfully used to measure protein markers at ~pg/mL levels [96,97].

Highly sensitive immunoassays that take advantage of the characteristics of microdevices have also been developed. For example, Rissin *et al.* [98] developed a digital ELISA using a ~50 fL microchamber. The beads on which the capture antibodies are immobilized are enclosed in a microchamber to capture the antigen, after which a single bead is added into one chamber and subjected to ELISA. Compared to the conventional method, this method enables fluorescence images to be quantified with higher sensitivities. As a result, we

successfully quantified prostate-specific antigen (PSA) at a detection limit of 14 fg/mL (0.4 fM). Based on this research, digital ELISAs, as highly sensitive immunoassay systems, were expanded through applied research [99–101]. As a similar method, Liu *et al.* [102] reported the immunoassaying of microdroplets generated in a microchannel. Antibody-immobilized magnetic beads were encapsulated in droplets and used in ELISA. In a similar manner to digital ELSIA, fluorescence images can be digitally quantified, which led to the successful analysis of exosomes to a sensitivity of ~10 aM. These methods are overwhelmingly more sensitive than conventional microplate-based immunoassays. Therefore, it can be said that they are effective methods for measuring trace markers such as exosomes. However, dedicated and expensive detection equipment is required. In addition, it is still difficult to miniaturize the system, including the detection system; therefore, it is not a method suitable for PONT.

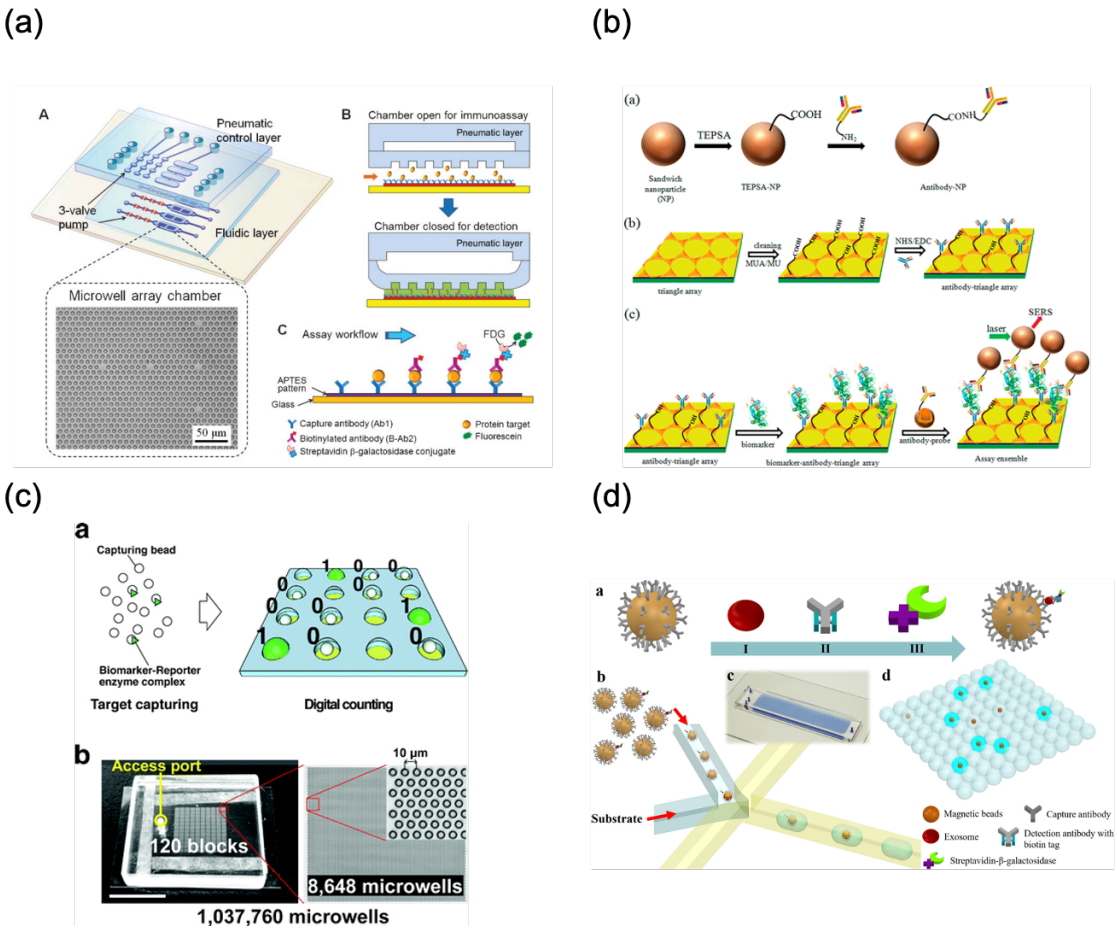


Figure 1.5 Examples of immunoassay system for highly sensitive detection. (a) An ELISA device. Reprinted with permission from reference [91]. Copyright 2013 The Royal Society of Chemistry. (b) A SERS device. Reprinted with permission from reference [97]. Copyright 2013 American Chemical Society (c) A digital ELISA device. Reprinted with permission from reference [99]. Copyright 2012 The Royal Society of Chemistry (d) A droplet digital ELISA device. Reprinted with permission from reference [102]. Copyright 2018 American Chemical Society.

1.4 Objectives of the Thesis

The objective of the present research was the development of a system for the analytical quantification of biomolecules for PONT based on immunoassays and microfluidic devices. As mentioned above, many immunoassay systems reportedly use microfluidic devices. However, despite the development of these elemental technologies, the number of immunoassay systems based on microfluidic devices that are practically used are still limited. Many immunoassay devices exhibit trade-off relationships between detection

sensitivity, analysis time, and procedural complexity, which is a major issue. These factors need to be compatible for practical use. In addition, miniaturizing such systems, including detection systems, will bring immunoassay technologies that use microfluidic devices closer to practical use. A PONT application also requires the analytical system to be easily handled in any location without the need for a professional engineer, and the rapid detection of the required analyte with the required sensitivity. To apply PONT to many applications in various fields, a microfluidic-device-based immunoassay system that meets these requirements of PONT was developed in this research. The target analytes in this research are proteins and viruses in biological samples, which are used in a wide range of PONT applications. In order to apply the system to various biomarkers and pathogens, two types of immunoassay system based on the detection of fluorescence signals were developed. In order to detect trace amounts of analyte-like protein biomarkers for cancer diagnosis, a highly sensitive immunoassay system based on a heterogeneous immunoassay was developed. To detect proteins that require rapidity, a simple and rapid immunoassay system based on a homogeneous immunoassay was developed. These two types of immunoassay system cover a wide range of PONT applications.

Chapter 2 describes the development of an ultrasensitive immunoassay system based on an enzyme sandwich immunoassay. A three-dimensional polymer structure (immuno-wall) was constructed in the microchannel, and capture antibodies were immobilized on this immuno-wall. In addition, in order to significantly improve detection sensitivity, a unique fluorescence signal amplification method that combines enzyme amplification and molecular concentration by the immuno-wall was developed. The sensitivity of the developed device was evaluated using human C-reactive protein (CRP) in serum as a model substance. Chapter 3 describes the fluorescence-signal amplification method developed in Chapter 2, and also discusses the mechanism of fluorescence-signal enhancement.

Chapter 4 describes the development of a non-competitive FPIA for protein quantification. Conventional FPIA is used as a homogeneous competitive immunoassay, but proteins, in principle, are difficult to analyze. The non-competitive FPIA concept was verified using a fluorescently labeled Fab fragment for protein quantification; it was also evaluated using serum CRP as a model substance. Chapter 5 describes the

detection of avian influenza virus antigens and antibodies as examples of non-competitive FPIA applications. A system capable of implementing non-competitive FPIA onsite was constructed using a portable FP analyzer and a microfluidic device.

The final chapter summarizes the findings of the present research, as well as several prospects for the future development of this research.

1.5 References

[1] Plebani, M. Does POCT Reduce the Risk of Error in Laboratory Testing? *Clin. Chim. Acta* **2009**, 404, 59–64.

[2] Zaloga, G. P. Evaluation of Bedside Testing Options for the Critical Care Unit. *Chest.* **1990**, 97, 185S-190.

[3] Jatlow, P. Point of Care Laboratory Testing in the Emergency Department *Am. J. Clin. Pathol.,* **1993**, 100, 591.

[4] Su, J.; Xu, J.; Chen, Y.; Xiang, Y.; Yuan, R.; Chai, Y. Personal Glucose Sensor for Point-of-Care Early Cancer Diagnosis. *Chem. Commun.* **2012**, 48, 6909.

[5] Lisi, F.; Peterson, J. R.; Gooding, J. J. The Application of Personal Glucose Meters as Universal Point-of-Care Diagnostic Tools. *Biosens. Bioelectron*. **2020**, 148, 111835.

[6] Werth, A.; Liakat, S.; Dong, A.; Woods, C. M.; Gmachl, C. F. Implementation of an Integrating Sphere for the Enhancement of Noninvasive Glucose Detection Using Quantum Cascade Laser Spectroscopy. *Appl. Phys. B* **2018**, 124, 75.

[7] Zhang, Y. J.; Kwon, H.; Miri, M.-A.; Kallos, E.; Cano-Garcia, H.; Tong, M. S.; Alu, A. Noninvasive Glucose Sensor Based on Parity-Time Symmetry. *Phys. Rev. Appl.* **2019**, 11, 044049.

[8] Keum, D. H.; Kim, S.-K.; Koo, J.; Lee, G.-H.; Jeon, C.; Mok, J. W.; Mun, B. H.; Lee, K. J.; Kamrani, E.; Joo, C.-K.; Shin, S.; Sim, J.-Y.; Myung, D.; Yun, S. H.; Bao, Z.; Hahn, S. K. Wireless Smart Contact Lens for Diabetic Diagnosis and Therapy. *Sci. Adv.* **2020**, 6, eaba3252.

[9] Moore, C. Point-of-Care Tests for Infection Control: Should Rapid Testing Be in the Laboratory or at the Front Line? *J. Hosp. Infect.* **2013**, 85, 1–7.

[10] Nair, C. B.; Manjula, J.; Subramani, P. A.; Nagendrappa, P. B.; Manoj, M. N.; Malpani, S.; Pullela, P. K.; Subbarao, P. V.; Ramamoorthy, S.; Ghosh, S. K. Differential Diagnosis of Malaria on Truelab Uno®, a

Portable, Real-Time, MicroPCR Device for Point-Of-Care Applications. *PLoS One* **2016**, 11, e0146961.

[11] Yu, S.-T.; Thi Bui, C.; Kim, D. T. H.; V. T. Nguyen, A.; Thi Trinh, T. T.; Yeo, S.-J. Clinical Evaluation of Rapid Fluorescent Diagnostic Immunochromatographic Test for Influenza A Virus (H1N1). *Sci. Rep.* **2018**, 8, 13468.

[12] Chen, C.; Xie, Q.; Yang, D.; Xiao, H.; Fu, Y.; Tan, Y.; Yao, S. Recent Advances in Electrochemical Glucose Biosensors: A Review. *RSC Adv.* **2013**, 3, 4473.

[13] Windmiller, J. R.; Wang, J. Wearable Electrochemical Sensors and Biosensors: A Review. *Electroanalysis* **2013**, 25, 29–46.

[14] Ciui, B.; Jambrec, D.; Sandulescu, R.; Cristea, C. Bioelectrochemistry for MiRNA Detection. *Curr. Opin. Electrochem.* **2017**, 5, 183–192.

[15] Cheng, Y.; Dong, L.; Zhang, J.; Zhao, Y.; Li, Z. Recent Advances in MicroRNA Detection. *Analyst* **2018**, 143, 1758–1774.

[16] Gou, T.; Hu, J.; Wu, W.; Ding, X.; Zhou, S.; Fang, W.; Mu, Y. Smartphone-Based Mobile Digital PCR Device for DNA Quantitative Analysis with High Accuracy. *Biosens. Bioelectron.* **2018**, 120, 144–152.

[17] Warsinke, A. Point-of-Care Testing of Proteins. *Anal. Bioanal. Chem.* **2009**, 393, 1393–1405.

[18] Jung, W.; Han, J.; Choi, J.-W.; Ahn, C. H. Point-of-Care Testing (POCT) Diagnostic Systems Using Microfluidic Lab-on-a-Chip Technologies. *Microelectron. Eng.* **2015**, 132, 46–57.

[19] MarketsandMarket Immunoassay Market by Product & Service (Reagents & Kits, Analyzers, Software), Technology (ELISA, Rapid Test), Platform (Radioimmunoassay), Specimen, Application (Infectious Diseases, Oncology, Cardiology), End User (Hospitals) – Global Forecast to 2023 https://www.marketsandmarkets.com/Market-Reports/immunoassay-market-436.html (accessed 1 December 2020)

[20] Yalow, R. S.; Berson, S. A. Assay of Plasma Insulin in Human Subjects by Immunological Methods. *Nature* **1959**, 184, 1648–1649.

[21] Rubenstein, K. E.; Schneider, R. S.; Ullman, E. F. "Homogeneous" Enzyme Immunoassay. A New Immunochemical Technique. Biochem. Biophys. *Res. Commun.* **1972**, 47, 846–851.

[22] Belanger, L.; Sylvestre, C.; Dufour, D. Enzyme-Linked Immunoassay for Alpha-Fetoprotein by Competitive and Sandwich Procedures. *Clin. Chim. Acta* **1973**, 48, 15–18.

[23] Pratt, J. J.; Woldring, M. G.; Villerius, L. Chemiluminescence-Linked Immunoassay. *J. Immunol. Methods* **1978**, 21, 179–184.

[24] Leuvering, J. H. W.; Thal, P. J. H. M.; Waart, M. van der; Schuurs, A. H. W. M. Sol Particle Immunoassay (SPIA). *J. Immunoassay* **1980**, 1, 77–91.

[25] Lequin, R. M. Enzyme Immunoassay (EIA)/Enzyme-Linked Immunosorbent Assay (ELISA). *Clin. Chem.* **2005**, 51, 2415–2418.

[26] Aydin, S. A Short History, Principles, and Types of ELISA, and Our Laboratory Experience with Peptide/Protein Analyses Using ELISA. *Peptides* **2015**, 72, 4–15.

[27] Hust, M. Mating Antibody Phage Display with Proteomics. *Trends Biotechnol.* **2004**, 22, 8–14.

[28] Rami, A.; Behdani, M.; Yardehnavi, N.; Habibi-Anbouhi, M.; Kazemi-Lomedasht, F. An Overview on Application of Phage Display Technique in Immunological Studies. *Asian Pac. J. Trop. Biomed.* **2017**, 7, 599–602.

[29] Grigorenko, V.; Andreeva, I.; Börchers, T.; Spener, F.; Egorov, A. A Genetically Engineered Fusion Protein with Horseradish Peroxidase as a Marker Enzyme for Use in Competitive Immunoassays. *Anal. Chem.* **2001**, 73, 1134–1139.

[30] Wang, F.; Li, Z.-F.; Yang, Y.-Y.; Wan, D.-B.; Vasylieva, N.; Zhang, Y.-Q.; Cai, J.; Wang, H.; Shen, Y.-D.; Xu, Z.-L.; Hammock, B. D. Chemiluminescent Enzyme Immunoassay and Bioluminescent Enzyme Immunoassay for Tenuazonic Acid Mycotoxin by Exploitation of Nanobody and Nanobody–Nanoluciferase Fusion. *Anal. Chem.* **2020**, 92, 11935–11942.

[31] Wu, J.; Fu, Z.; Yan, F.; Ju, H. Biomedical and Clinical Applications of Immunoassays and Immunosensors for Tumor Markers. *TrAC Trends Anal. Chem.* **2007**, 26, 679–688.

[32] Nimse, S. B.; Sonawane, M. D.; Song, K.-S.; Kim, T. Biomarker Detection Technologies and Future Directions. *Analyst* **2016**, 141, 740–755.

[33] Song, L.-W.; Wang, Y.-B.; Fang, L.-L.; Wu, Y.; Yang, L.; Chen, J.-Y.; Ge, S.-X.; Zhang, J.; Xiong, Y.-Z.; Deng, X.-M.; Min, X.-P.; Zhang, J.; Chen, P.-J.; Yuan, Q.; Xia, N.-S. Rapid Fluorescent Lateral-Flow Immunoassay for Hepatitis B Virus Genotyping. *Anal. Chem.* **2015**, 87, 5173–5180.

[34] Wu, Z.; Zeng, T.; Guo, W.-J.; Bai, Y.-Y.; Pang, D.-W.; Zhang, Z.-L. Digital Single Virus Immunoassay for Ultrasensitive Multiplex Avian Influenza Virus Detection Based on Fluorescent Magnetic Multifunctional Nanospheres. *ACS Appl. Mater. Interfaces* **2019**, 11, 5762–5770.

[35] Su, X.-L.; Li, Y. Quantum Dot Biolabeling Coupled with Immunomagnetic Separation for Detection of Escherichia Coli O157:H7. *Anal. Chem.* **2004**, 76, 4806–4810.

[36] Dogan, Ü.; Kasap, E.; Cetin, D.; Suludere, Z.; Boyaci, I. H.; Türkyılmaz, C.; Ertas, N.; Tamer, U. Rapid Detection of Bacteria Based on Homogenous Immunoassay Using Chitosan Modified Quantum Dots. *Sensors Actuators B Chem.* **2016**, 233, 369–378.

[37] Lyashchenko, K. P.; Singh, M.; Colangeli, R.; Gennaro, M. L. A Multi-Antigen Print Immunoassay for the Development of Serological Diagnosis of Infectious Diseases. *J. Immunol. Methods* **2000**, 242, 91–100.

[38] Alves, D.; Curvello, R.; Henderson, E.; Kesarwani, V.; Walker, J. A.; Leguizamon, S. C.; McLiesh, H.; Raghuwanshi, V. S.; Samadian, H.; Wood, E. M.; McQuilten, Z. K.; Graham, M.; Wieringa, M.; Korman,

T. M.; Scott, T. F.; Banaszak Holl, M. M.; Garnier, G.; Corrie, S. R. Rapid Gel Card Agglutination Assays for Serological Analysis Following SARS-CoV-2 Infection in Humans. *ACS Sensors* **2020**, 5, 2596–2603.

[39] Maragos, C. M.; Plattner, R. D. Rapid Fluorescence Polarization Immunoassay for the Mycotoxin Deoxynivalenol in Wheat. *J. Agric. Food Chem*. **2002**, 50, 1827–1832.

[40] Song, S.; Liu, N.; Zhao, Z.; Njumbe Ediage, E.; Wu, S.; Sun, C.; De Saeger, S.; Wu, A. Multiplex Lateral Flow Immunoassay for Mycotoxin Determination. *Anal. Chem.* **2014**, 86, 4995–5001.

[41] Li, W.; Wu, W. Z.; Barbara, R. B.; Schramm, K.-W.; Kettrup, A. A New Enzyme Immunoassay for PCDD/F TEQ Screening in Environmental Samples: Comparison to Micro-EROD Assay and to Chemical Analysis. *Chemosphere* **1999**, 38, 3313–3318.

[42] Marchesini, G. R.; Meulenberg, E.; Haasnoot, W.; Irth, H. Biosensor Immunoassays for the Detection of Bisphenol A. *Anal. Chim. Acta* **2005**, 528, 37–45.

[43] Blake, C.; Gould, B. J. Use of Enzymes in Immunoassay Techniques. A Review. *Analyst* **1984**, 109, 533.

[44] Towbin, H.; Motz, J.; Oroszlan, P.; Zingel, O. Sandwich Immunoassay for the Hapten Angiotensin II a Novel Assay Principle Based on Antibodies against Immune Complexes. *J. Immunol. Methods* **1995**, 181, 167–176.

[45] Kobayashi, N.; Oiwa, H.; Kubota, K.; Sakoda, S.; Goto, J. Monoclonal Antibodies Generated against an Affinity-Labeled Immune Complex of an Anti-Bile Acid Metabolite Antibody: An Approach to Noncompetitive Hapten Immunoassays Based on Anti-Idiotype or Anti-Metatype Antibodies. *J. Immunol. Methods* **2000**, 245, 95–108.

[46] Smith, D. S.; Al-Hakiem, M. H. H.; Landon, J. A Review of Fluoroimmunoassay and Immunofluorometric Assay. Ann. Clin. Biochem. *An Int. J. Biochem. Lab. Med.* **1981**, 18, 253–274.

[47] Zhao, L.; Sun, L.; Chu, X. Chemiluminescence Immunoassay. *TrAC Trends Anal. Chem.* **2009**, 28 (4), 404–415.

[48] The Immunoassay Handbook: Theory and Applications of Ligand Binding, ELISA and Related Techniques , D. WildElsevier, Amsterdam, Netherlands, 2013

[49] Henderson, D. R.; Friedman, S. B.; Harris, J. D.; Manning, W. B.; Zoccoli, M. A. CEDIA, a New Homogeneous Immunoassay System. *Clin. Chem.* **1986**, 32, 1637–1641.

[50] Dandliker, W. B.; Schapiro, H. .; Meduski, J. .; Alonso, R.; Feigen, G. A.; Hamrick, J. . Application of Fluorescence Polarization to the Antigen-Antibody Reaction. *Immunochemistry* **1964**, 1, 165–191.

[51] Dandliker, W. B.; Kelly, R. J.; Dandliker, J.; Farquhar, J.; Levin, J. Fluorescence Polarization Immunoassay. Theory and Experimental Method. *Immunochemistry* **1973**, 10, 219–227.

[52] Smith, D. S.; Eremin, S. A. Fluorescence Polarization Immunoassays and Related Methods for Simple, High-Throughput Screening of Small Molecules. *Anal. Bioanal. Chem.* **2008**, 391, 1499–1507.

[53] Ullman, E. F.; Kirakossian, H.; Switchenko, A. C.; Ishkanian, J.; Ericson, M.; Wartchow, C. A.; Pirio, M.; Pease, J.; Irvin, B. R.; Singh, S.; Singh, R.; Patel, R.; Dafforn, A.; Davalian, D.; Skold, C.; Kurn, N.; Wagner, D. B. Luminescent Oxygen Channeling Assay (LOCI): Sensitive, Broadly Applicable Homogeneous Immunoassay Method. *Clin. Chem.* **1996**, 42, 1518–1526.

[54] Lim, S.-L.; Ichinose, H.; Shinoda, T.; Ueda, H. Noncompetitive Detection of Low Molecular Weight Peptides by Open Sandwich Immunoassay. *Anal. Chem.* **2007**, 79, 6193–6200.

[55] Xia, Y.; Whitesides, G. M. Soft Lithography. *Angew. Chemie Int. Ed.* **1998**, 37, 550–575.

[56] Lab on a Chip Technology Volume 1: Fabrication and Microfluidics, K. E. Herold and A. Rasooly, Caister Academic Press, Norfolk, UK, 2009.

[57] Terry, S. C.; Jerman, J. H.; Angell, J. B. A Gas Chromatographic Air Analyzer Fabricated on a Silicon Wafer. IEEE Trans. *Electron Devices* **1979**, 26, 1880–1886.

[58] Manz, A.; Graber, N.; Widmer, H. M. Miniaturized Total Chemical Analysis Systems: A Novel Concept for Chemical Sensing. *Sensors Actuators B Chem.* **1990**, 1, 244–248.

[59] Terry, S. C.; Jerman, J. H.; Angell, J. B. A Gas Chromatographic Air Analyzer Fabricated on a Silicon Wafer. *IEEE Trans. Electron Devices* **1979**, 26, 1880–1886.

[60] Haapala, M.; Luosujärvi, L.; Saarela, V.; Kotiaho, T.; Ketola, R. A.; Franssila, S.; Kostiainen, R. Microchip for Combining Gas Chromatography or Capillary Liquid Chromatography with Atmospheric Pressure Photoionization-Mass Spectrometry. *Anal. Chem.* **2007**, 79, 4994–4999.

[61] Ishida, A.; Fujii, M.; Fujimoto, T.; Sasaki, S.; Yanagisawa, I.; Tani, H.; Tokeshi, M. A Portable Liquid Chromatograph with a Battery-Operated Compact Electroosmotic Pump and a Microfluidic Chip Device with a Reversed Phase Packed Column. *Anal. Sci.* **2015**, 31, 1163–1169.

[62] Li, D.; Chen, H.; Ren, S.; Zhang, Y.; Yang, Y.; Chang, H. Portable Liquid Chromatography for Point-of-Care Testing of Glycated Haemoglobin. *Sensors Actuators B Chem.* **2020**, 305, 127484.

[63] Harrison, D. J.; Manz, A.; Fan, Z.; Luedi, H.; Widmer, H. M. Capillary Electrophoresis and Sample Injection Systems Integrated on a Planar Glass Chip. *Anal. Chem.* **1992**, 64, 1926–1932.

[64] Woolley, A. T.; Mathies, R. A. Ultra-High-Speed DNA Sequencing Using Capillary Electrophoresis Chips. *Anal. Chem.* **1995**, 67, 3676–3680.

[65] Fluri, K.; Fitzpatrick, G.; Chiem, N.; Harrison, D. J. Integrated Capillary Electrophoresis Devices with an Efficient Postcolumn Reactor in Planar Quartz and Glass Chips. *Anal. Chem.* **1996**, 68, 4285–4290.

[66] Waters, L. C.; Jacobson, S. C.; Kroutchinina, N.; Khandurina, J.; Foote, R. S.; Ramsey, J. M. Microchip Device for Cell Lysis, Multiplex PCR Amplification, and Electrophoretic Sizing. *Anal. Chem.* **1998**, 70, 158–162.

[67] Tokeshi, M.; Uchida, M.; Hibara, A.; Sawada, T.; Kitamori, T. Determination of Subyoctomole Amounts of Nonfluorescent Molecules Using a Thermal Lens Microscope: Subsingle-Molecule Determination. *Anal. Chem.* **2001**, 73, 2112–2116.

[68] Tamaki, E.; Sato, K.; Tokeshi, M.; Sato, K.; Aihara, M.; Kitamori, T. Single-Cell Analysis by a Scanning Thermal Lens Microscope with a Microchip: Direct Monitoring of Cytochrome c Distribution during Apoptosis Process. *Anal. Chem.* **2002**, 74, 1560–1564.

[69] Sato, K.; Tokeshi, M.; Odake, T.; Kimura, H.; Ooi, T.; Nakao, M.; Kitamori, T. Integration of an Immunosorbent Assay System: Analysis of Secretory Human Immunoglobulin A on Polystyrene Beads in a Microchip. *Anal. Chem.* **2000**, 72, 1144–1147.

[70] Sato, K.; Tokeshi, M.; Kimura, H.; Kitamori, T. Determination of Carcinoembryonic Antigen in Human Sera by Integrated Bead-Bed Immunoasay in a Microchip for Cancer Diagnosis. *Anal. Chem.* **2001**, 73, 1213–1218.

[71] Sia, S. K.; Linder, V.; Parviz, B. A.; Siegel, A.; Whitesides, G. M. An Integrated Approach to a Portable and Low-Cost Immunoassay for Resource-Poor Settings. *Angew. Chemie Int. Ed.* **2004**, 43, 498–502.

[72] Hu, W.; Lu, Z.; Liu, Y.; Chen, T.; Zhou, X.; Li, C. M. A Portable Flow-through Fluorescent Immunoassay Lab-on-a-Chip Device Using ZnO Nanorod-Decorated Glass Capillaries. *Lab Chip* **2013**, 13, 1797.

[73] Rivas, L.; Medina-Sánchez, M.; de la Escosura-Muñiz, A.; Merkoçi, A. Improving Sensitivity of Gold Nanoparticle-Based Lateral Flow Assays by Using Wax-Printed Pillars as Delay Barriers of Microfluidics. *Lab Chip* **2014**, 14, 4406–4414.

[74] Wang, Z.; Li, H.; Li, C.; Yu, Q.; Shen, J.; De Saeger, S. Development and Application of a Quantitative Fluorescence-Based Immunochromatographic Assay for Fumonisin B1 in Maize. *J. Agric. Food Chem.* **2014**, 62, 6294–6298.

[75] López_Marzo, A. M.; Pons, J.; Blake, D. A.; Merkoçi, A. High Sensitive Gold-Nanoparticle Based Lateral Flow Immunodevice for Cd^{2+} Detection in Drinking Waters. *Biosens. Bioelectron.* **2013**, 47, 190–198.

[76] Koizumi, D.; Shirota, K.; Akita, R.; Oda, H.; Akiyama, H. Development and Validation of a Lateral Flow Assay for the Detection of Crustacean Protein in Processed Foods. *Food Chem.* **2014**, 150, 348–352.

[77] Martinez, A. W.; Phillips, S. T.; Butte, M. J.; Whitesides, G. M. Patterned Paper as a Platform for Inexpensive, Low-Volume, Portable Bioassays. *Angew. Chemie Int. Ed.* **2007**, 46, 1318–1320.

[78] Liu, W.; Cassano, C. L.; Xu, X.; Fan, Z. H. Laminated Paper-Based Analytical Devices (LPAD) with Origami-Enabled Chemiluminescence Immunoassay for Cotinine Detection in Mouse Serum. *Anal. Chem.* **2013**, 85, 10270–10276.

[79] Li, S.; Wang, Y.; Ge, S.; Yu, J.; Yan, M. Self-Powered Competitive Immunosensor Driven by Biofuel Cell Based on Hollow-Channel Paper Analytical Devices. *Biosens. Bioelectron.* **2015**, 71, 18–24.

[80] Busa, L. S. A.; Mohammadi, S.; Maeki, M.; Ishida, A.; Tani, H.; Tokeshi, M. A Competitive Immunoassay System for Microfluidic Paper-Based Analytical Detection of Small Size Molecules. *Analyst* **2016**, 141, 6598–6603.

[81] Apilux, A.; Ukita, Y.; Chikae, M.; Chailapakul, O.; Takamura, Y. Development of Automated Paper-Based Devices for Sequential Multistep Sandwich Enzyme-Linked Immunosorbent Assays Using Inkjet Printing. *Lab Chip* **2013**, 13, 126–135.

[82] Chen, C.-A.; Yeh, W.-S.; Tsai, T.-T.; Li, Y.-D.; Chen, C.-F. Three-Dimensional Origami Paper-Based Device for Portable Immunoassay Applications. *Lab Chip* **2019**, 19, 598–607.

[83] Hu, J.; Wang, S.; Wang, L.; Li, F.; Pingguan-Murphy, B.; Lu, T. J.; Xu, F. Advances in Paper-Based Point-of-Care Diagnostics. *Biosens. Bioelectron.* **2014**, 54, 585–597.

[84] Strohmeier, O.; Keller, M.; Schwemmer, F.; Zehnle, S.; Mark, D.; von Stetten, F.; Zengerle, R.; Paust, N. Centrifugal Microfluidic Platforms: Advanced Unit Operations and Applications. *Chem. Soc. Rev.* **2015**, 44, 6187–6229.

[85] Lee, B. S.; Lee, Y. U.; Kim, H.-S.; Kim, T.-H.; Park, J.; Lee, J.-G.; Kim, J.; Kim, H.; Lee, W. G.; Cho, Y.-K. Fully Integrated Lab-on-a-Disc for Simultaneous Analysis of Biochemistry and Immunoassay from Whole Blood. *Lab Chip* **2011**, 11, 70–78.

[86] Park, J.; Sunkara, V.; Kim, T.-H.; Hwang, H.; Cho, Y.-K. Lab-on-a-Disc for Fully Integrated Multiplex Immunoassays. *Anal. Chem.* **2012**, 84, 2133–2140.

[87] Czilwik, G.; Vashist, S. K.; Klein, V.; Buderer, A.; Roth, G.; von Stetten, F.; Zengerle, R.; Mark, D. Magnetic Chemiluminescent Immunoassay for Human C-Reactive Protein on the Centrifugal Microfluidics Platform. *RSC Adv.* **2015**, 5, 61906–61912.

[88] Nwankire, C. E.; Donohoe, G. G.; Zhang, X.; Siegrist, J.; Somers, M.; Kurzbuch, D.; Monaghan, R.; Kitsara, M.; Burger, R.; Hearty, S.; Murrell, J.; Martin, C.; Rook, M.; Barrett, L.; Daniels, S.; McDonagh, C.; O'Kennedy, R.; Ducrée, J. At-Line Bioprocess Monitoring by Immunoassay with Rotationally Controlled Serial Siphoning and Integrated Supercritical Angle Fluorescence Optics. *Anal. Chim. Acta* **2013**, 781, 54–62.

[89] Torabi, F.; Mobini Far, H. R.; Danielsson, B.; Khayyami, M. Development of a Plasma Panel Test for Detection of Human Myocardial Proteins by Capillary Immunoassay. *Biosens. Bioelectron.* **2007**, 22, 1218–1223.

[90] Herrmann, M.; Veres, T.; Tabrizian, M. Quantification of Low-Picomolar Concentrations of TNF-α in Serum Using the Dual-Network Microfluidic ELISA Platform. *Anal. Chem.* **2008**, 80, 5160–5167.

[91] Wang, T.; Zhang, M.; Dreher, D. D.; Zeng, Y. Ultrasensitive Microfluidic Solid-Phase ELISA Using an Actuatable Microwell-Patterned PDMS Chip. *Lab Chip* **2013**, 13, 4190-4197.

[92] Mohamadi, M. R.; Kaji, N.; Tokeshi, M.; Baba, Y. Online Preconcentration by Transient Isotachophoresis in Linear Polymer on a Poly(Methyl Methacrylate) Microchip for Separation of Human Serum Albumin Immunoassay Mixtures. *Anal. Chem.* **2007**, 79, 3667–3672.

[93] Huang, Y.; Shi, M.; Zhao, S.; Liang, H. A Sensitive and Rapid Immunoassay for Quantification of Testosterone by Microchip Electrophoresis with Enhanced Chemiluminescence Detection. *Electrophoresis* **2011**, 32, 3196–3200.

[94] Han, X. X.; Zhao, B.; Ozaki, Y. Surface-Enhanced Raman Scattering for Protein Detection. *Anal. Bioanal. Chem.* **2009**, 394, 1719–1727.

[95] Pang, S.; Yang, T.; He, L. Review of Surface Enhanced Raman Spectroscopic (SERS) Detection of Synthetic Chemical Pesticides. *TrAC Trends Anal. Chem.* **2016**, 85, 73–82.

[96] Yoon, K.-J.; Seo, H.-K.; Hwang, H.; Pyo, D.; Eom, I.-Y.; Hahn, J.-H.; Jung, Y.-M. Bioanalytical Application of SERS Immunoassay for Detection of Prostate-Specific Antigen. *Bull. Korean Chem. Soc.* **2010**, 31, 1215–1218.

[97] Li, M.; Cushing, S. K.; Zhang, J.; Suri, S.; Evans, R.; Petros, W. P.; Gibson, L. F.; Ma, D.; Liu, Y.; Wu, N. Three-Dimensional Hierarchical Plasmonic Nano-Architecture Enhanced Surface-Enhanced Raman Scattering Immunosensor for Cancer Biomarker Detection in Blood Plasma. *ACS Nano* **2013**, 7, 4967–4976.

[98] Rissin, D. M.; Kan, C. W.; Campbell, T. G.; Howes, S. C.; Fournier, D. R.; Song, L.; Piech, T.; Patel, P. P.; Chang, L.; Rivnak, A. J.; Ferrell, E. P.; Randall, J. D.; Provuncher, G. K.; Walt, D. R.; Duffy, D. C. Single-Molecule Enzyme-Linked Immunosorbent Assay Detects Serum Proteins at Subfemtomolar Concentrations. *Nat. Biotechnol.* **2010**, 28, 595–599.

[99] Kim, S. H.; Iwai, S.; Araki, S.; Sakakihara, S.; Iino, R.; Noji, H. Large-Scale Femtoliter Droplet Array for Digital Counting of Single Biomolecules. *Lab Chip* **2012**, 12, 4986-4991.

[100] Leirs, K.; Tewari Kumar, P.; Decrop, D.; Pérez-Ruiz, E.; Leblebici, P.; Van Kelst, B.; Compernolle, G.; Meeuws, H.; Van Wesenbeeck, L.; Lagatie, O.; Stuyver, L.; Gils, A.; Lammertyn, J.; Spasic, D. Bioassay Development for Ultrasensitive Detection of Influenza A Nucleoprotein Using Digital ELISA. *Anal. Chem.* **2016**, 88, 8450–8458.

[101] Pérez-Ruiz, E.; Decrop, D.; Ven, K.; Tripodi, L.; Leirs, K.; Rosseels, J.; van de Wouwer, M.; Geukens, N.; De Vos, A.; Vanmechelen, E.; Winderickx, J.; Lammertyn, J.; Spasic, D. Digital ELISA for the Quantification of Attomolar Concentrations of Alzheimer's Disease Biomarker Protein Tau in Biological Samples. *Anal. Chim. Acta* **2018**, 1015, 74–81.

[102] Liu, C.; Xu, X.; Li, B.; Situ, B.; Pan, W.; Hu, Y.; An, T.; Yao, S.; Zheng, L. Single-Exosome-Counting Immunoassays for Cancer Diagnostics. *Nano Lett.* **2018**, 18, 4226–4232.

CHAPTER 2 Ultrasensitive Detection of Disease Biomarkers Using an Immuno-wall Device with Enzymatic Amplification

2.1 Introduction

With the discovery of new biomarkers, there has been a growing interest in diagnosis of diseases by biomarker detection [1-3]. Numerous research studies on low cost and simple methods to detect biomarkers have been reported [4-8]. Among them, microfluidic devices are representative solutions for simple and rapid diagnosis. For example, devices based on lateral flow immunoassays for pregnancy and influenza tests are widely used and contribute to easy and early diagnosis [9,10]. There are also ever-increasing interests in detecting trace amounts of biomarkers in samples such as cancer biomarkers by easy-to-use and rapid detection methods [11-14].

Immunoassays are used for measuring biomarkers [15]. Various immunoassays have been realized using microdevices and applied to disease diagnosis [16-21]. Many immunoassays are based on optical detection. They are classified into colorimetric, fluorescence or chemiluminescent methods depending on the nature of the signal. Colorimetric methods offer simplicity and implementation by inexpensive detectors; however, they are generally less sensitive than fluorescence and chemiluminescence methods [22,23]. Chemiluminescence methods are highly sensitive and do not require an excitation light source. However, since chemiluminescence is strongly affected by environmental factors such as temperature and matrix components, it is necessary to use a system that takes these into consideration [24,25]. Fluorescence methods are highly sensitive and applicable to many analytes [26-28]. Moreover, some miniaturized detectors, consisting of simple components, for the fluorescence signal detection have been reported [29-30].

Tokeshi *et al.* [31-35] have reported microdevices based on a fluorescence method immunoassay for easy and rapid detection of disease biomarkers. In these previous papers, they used a cylindrical hydrogel structure (immuno-pillar) for the immunoassay reaction sites. However, it is difficult to wash thoroughly in the immuno-pillar and this difficulty leads to a large variation of results. Recently, Tokeshi *et al.* [36,37] also developed a new device called the immuno-wall device that has a 3-D wall-like structure made of photopolymer. The 3-D wall-like structure allow us to easily remove the nonspecifically binding molecules by just injecting washing buffer. In the immuno-wall device, the immunoassay is performed using an antibody immobilized on the wall

as a capture antibody and a fluorescence-labeled antibody as a labeling antibody. The fluorescence signal on the wall surface is detected after protein complex formation. The immuno-wall device provides rapid analysis (16 min), and requires only a small volume of sample (0.25 μL). However, the sensitivity of the immuno-wall device is equivalent to that of a commercially available microplate. Improving the sensitivity is indispensable to detect biomarkers that are only present in trace amounts in a sample.

In the chapter 2, the ultrasensitive immunoassay system using the immuno-wall device with an enzymatic amplification reaction was developed. Human C-reactive protein (CRP) was used as the model measurement substance because many microdevices have already been reported for CRP detection; [38-43] that means there are existing devices to which I can compare performance of our microdevice. A sandwich immunoassay was performed with an enzyme-labeled antibody, alkaline phosphatase-labeled antibody, as a labeling antibody and a high concentration of fluorescent molecules was generated by an enzyme reaction in the presence of an excess amount of substrate. From the fluorescence intensity profile analysis, I found that the immuno-wall efficiently accumulated the fluorescent molecules. I was able to accomplish ultrasensitive CRP detection with a small amount of sample by utilizing the wall properties for fluorescence detection.

2.2 Experimental

2.2.1 Materials and reagents

Bovine serum albumin (BSA), hydrochloric acid and magnesium chloride hexahydrate were purchased from FUJIFILM Wako Pure Chemical Corporation (Japan). Trizma® base and Tween 20 were purchased from Sigma-Aldrich Co. LLC (USA). Phosphate-buffered saline (PBS; pH 7.4) solution, 9H-(1,3-dichloro-9,9-dimethylacridin-2-one-7-yl) phosphate diammonium salt (DDAO phosphate), fluorescein diphosphate tetraammonium salt (FDP), 4-methylumbelliferyl phosphate free acid (MUP) and 6,8-difluoro-4-methylumbelliferyl phosphate (DiFMUP) were purchased from Thermo Fisher Scientific, Inc. (USA). 9H-(1,3-Dichloro-9,9-dimethylacridin-2-one-7-yl) (DDAO) was purchased from Cosmo Bio Corporation (Japan).

AttoPhos® substrate was purchased from Promega Corporation (USA). Rabbit anti-CRP monoclonal antibody, DyLight 650-labeled goat anti-rabbit polyclonal antibody and alkaline phosphatase-labeled goat anti-rabbit polyclonal antibody were purchased from Abcam (USA). Biotinylated mouse anti-CRP monoclonal antibody and streptavidin were purchased from ProSpec-Tany TechnoGene Ltd (USA). Human CRP and human CRP-free serum were purchased from Oriental Yeast Co., Ltd (Japan). Azide-unit pendant water-soluble photopolymer (AWP, 6%) was purchased from Toyo Gosei Co., Ltd (Japan). PBS containing 0.5% Tween-20 and 0.5% BSA was used as a washing buffer.

2.2.2 Fabrication of immuno-wall device

Figure 2.1 (a) shows a photograph and schematic drawing of the immuno-wall device. The immuno-walls having widths of 40 and 20 μm were fabricated for assays with DyLight 650-labeled antibody and alkaline phosphatase-labeled antibody, respectively. Although narrower immuno-walls were fragile, they allowed us to efficiently wash unimmobilized antibodies retained inside the wall. Enzymes of unimmobilized antibodies remained in the wall affected the reproducibility of the signal, which was amplified with the enzyme reaction. Therefore, I designed a narrow immuno-wall for the assay with alkaline phosphatase-labeled antibody. The microchip having 40 straight microchannels was fabricated with cyclic olefin copolymer in Sumitomo Bakelite Co., Ltd (Tokyo, Japan). Figure 2.1 (b) summarizes the fabrication procedure for the immuno-wall device. At first, the microchip was aligned with a photomask into the home-made holder. Second, a microchannel was filled with a mixture (0.25 μL, volume ratio 1 : 1) of AWP and 10 mg mL^{-1} streptavidin by using a pipette (PIPETMAN; Gilson S.A.S.; France). Then, the UV light (365 nm, 20 mW) from a mercury lamp (LA-410UV; Hayashi Watch Works; Japan) was irradiated onto the mixture through the photomask for 8 s. Subsequently, the uncured AWP was removed by a vacuum pump (SP 20; Air Liquide Medical Systems; France). Finally, a microchannel was washed with a washing buffer to reveal the resulting structure.

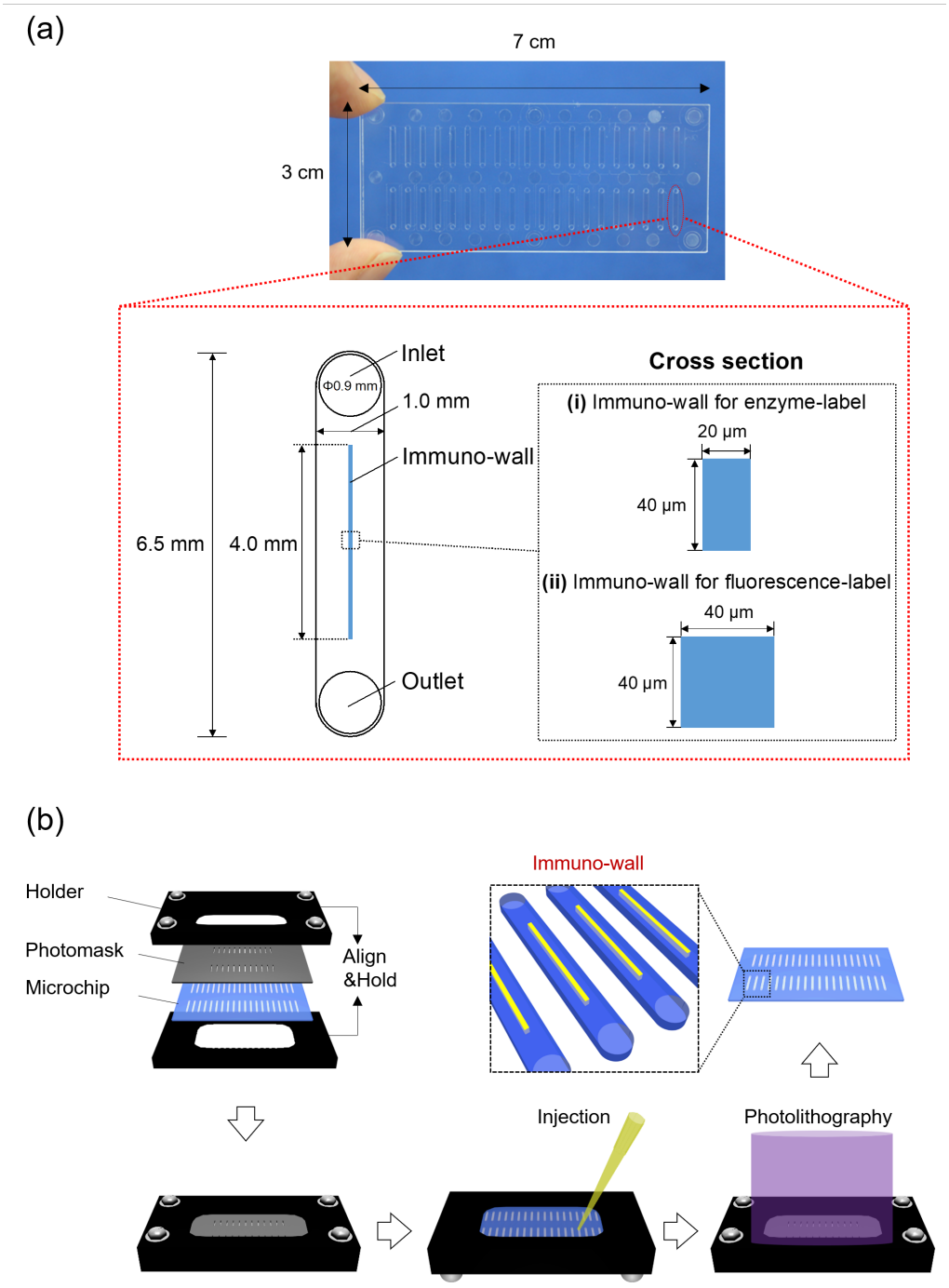


Figure 2.1 (a) Photograph and schematic illustration of the immuno-wall device. Two types of immuno-wall devices were fabricated for the detection with (i) enzyme-labeled antibody and (ii) fluorescence-labeled antibody. (b) Schematic illustration of the immuno-wall device fabrication procedure.

2.2.3 Assay procedure

A schematic flow diagram of the assay procedure is shown in Figure 2.2. All solutions (0.25 μL each) were introduced into a microchannel in the device by using a pipette within 1 s. The solutions remained in the microchannel during respective incubations. For immobilizing capture antibodies at the streptavidin-modified wall, biotinylated anti-CRP monoclonal antibody (50 μg mL^{-1}) in 1% BSA–PBS was introduced into the microchannel and incubated for 1 h. Then, the antibody solution was sucked with a vacuum pump and the wall was washed with the washing buffer. CRP in PBS or CRP-free serum was injected and incubated for 15 min. Then, anti-CRP antibody (detection antibody) (50 μg mL^{-1}) in 1% BSA–PBS was injected and incubated for 30 s. Next, DyLight 650-labeled antibody (labeling antibody) (50 μg mL^{-1}) in 1% BSA–PBS or alkaline phosphatase-labeled antibody (labeling antibody) (50 μg mL^{-1}) in 1% BSA–PBS was injected and incubated for 30 s. The microchannel was washed after each incubation in the same manner as I mentioned above. For alkaline phosphatase-labeled antibody, 3 μM fluorogenic substrate such as DiFMUP, MUP, AttoPhos, FDP or DDAO phosphate in Tris-HCl buffer (pH 8.0, 1 μM Mg^{2+}) was introduced into the microchannel. Afterwards, the immuno-wall device was immediately placed onto a clear heating stage (TPi-KIX; Tokai Hit; Shizuoka, Japan) equipped with a fluorescence microscope to control the reaction temperature. The fluorescence image of the immuno-wall device was captured without removing the solution of the reaction mixture remained in the microchannel.

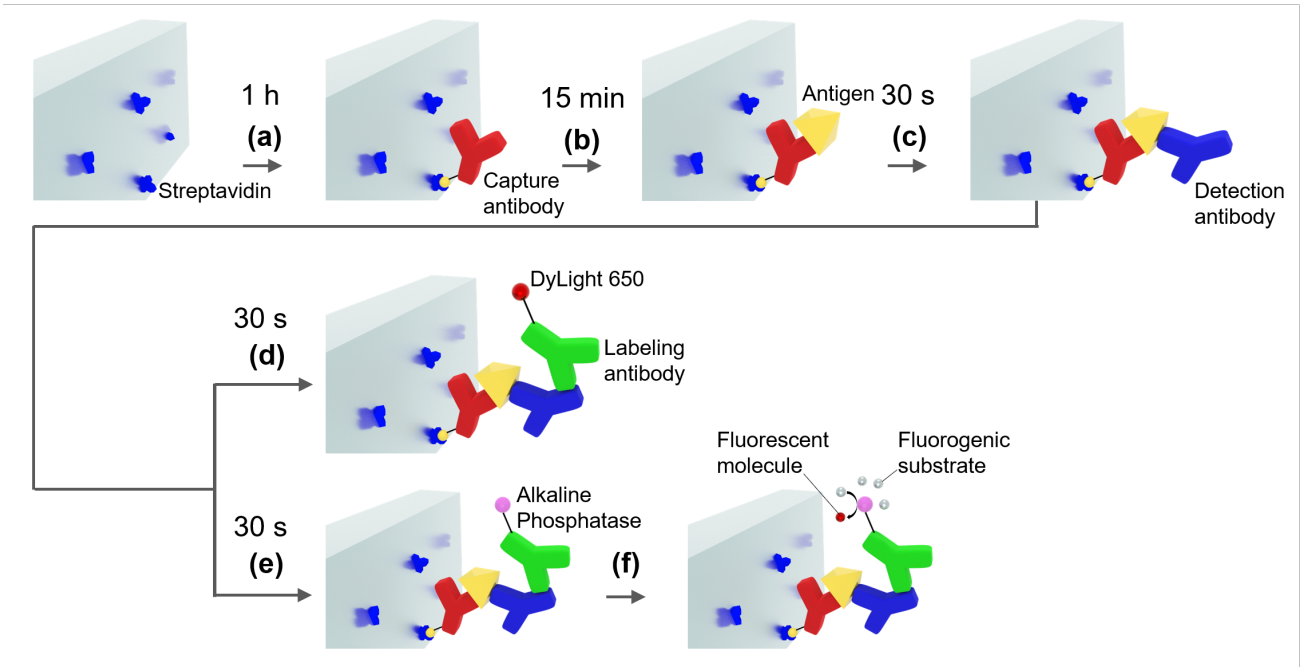


Figure 2.2 Schematic illustration of the assay procedure flow. Injection of: (a) a capture antibody; (b) an antigen; (c) a detection antibody; (d) a DyLight 650-labeled antibody; (e) the alkaline phosphatase-labeled antibody; and (f) a fluorogenic substrate. Incubation times are: (a) 1 h; (b) 15 min; (c) 30 s; (d) 30 s; and (e) 30 s.

2.2.4 Fluorescence microscope

The fluorescence signal was detected by an inverted fluorescence microscope (BZ-9000; Keyence; Japan) after assay. Three filter cubes were used: DAPI filter (OP-87762; excitation 360/40 nm, emission 460/50 nm; Keyence; Japan) for DiFMUP and MUP; GFP-B filter (OP-66836; excitation 470/40 nm, emission 535/50 nm; Keyence; Japan) for AttoPhos and FDP; and Cy5 filter (OP-87766; excitation 620/60 nm, emission 700/75 nm; Keyence; Japan) for DDAO phosphate and DyLight 650. Exposure times of the CCD camera were adjusted to 0.1 s for DiFMUP and MUP, 2.0 s for AttoPhos and FDP, 3.0 s for DyLight 650 and 5.0 s for DDAO phosphate. Reaction temperatures of the immuno-wall device were kept using the thermo plate on the microscope stage.

2.3 Results and Discussion

2.3.1 Biomarker detection with fluorescence-labeled antibody

CRP is widely used as a biomarker for inflammation and arteriosclerosis. The cutoff value of CRP is 10 μg mL^{-1} for inflammation and 1 μg mL^{-1} for arteriosclerosis [44]. In order to evaluate the performance with the DyLight 650-labeled antibody that has been used in the conventional immuno-wall device [36], I prepared a calibration curve for the standard CRP solution in PBS (Figure 2.3 (b)). Fluorescence was observed from both sides of the immuno-wall on which the antibody was immobilized (Figure 2.3 (a)). Fluorescence intensity of the calibration curve was defined as the average value of the fluorescence intensity of each pixel within the rectangle, red dotted line in Figure 2.3 (a). Increasing fluorescence intensity was confirmed as the concentration increased. The limit of detection (LOD) was 1.7 ng mL^{-1} which gave a signal at 3 standard deviations (SDs) above the background. This value was well below the cutoff values. In addition, the total incubation time was 16 min and the required sample volume was 0.25 μL. The detection range of CRP was from 1.7 to 10 000 ng mL^{-1}.

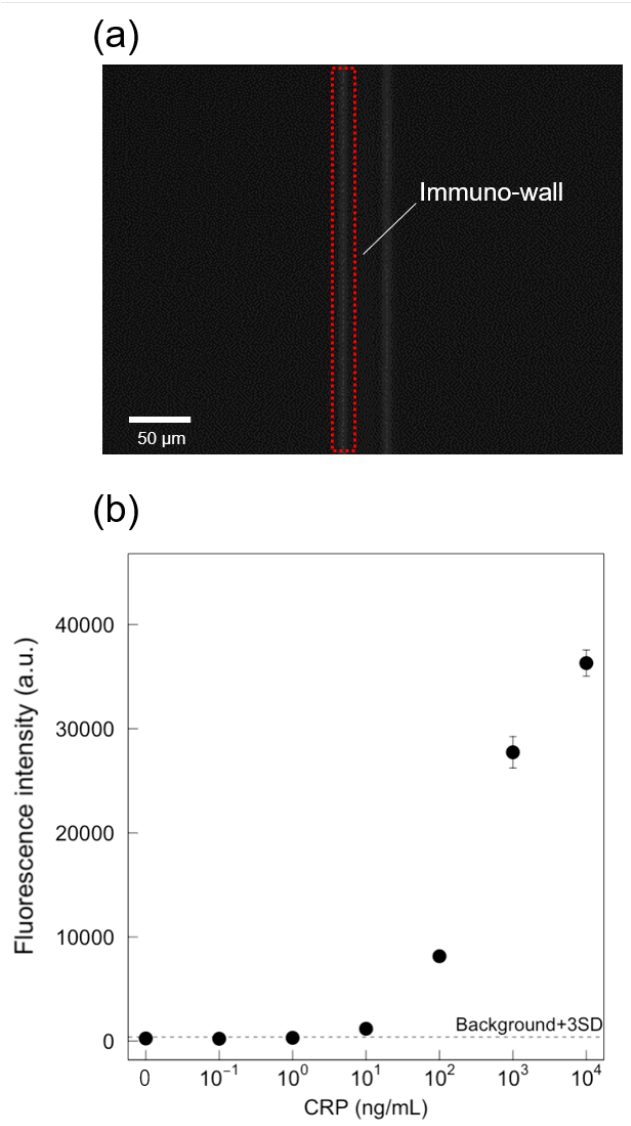


Figure 2.3 (a) Photograph of a fluorescence image of the immuno-wall device with fluorescence-labeled antibody. CPR concentration was 1000 ng mL^{-1}. (b) Calibration curve of standard CRP solution in PBS. The dashed line represents the signal level at 3 SDs above the background. BG means the background signal of the immuno-wall. Exposure time of the CCD camera was 3 s.

2.3.2 Selection of fluorogenic substrates for enzymatic amplification

In order to obtain ultrahigh sensitivity with the immuno-wall device, I investigated whether or not signal amplification by an enzyme reaction could be applied to the immuno-wall device. The alkaline phosphatase-labeled antibody was used as a labeling antibody. Fluorescence signals are amplified by an enzyme

reaction in the presence of an excessive amount of fluorogenic substrate. In order to select the most sensitive fluorogenic substrate suitable for the immuno-wall device, I examined five representative alkaline phosphatase fluorogenic substrates: DiFMUP (ex/em 358/455 nm); MUP (ex/em 360/449 nm); AttoPhos (ex/em 435/555 nm); FDP (ex/em 490/514 nm); and DDAO phosphate (ex/em 646/659 nm). In this device, the fluorescent molecules generated by the enzyme reaction diffuse through the solution. This is distinct from the conventional device in which the fluorescence-labeled antibody is placed beside the immuno-wall. Therefore, the behavior of the fluorescent molecules in the microchannel over time was observed in the area around the immuno-wall (Figure 2.4 (a)). Since the excitation and emission wavelengths are greatly different for each substrate, three types of fluorescence filters of the fluorescence microscope were used for the experiment. Figure 2.5 shows the background signal of the immuno-wall of each filter. Using a short wavelength filter led to a high background signal. This was due to the autofluorescence of AWP having a peak absorption wavelength on the short wavelength side (~310 nm). Then I confirmed the sensitive detection range of the fluorescence microscope. Figure 2.6 shows the calibration curves of DDAO in microchannel without the immuno-wall. DDAO is a fluorescent molecule formed as a product of the enzymatic reaction from DDAO phosphate. The fluorescence microscope could sensitively detect DDAO when the fluorescence intensity was in the range of 5000–35 000. In order to measure the fluorescence intensity in this range after injection of a fluorogenic substrate, I set the exposure time of the CCD camera in fluorescence microscope to 0.1 s for DiFMUP and MUP, 2.0 s for AttoPhos and FDP, and 5.0 s for DDAO phosphate.

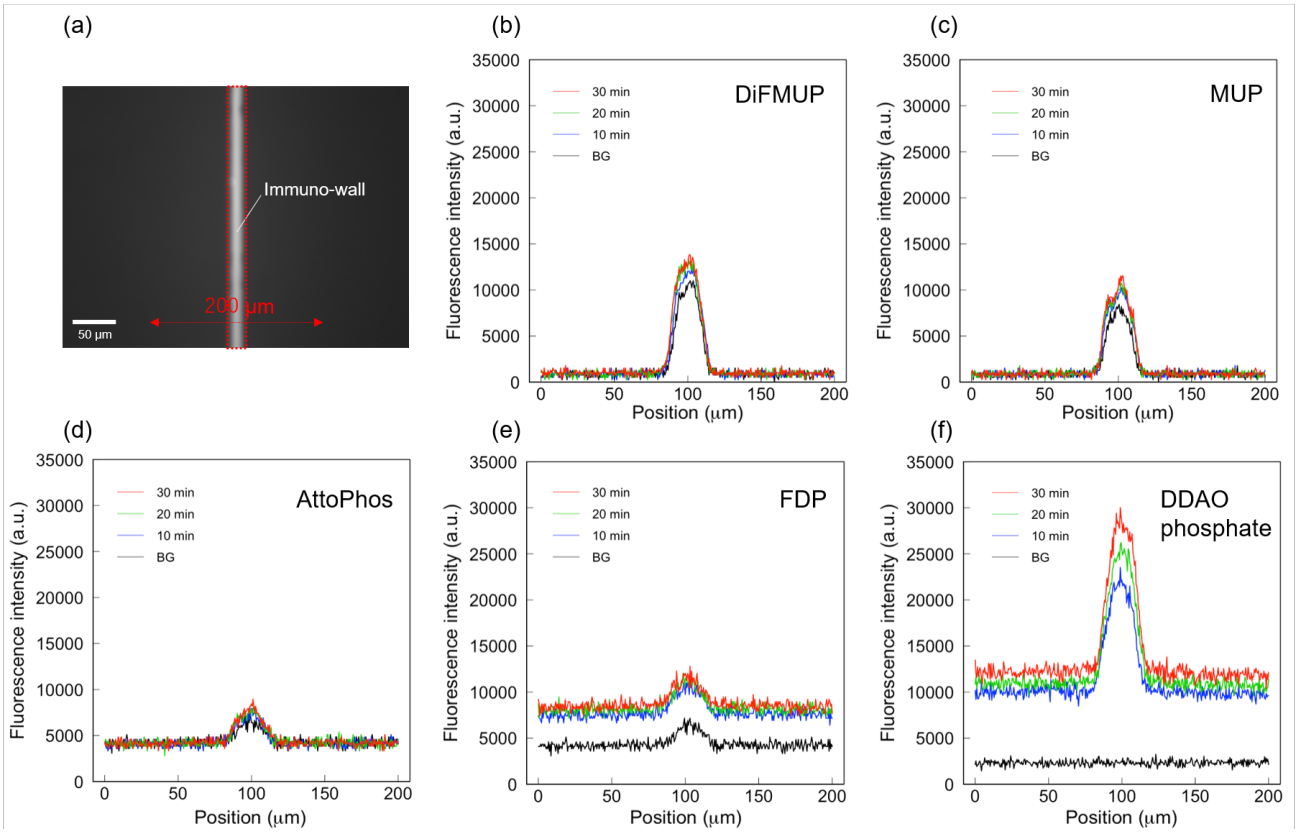


Figure 2.4 (a) Photograph of a fluorescence image of the immuno-wall device with enzyme-labeled antibody. The red arrow shows the detection range of the fluorescence intensity profile (200 µm). Fluorescence intensity profiles as a function of the position with: (b) DiFMUP; (c) MUP; (d) AttoPhos; (e) FDP; and (f) DDAO phosphate during a single measurement. The fluorescence intensity profiles were obtained at 0 min (black), 10 min (blue), 20 min (green) and 30 min (red) after injection of the fluorogenic substrate. Exposure times of the CCD camera were (b) and (c) 0.1 s; (d) and (e) 2 s; and (f) 5 s.

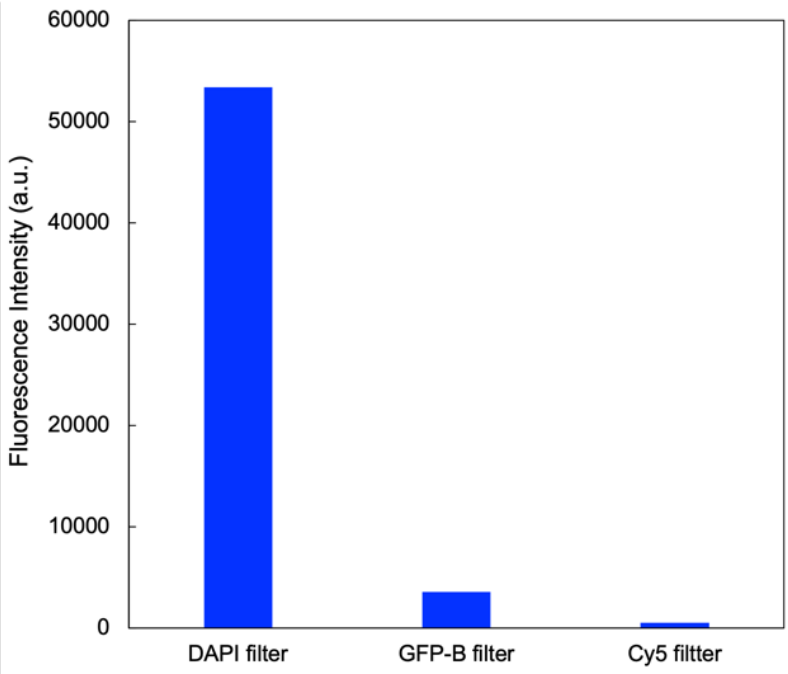


Figure 2.5 Background signal of the immuno-wall obtained using various filters. Exposure time of the CCD camera was 1 s for all filters.

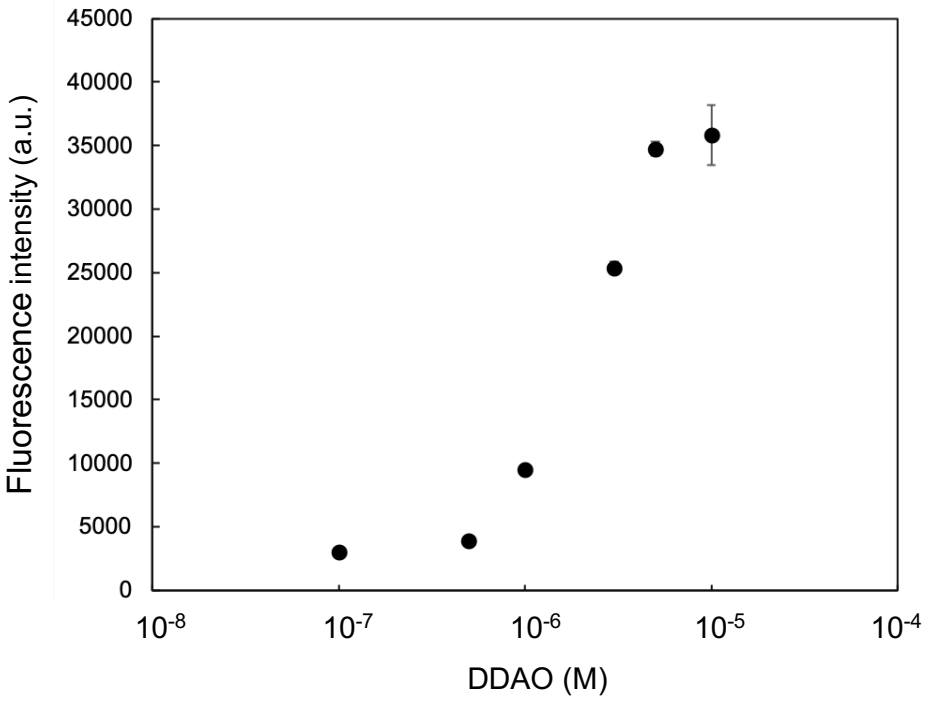


Figure 2.6 Calibration curves of 9H-(1,3-dichloro-9,9-dimethylacridin-2-one-7-yl) (DDAO) in a microchannel without the immuno-wall. Exposure time of the CCD camera was 5 s.

Figure 2.4 (b)–(f) show the fluorescence profiles after substrate injection. 1 ng mL^{-1} CRP was used as an antigen. The time was defined as 0 min when the substrate was injected into the microchannel. Unlike the fluorescence image shown in Figure 2.3 (a), the fluorescence was observed from the entire immuno-wall area in this device. A peak at the background (0 min) was due to the autofluorescence of AWP. As described above, the intensity of the autofluorescence of AWP depends on the filter. As for DiFMUP, MUP and AttoPhos, the fluorescence intensity slightly increased only in the wall area over time. The signals of FDP and DDAO phosphate showed a large difference from their background signals. Particularly in DDAO phosphate, the fluorescence intensity inside the wall greatly increased with the time. DDAO phosphate provided the highest signal/background (S/B) ratio among all substrates examined. In order to examine the reason why the fluorescence intensity increased in the wall area, 0.5 μM DDAO was introduced into a microchannel without any antigen and antibodies injection (Figure 2.7). The fluorescence intensity of the wall area remarkably increased over time in the same manner as for the DDAO phosphate introduction. I inferred from this result that DDAO molecules could penetrate into the wall by diffusion and they accumulated inside the wall.

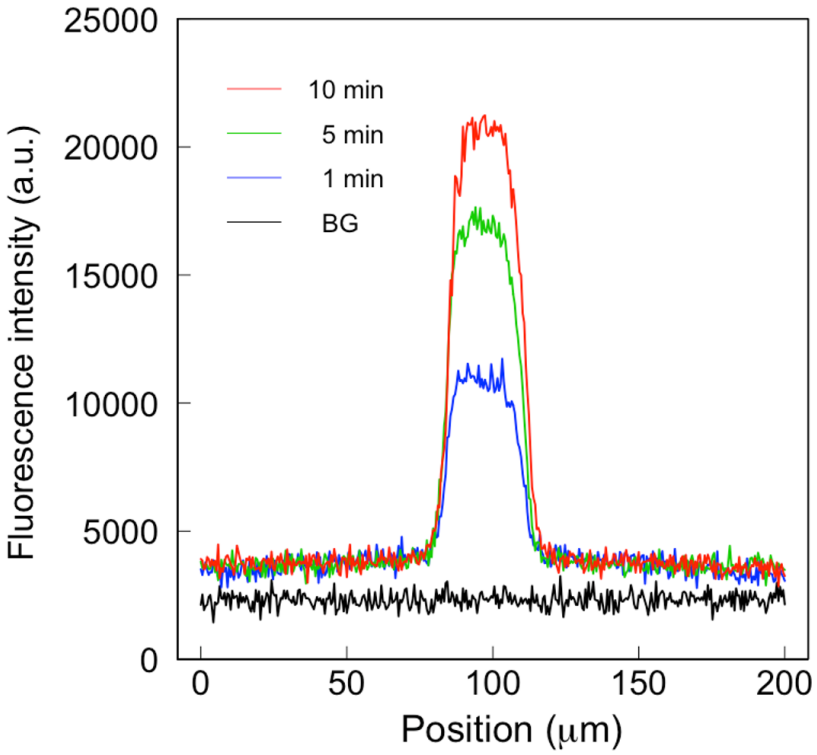


Figure 2.7 Fluorescence intensity profile as a function of the position with injection of 0.5 μM DDAO. Exposure time of the CCD camera was 5 s.

From all these results, I concluded that using DDAO phosphate as a substrate and defining the fluorescence intensity in the wall area as a signal led to the highest sensitivity. DDAO phosphate was used as the substrate in subsequent experiments.

2.3.3 Biomarker detection with the enzyme-labeled antibody, alkaline phosphatase-labeled antibody

Standard CRP solution in PBS was measured with the alkaline phosphatase-labeled antibody and DDAO phosphate substrate. The fluorescence intensity was defined as the average value of the fluorescence intensity of each pixel within the rectangle, red dotted lines in Figure 2.4 (a). The calibration curves of CRP are shown in Figure 2.8. The reaction temperature after DDAO phosphate injection was set at 25 °C or 45 °C. Figure 2.8

(a) shows the curves for the alkaline phosphate-labeled antibody (standard samples) and the fluorescence intensity increased as the concentration increased for both temperature conditions. The LODs of CRP in PBS were 58 pg mL^{-1} at 25 °C and 2.5 pg mL^{-1} at 45 °C. This value was much lower than the that of obtained for the conventional device with fluorescence-labeled antibody. This sensitivity was comparable or superior to that of related studies of microdevices based on immunoassay (Table 2.1) [38–43]. Figure 2.8 (b) compares calibration curves between fluorescence-labeled antibody (25 °C) and enzyme-labeled antibody (45 °C). The enzyme-labeled antibody showed a sharp increase in the signal in the low concentration region. Comparing the slope of the calibration curve of 1–10 ng mL^{-1} that is near the LOD when using the fluorescence-labeled antibody, I saw that the slope of the calibration curve was increased about 40 times.

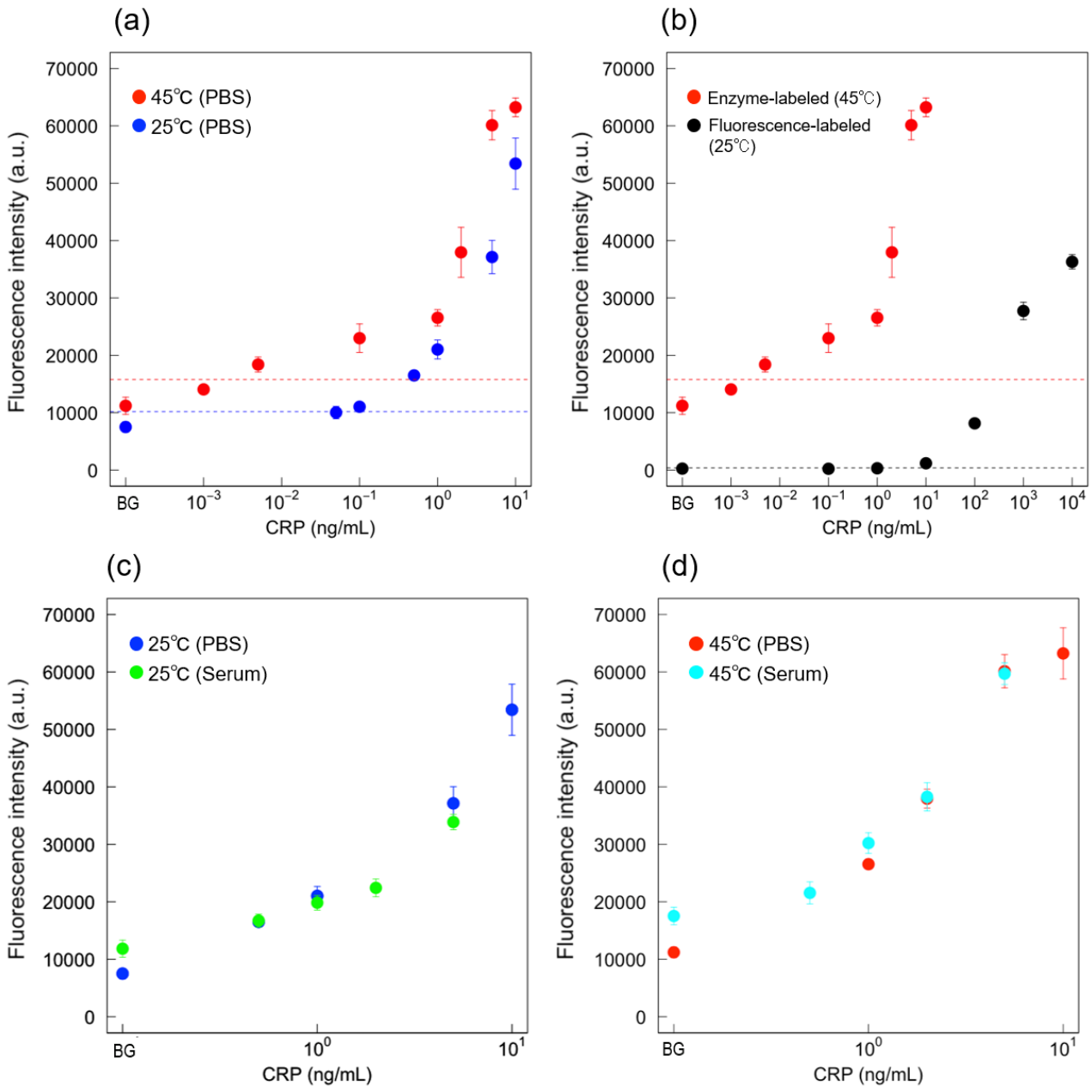


Figure 2.8 Calibration curves of CRP. (a) Reaction temperature was 25 °C or 45 °C with the enzyme-labeled antibody, alkaline phosphate-labeled antibody (standard samples). Exposure time of the CCD camera was 3 s. (b) Comparison between using enzyme-labeled antibody (45 °C) and fluorescence-labeled antibody (25 °C). (c) Reaction temperature was 25 °C with standard sample or serum sample. (d) Reaction temperature was 45 °C with standard sample or serum sample. The dashed lines in (a) and (b) represent the signal level at 3 SDs above the background. All incubation times of DDAO phosphate were 30 min. BG means the background signal of the immuno-wall. All data points are means ± standard deviations (n = 3).

Table 2.1 Analytical performance of correlative devices for C-reactive protein (CRP) detection

Method	LOD[a]	Assay time (min)	Sample volume (μL)	Ref.
Immunoassay on a power-free microchip	17 pg/mL	23	0.5	(38)
Surface plasmon resonance-based immunoassay	1.2 ng/mL	5	50	(39)
Label-free immunoassay based on electron transfer	40 pg/mL	50	10	(40)
Paper-based device	5.0 μg/mL	22	0.5	(41)
Nanoribon sensors using a miniature bead-based enzyme-linked immunosorbent assay	50 pg/mL	60	10	(42)
Graphene/polyethylene glycol hybrids for single-step immunoassay microdevice	400 ng/mL	2	-	(43)
Immuno-wall device (Fluorescence-label)	**1.7 ng/mL**	**16**	**0.25**	**This work**
Immuno-wall device (Enzyme-label)	**2.5 pg/ mL**	**46**	**0.25**	**This work**

[a] LOD, limit of detection

Subsequently, CRP was spiked into a CRP-free serum and I prepared calibration curves of CRP in CRP-free serum (Figure 2.8 (c) and (d)). The value of 0 ng mL^{-1} CRP in serum (blank) was higher than that of CRP in PBS at both temperatures. CRP concentration of the CRP-free serum was guaranteed only below 8 ng mL^{-1}. Therefore, there was a fair possibility that CRP-free serum contained CRP below the guaranteed concentration and it affected the signal of the blank. However, the calibration curves of CRP in serum were consistent with these of CRP in PBS except for the blank at both temperatures of 25 °C and 45 °C. Moreover, there was no constant tendency in the difference between CRP in serum and CRP in PBS. In conclusion, there was almost no influence by the blood matrix.

From these results, I judged the sensitivity of detecting CRP to be improved greatly by using alkaline phosphatase-labeled antibody and DDAO phosphate.

2.4 Conclusions

In chapter 2, I improved the sensitivity of the immuno-wall device by using enzymatic amplification. Alkaline phosphatase-labeled antibody was used as a labeling antibody and five representative alkaline phosphatase fluorogenic substrates were examined. When DDAO phosphate was used, a significant time-dependent change in fluorescence intensity was observed. The LOD of standard human CRP solution in PBS was 2.5 pg mL^{-1} with DDAO phosphate. The CRP detection range of this device was 0.0025–10 ng mL^{-1}. I succeeded in developing an ultra-sensitive and simple immunoassay system that can be applied to immunoassays of a wide range of targets and measurement applications.

In the future, I need to investigate the assay conditions of the enzymatic reaction in detail to further improve the device sensitivity. Furthermore, I need to consider miniaturizing the fluorescence detection system for point-of-care diagnosis.

2.5 References

[1] Kumar, S.; Mohan, A.; Guleria, R. Biomarkers in Cancer Screening, Research and Detection: Present and Future: A Review. *Biomarkers* **2006**, 11, 385–405.

[2] Ptolemy, A. S.; Rifai, N. What Is a Biomarker? Research Investments and Lack of Clinical Integration Necessitate a Review of Biomarker Terminology and Validation Schema. *Scand. J. Clin. Lab. Invest.* **2010**, 70, 6–14.

[3] Kaptoge, S.; Di Angelantonio, E.; Pennells, L.; Wood, A. M.; White, I. R.; Gao, P.; Walker, M.; Thompson, A.; Sarwar, N.; Caslake, M.; Butterworth, A. S.; Amouyel, P.; Assmann, G.; Bakker, S. J. L.; Barr, E. L. M. *et al.*, X. C-Reactive Protein, Fibrinogen, and Cardiovascular Disease Prediction. *N. Engl. J. Med.* **2012**, 367, 1310–1320.

[4] Kulinsky, L.; Noroozi, Z.; Madou, M. Present Technology and Future Trends in Point-of-Care Microfluidic Diagnostics. In *Methods in Molecular Biology*; **2013**; 3–23.

[5] Vashist, S. K.; Luppa, P. B.; Yeo, L. Y.; Ozcan, A.; Luong, J. H. T. Emerging Technologies for Next-Generation Point-of-Care Testing. *Trends Biotechnol.* **2015**, 33, 692–705.

[6] Sanjay, S. T.; Fu, G.; Dou, M.; Xu, F.; Liu, R.; Qi, H.; Li, X. Biomarker Detection for Disease Diagnosis Using Cost-Effective Microfluidic Platforms. *Analyst* **2015**, 140, 7062–7081.

[7] Sonker, M.; Sahore, V.; Woolley, A. T. Recent Advances in Microfluidic Sample Preparation and Separation Techniques for Molecular Biomarker Analysis: A Critical Review. *Anal. Chim. Acta* **2017**, 986, 1–11.

[8] Tian, T.; Bi, Y.; Xu, X.; Zhu, Z.; Yang, C. Integrated Paper-Based Microfluidic Devices for Point-of-Care Testing. *Anal. Methods* **2018**, 10, 3567–3581.

[9] Posthuma-Trumpie, G. A.; Korf, J.; van Amerongen, A. Lateral Flow (Immuno)Assay: Its Strengths, Weaknesses, Opportunities and Threats. A Literature Survey. *Anal. Bioanal. Chem.* **2009**, 393, 569–582.

[10] Li, J.; Macdonald, J. Multiplexed Lateral Flow Biosensors: Technological Advances for Radically Improving Point-of-Care Diagnoses. *Biosens. Bioelectron.* **2016**, 83, 177–192.

[11] Choi, Y.-E.; Kwak, J.-W.; Park, J. W. Nanotechnology for Early Cancer Detection. *Sensors* **2010**, 10, 428–455.

[12] Mousa, S. Biosensors: The New Wave in Cancer Diagnosis. *Nanotechnol. Sci.* **2010**, 2011:4, 1–10.

[13] Yasui, T.; Yanagida, T.; Ito, S.; Konakade, Y.; Takeshita, D.; Naganawa, T.; Nagashima, K.; Shimada, T.; Kaji, N.; Nakamura, Y.; Thiodorus, I. A.; He, Y.; Rahong, S.; Kanai, M.; Yukawa, H.; Ochiya, T.; Kawai, T.; Baba, Y. Unveiling Massive Numbers of Cancer-Related Urinary-MicroRNA Candidates via Nanowires. *Sci. Adv.* **2017**, 3, e1701133.

[14] Lewis, J. M.; Vyas, A. D.; Qiu, Y.; Messer, K. S.; White, R.; Heller, M. J. Integrated Analysis of Exosomal Protein Biomarkers on Alternating Current Electrokinetic Chips Enables Rapid Detection of Pancreatic Cancer in Patient Blood. *ACS Nano* **2018**, 12, 3311–3320.

[15] The Immunoassay Handbook: Theory and Applications of Ligand Binding, ELISA and Related Techniques , D. WildElsevier, Amsterdam, Netherlands, 2013

[16] Sato, K.; Tokeshi, M.; Odake, T.; Kimura, H.; Ooi, T.; Nakao, M.; Kitamori, T. Integration of an Immunosorbent Assay System: Analysis of Secretory Human Immunoglobulin A on Polystyrene Beads in a Microchip. *Anal. Chem.* **2000**, 72, 1144–1147.

[17] Sato, K.; Tokeshi, M.; Kimura, H.; Kitamori, T. Determination of Carcinoembryonic Antigen in Human Sera by Integrated Bead-Bed Immunoasay in a Microchip for Cancer Diagnosis. *Anal. Chem.* **2001**, 73, 1213–1218.

[18] Sato, K.; Yamanaka, M.; Hagino, T.; Tokeshi, M.; Kimura, H.; Kitamori, T. Microchip-Based Enzyme-Linked Immunosorbent Assay (MicroELISA) System with Thermal Lens Detection. *Lab Chip* **2004**, 4, 570.

[19] Han, K. N.; Li, C. A.; Seong, G. H. Microfluidic Chips for Immunoassays. *Annu. Rev. Anal. Chem.* **2013**, 6, 119–141.

[20] Akama, K.; Shirai, K.; Suzuki, S. Droplet-Free Digital Enzyme-Linked Immunosorbent Assay Based on a Tyramide Signal Amplification System. *Anal. Chem.* **2016**, 88, 7123–7129.

[21] Nishiyama, K.; Sugiura, K.; Kaji, N.; Tokeshi, M.; Baba, Y. Development of a Microdevice for Facile Analysis of Theophylline in Whole Blood by a Cloned Enzyme Donor Immunoassay. *Lab Chip* **2019**, 19, 233–240.

[22] Ishida, A.; Yamada, Y.; Kamidate, T. Colorimetric Method for Enzymatic Screening Assay of ATP Using Fe(III)-Xylenol Orange Complex Formation. *Anal. Bioanal. Chem.* **2008**, 392, 987–994.

[23] Busa, L. S. A.; Maeki, M.; Ishida, A.; Tani, H.; Tokeshi, M. Simple and Sensitive Colorimetric Assay System for Horseradish Peroxidase Using Microfluidic Paper-Based Devices. *Sensors Actuators B Chem.* **2016**, 236, 433–441.

[24] Baeyens, W. R. .; Schulman, S. .; Calokerinos, A. .; Zhao, Y.; García Campaña, A. M.; Nakashima, K.; De Keukeleire, D. Chemiluminescence-Based Detection: Principles and Analytical Applications in Flowing Streams and in Immunoassays. *J. Pharm. Biomed. Anal.* **1998**, 17, 941–953.

[25] García-Campaña, A. M.; Baeyens, W. R. G.; Zhang, X. R.; Smet, E.; Van Der Weken, G.; Nakashima, K.; Calokerinos, A. C. Detection in the Liquid Phase Applying Chemiluminescence. Biomed. *Chromatogr.* **2000**, 14, 166–172.

[26] Garcia-Cordero, J. L.; Maerkl, S. J. A 1024-Sample Serum Analyzer Chip for Cancer Diagnostics. *Lab Chip* **2014**, 14, 2642–2650.

[27] Kai, J.; Puntambekar, A.; Santiago, N.; Lee, S. H.; Sehy, D. W.; Moore, V.; Han, J.; Ahn, C. H. A Novel Microfluidic Microplate as the next Generation Assay Platform for Enzyme Linked Immunoassays (ELISA). *Lab Chip* **2012**, 12, 4257.

[28] Peltomaa, R.; Amaro-Torres, F.; Carrasco, S.; Orellana, G.; Benito-Peña, E.; Moreno-Bondi, M. C. Homogeneous Quenching Immunoassay for Fumonisin B 1 Based on Gold Nanoparticles and an Epitope-Mimicking Yellow Fluorescent Protein. *ACS Nano* **2018**, 12, 11333–11342.

[29] Fang, X.-X.; Li, H.-Y.; Fang, P.; Pan, J.-Z.; Fang, Q. A Handheld Laser-Induced Fluorescence Detector for Multiple Applications. *Talanta* **2016**, 150, 135–141.

[30] Wakao, O.; Satou, K.; Nakamura, A.; Sumiyoshi, K.; Shirokawa, M.; Mizokuchi, C.; Shiota, K.; Maeki, M.; Ishida, A.; Tani, H.; Shigemura, K.; Hibara, A.; Tokeshi, M. A Compact Fluorescence Polarization Analyzer with High-Transmittance Liquid Crystal Layer. *Rev. Sci. Instrum.* **2018**, 89, 024103.

[31] Ikami, M.; Kawakami, A.; Kakuta, M.; Okamoto, Y.; Kaji, N.; Tokeshi, M.; Baba, Y. Immuno-Pillar Chip: A New Platform for Rapid and Easy-to-Use Immunoassay. *Lab Chip* **2010**, 10, 3335.

[32] Jin, W.; Yamada, K.; Ikami, M.; Kaji, N.; Tokeshi, M.; Atsumi, Y.; Mizutani, M.; Murai, A.; Okamoto, A.; Namikawa, T.; Baba, Y.; Ohta, M. Application of IgY to Sandwich Enzyme-Linked Immunosorbent Assays, Lateral Flow Devices, and Immunopillar Chips for Detecting Staphylococcal Enterotoxins in Milk and Dairy Products. *J. Microbiol. Methods* **2013**, 92, 323–331.

[33] Kasama, T.; Ikami, M.; Jin, W.; Yamada, K.; Kaji, N.; Atsumi, Y.; Mizutani, M.; Murai, A.; Okamoto, A.; Namikawa, T.; Ohta, M.; Tokeshi, M.; Baba, Y. Rapid, Highly Sensitive, and Simultaneous Detection of Staphylococcal Enterotoxins in Milk by Using Immuno-Pillar Devices. *Anal. Methods* **2015**, 7, 5092–5095.

[34] Mohammadi, S.; Busa, L. S. A.; Maeki, M.; Mohammadi, R. M.; Ishida, A.; Tani, H.; Tokeshi, M. Rapid Detection of Cat Cystatin C (CCys-C) Using Immuno-Pillar Chips. *Anal. Sci.* **2016**, 32, 1359–1362.

[35] Kasama, T.; Kaji N.; Tokeshi, M.; Baba, Y., Microchip Diagnostics, Methods in Molecular Biology , V. Taly, J.-L. Viovy and S. Descroix, Springer, New York, 2017, 49-55.

[36] Yamamichi, A.; Kasama, T.; Ohka, F.; Suzuki, H.; Kato, A.; Motomura, K.; Hirano, M.; Ranjit, M.; Chalise, L.; Kurimoto, M.; Kondo, G.; Aoki, K.; Kaji, N.; Tokeshi, M.; Matsubara, T.; Senga, T.; Kaneko, M. K.;

Suzuki, H.; Hara, M.; Wakabayashi, T.; Baba, Y.; Kato, Y.; Natsume, A. An Immuno-Wall Microdevice Exhibits Rapid and Sensitive Detection of IDH1-R132H Mutation Specific to Grade II and III Gliomas. *Sci. Technol. Adv. Mater*. **2016**, 17, 618–625.

[37] Kasama, T.; Baba, Y.; Tokeshi, M. Microfluidic Immunoassay Devices Realize Next Generation Clinical Diagnostics, Next Generation Point-of-Care Biomedical Sensors Technologies for Cancer Diagnosis , P. Chandra, Y. N. Tan and S. P. Singh, Springer, 2017, 305–322.

[38] Hosokawa, K.; Omata, M.; Maeda, M. Immunoassay on a Power-Free Microchip with Laminar Flow-Assisted Dendritic Amplification. *Anal. Chem.* **2007**, 79, 6000–6004.

[39] Vashist, S. K.; Schneider, E. M.; Luong, J. H. T. Surface Plasmon Resonance-Based Immunoassay for Human C-Reactive Protein. *Analyst* **2015**, 140, 4445–4452.

[40] Liu, T.-Z.; Hu, R.; Zhang, X.; Zhang, K.-L.; Liu, Y.; Zhang, X.-B.; Bai, R.-Y.; Li, D.; Yang, Y.-H. Metal–Organic Framework Nanomaterials as Novel Signal Probes for Electron Transfer Mediated Ultrasensitive Electrochemical Immunoassay. *Anal. Chem.* **2016**, 88, 12516–12523.

[41] Mohammadi, S.; Busa, L. S. A.; Maeki, M.; Mohamadi, R. M.; Ishida, A.; Tani, H.; Tokeshi, M. Novel Concept of Washing for Microfluidic Paper-Based Analytical Devices Based on Capillary Force of Paper Substrates. *Anal. Bioanal. Chem.* **2016**, 408 , 7559–7563.

[42] Hu, C.; Zeimpekis, I.; Sun, K.; Anderson, S.; Ashburn, P.; Morgan, H. Low-Cost Nanoribbon Sensors for Protein Analysis in Human Serum Using a Miniature Bead-Based Enzyme-Linked Immunosorbent Assay. *Anal. Chem.* **2016**, 88 (9), 4872–4878

[43] Shirai, A.; Sueyoshi, K.; Endo, T.; Hisamoto, H. Graphene/Polyethylene Glycol Hybrids for Single-Step Immunoassay Microdevice. *FlatChem* **2019**, 13, 34–39.

[44] Koenig, W. High-Sensitivity C-Reactive Protein and Atherosclerotic Disease: From Improved Risk Prediction to Risk-Guided Therapy. *Int. J. Cardiol.* **2013**, 168, 5126–5134.

CHAPTER 3 Simple Approach for Fluorescence Signal Amplification Utilizing a Poly(vinyl alcohol)-based Polymer Structure in a Microchannel

3.1 Introduction

A lot of efforts have been put into detecting trace amounts of analytes in complex samples like biological materials in recent years, and the detection of trace amounts of biomarkers in body fluids has attracted attention for early diagnosis of serious diseases [1,2]. For example, there are demands for sensitive detection (~ng/mL level) of cancer biomarkers such as prostate specific antigen and carcinoembryonic antigen [3,4]. To meet these demands, various detection methods for biomarkers using microfluidic devices have been reported [5-8]. Microfluidic devices are useful tools for miniaturized detection systems. However, it remains challenging to achieve both high sensitivity and construction of an easy-to-use and rapid detection system.

For point-of-care testing with protein biomarkers, Tokeshi *et al.* [9-12] have previously developed a microfluidic device (immuno-wall device) for highly sensitive immunoassay. Capture antibodies were immobilized on the wall-like structure made from azide-unit pendant water-soluble photopolymer (AWP-wall) in a microfluidic channel. A sandwich immunoassay was performed by pipette operations, and all reactions for the immunoassay were completed in an incubation time of several tens of minutes. At the same time, I found a phenomenon in which the fluorescence signal increased locally inside the AWP-wall. This property was combined with an enzymatic reaction, which resulted in significant improvement in detection sensitivity of the immuno-wall device [10]. Since the fluorescence signal was amplified only by injecting the solution into the microchannel having the AWP structure, the process of signal amplification was simple. However, the characteristics and mechanism of AWP-wall as a fluorescence signal amplifier have not been discussed. Clarifying these issues is important for constructing a better method of signal amplification.

In chapter 3, I report that the AWP-wall in the microchannel plays a role as an amplifier of the fluorescence signal. The proposed method was based on the spontaneous concentration by accumulation of fluorescent molecules in the AWP-wall. Typical concentration methods of molecules with microdevices include using liquid-liquid extraction [13,14], nanoporous membranes [15,16], and electrophoresis [17,18]. Although the concentration efficiency of these methods is high, expensive external equipment and complicated operations are required for concentration. In the proposed method, fluorescence signal amplification was accomplished

without external equipment or additional operations (Figure 3.1). I describe the work to characterize the AWP-wall as a fluorescence signal amplifier in the microchannel and I elucidate the mechanism of fluorescence signal amplification.

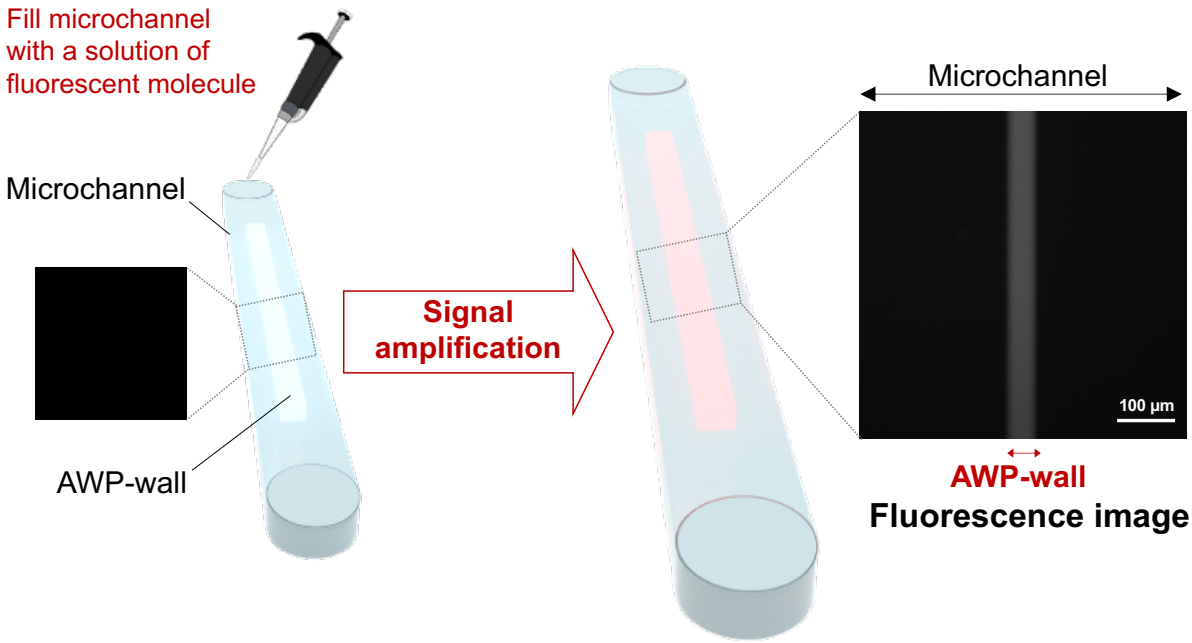


Figure 3.1 Schematic illustration of fluorescence signal amplification by the AWP-wall. The right inset photo is the fluorescence image of the AWP-wall in a microchannel after the injection of 1 μM DDAO.

3.2 Experimental

3.2.1 Materials

Hydrochloric acid was purchased from FUJIFILM Wako Pure Chemical Corporation (Japan). Trizma® base was purchased from Sigma-Aldrich Co. LLC (USA). Phosphate-buffered saline (PBS; pH 7.4) solution and Alexa Fluor™ 647 carboxylic acid were purchased from Thermo Fisher Scientific, Inc. (USA). ATTO 647N free COOH was purchased from Atto-Tec GmbH (Germany). Cy3 carboxylic acid and Cy5 carboxylic acid were purchased from Lumiprobe Corporation (USA). 9H-(1,3-Dichloro-9,9-dimethylacridin-2-one-7-yl) (DDAO) was purchased from Santa Cruz Biotechnology, Inc. (USA). Azide-unit pendant water-soluble photopolymer (AWP, 6%) was purchased from Toyo Gosei Co., Ltd. (Japan).

3.2.2 AWP-wall in a microchannel

The AWP-wall in a microchannel was fabricated in accordance with the literature with slight modifications [10]. In short, I used the microchip having 40 straight microchannels which was made from cyclic olefin copolymer (Sumitomo Bakelite Co., Ltd.; Japan). A microchannel was filled with a mixture of AWP and PBS (volume ratio 1:1). Then, the UV light from a mercury lamp (Hayashi Watch Works LA-410 UV) was irradiated onto the mixture in the microchannel through the photomask for 8 s. Subsequently, the uncured AWP was removed by a vacuum pump (SP 20; Air Liquide Medical Systems; France) and washed with PBS to reveal the resulting structure (AWP-wall). Fig. S1 shows a photograph and schematic illustration of the microchip and the AWP-wall.

3.2.3 Evaluation of AWP-wall in a microchannel as a fluorescence signal amplifier

The fluorescent molecule species (DDAO, Alexa Fluor™ 647, ATTO647N, Cy5 or Cy3) in 1 M Tris-HCl buffer (pH 8.0) was injected into the microchannel having the AWP-wall. After a certain incubation time, the fluorescence image of the microchannel was captured without removing the solution with an inverted fluorescence microscope (Keyence BZ-9000). Two filter cubes of the fluorescence microscope were used: TRITC filter (Keyence OP-66837; excitation 540/25 nm, emission 605/55 nm) for Cy3; and Cy5 filter (Keyence OP-87766; excitation 620/60 nm, emission 700/75 nm) for DDAO, Alexa Fluor™ 647, ATTO 647N and Cy5. The exposure time of the microscope was adjusted appropriately according to each experiment. The fluorescence image was analyzed with ImageJ software to calculate the fluorescence intensity. The fluorescence intensity was calculated as the average value of the fluorescence signals from all pixels in the selected area.

3.2.4 Evaluation of transfer of fluorescent molecules to AWP in a microplate

AWP (50 μL) was injected into a well in a 96-well microplate (Thermo Fisher Scientific Nunc™ F96 MicroWell™ Black Polystyrene Plate). Then, the UV light from a mercury lamp (Hayashi Watch Works LA-410 UV) was irradiated onto the microplate for 16 s. Subsequently, the 1 μM concentration of fluorescent molecule species (DDAO, Alexa Fluor™ 647, ATTO 647N, Cy5 or Cy3) in 1M Tris-HCl buffer (pH 8.0, 200 μL) was injected into the microplate containing the AWP. After the 2 h incubation, 100 μL supernatant liquid in the well was moved to an empty well (~10 μL solution of fluorescent molecules was absorbed into the AWP). The fluorescence intensity of this supernatant liquid was measured with a microplate reader (Tecan Infinite 200 PRO). The excitation filter at 620/20 nm and emission filter at 670/25 nm were used for DDAO, Alexa Fluor™ 647, ATTO647N, and Cy5. The excitation filter at 540/25 nm and emission filter at 590/20 nm were used for Cy3.

3.2.5 Fluorescence spectrum of DDAO

AWP was added to DDAO in 1 M Tris-HCl buffer (pH 8.0). The final concentration of DDAO in the mixture was 5 μM and that of AWP was adjusted to 5, 10 or 50% (v/v). After the mixing of the DDAO solution and AWP by the vortex mixer (Scientific Industries Vortex-Genie 2), the mixture (3 mL) was added into a disposable poly methyl methacrylate cell (Kartell, Italy). Then, the UV light from the mercury lamp was irradiated onto the mixture for 16 s. The fluorescence emission spectrum of the cured mixture was measured by a fluorescence spectrophotometer (Hitachi F-7000). The excitation wavelength was 620 nm.

3.2.6 Prediction of octanol-water partition coefficient

Octanol-water partition coefficient (log *P*) of the fluorescent molecules was calculated by Swiss ADME predictor software (http://www.swissadme.ch/). This software predicts log *P* by combining the generalized Born and solvent accessible surface area models into a method known as the iLogP method [19].

3.3 Results and discussion

The AWP-wall (40 μm × 4 mm × 40 μm) was fabricated in a microchannel as a simple model of the fluorescence signal amplification by an AWP structure. In chapter 2, I found high fluorescence intensity locally inside the AWP-wall when alkaline phosphatase was reacted with DDAO phosphate (fluorogenic substrate) outside the AWP-wall. Therefore, I first investigated the fluorescence signal amplification by the AWP-wall using DDAO, which is a fluorescent species formed as a product of the enzymatic reaction from DDAO phosphate. 1 μM DDAO solution was injected into the microchannel having the AWP-wall, and fluorescence intensity around the AWP-wall was measured (Figure 3.2). Figure 3.2 (a) and (b) show that the fluorescence intensity inside the AWP-wall was high locally at 1 min after the solution injection. Additionally, the fluorescence intensity inside the AWP-wall increased over time and reached a plateau at 10 min after the DDAO injection. I clarified that the AWP-wall worked as a fluorescence signal amplifier even if DDAO was introduced into the microchannel having the AWP-wall.

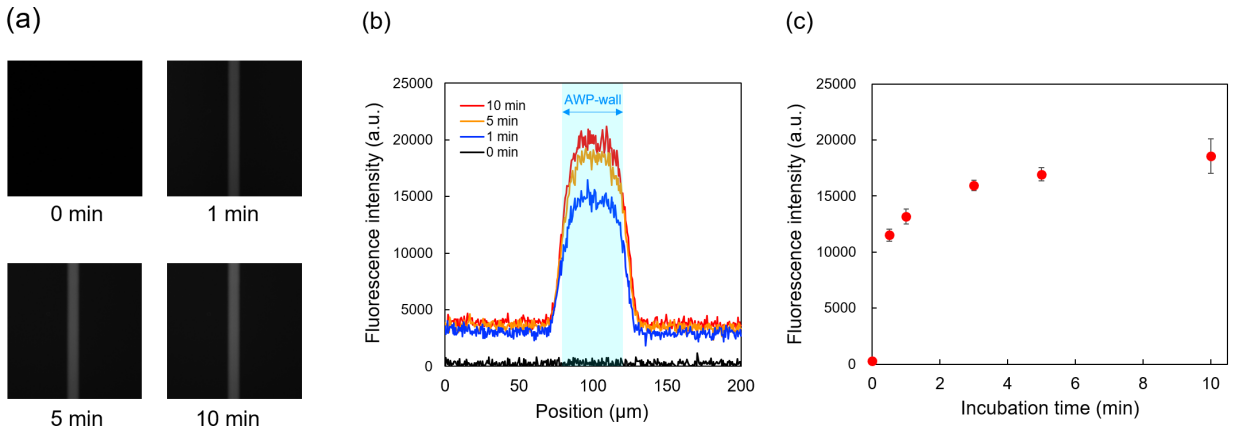


Figure 3.2 Fluorescence signal amplification of DDAO by the AWP-wall. 1 μM DDAO was injected into a microchannel and incubated for 10 min. The time in this figure refers to incubation time. (a) Fluorescence image of the AWP-wall in the microchannel. (b) Fluorescence intensity profile as a function of the position around the AWP-wall. (c) Fluorescence intensity inside the AWP-wall.

Next, I investigated the dependence of DDAO concentration on the fluorescence intensity inside the AWP-wall. Calibration curves of the DDAO were prepared using the fluorescence intensity inside and outside the AWP-wall to compare both sensitivities (Figure 3.3). The average value of the fluorescence intensity of each pixel inside the AWP-wall was defined as I_{wall}, and that outside the AWP-wall was defined as $I_{channel}$ (Figure 3.3 (a)). Figure 3.3 (b) shows calibration curves with I_{wall} and $I_{channel}$. I_{wall} and $I_{channel}$ increased linearly as the DDAO concentration increased. The slope of the calibration curve using I_{wall} was about five times higher than that of $I_{channel}$ (Figure 3.3 (b)). The limit of detection (LOD) of DDAO was 2.7 nM when using I_{wall}. From the above results, I found that I_{wall} was dependent on the DDAO concentration and it could be used for highly sensitive detection of DDAO.

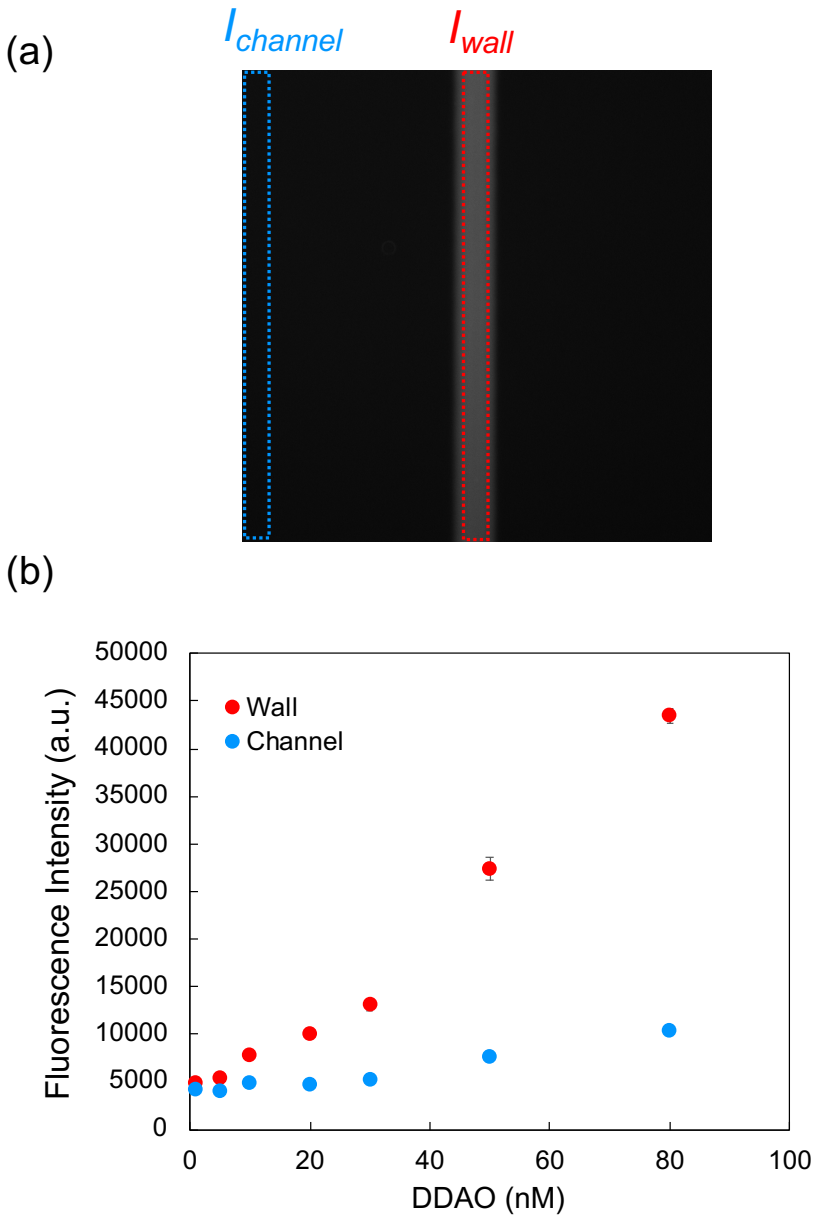


Figure 3.3 (a) Photograph of a fluorescence image of the AWP-wall in a microchannel after injection of 1 μM DDAO. The red dotted rectangle represents the detection area of the AWP-wall. The blue one represents the detection area of the microchannel. (b) Calibration curves of DDAO with different detection areas. Incubation time: 10 min.

The increase in fluorescence intensity of DDAO inside the AWP-wall was presumably due to one or both of the following two factors. The first factor is the increment of the fluorescence quantum yield of DDAO in the AWP environment. The second one is the accumulation of DDAO inside the AWP-wall. At first, to

discuss the possibility of increasing the fluorescence quantum yield of DDAO in the AWP, I obtained the fluorescence spectrum of a mixture of AWP and DDAO solution (Figure 3.4). After thoroughly mixing AWP and DDAO, the mixture was irradiated with UV light to polymerize it, and then the fluorescence spectrum was measured. When the AWP percentage in the mixture was 10% or less, there were almost no changes in the fluorescence peak wavelength and fluorescence intensity. When the AWP percentage was 50% (the same as in the AWP-wall), fluorescence intensity was increased and fluorescence peak wavelength was shifted slightly (from 658 nm to 662 nm). Although there are few reports available on the fluorescence quantum yield of DDAO, Gong *et al.* [20] reported that the fluorescence intensity of DDAO was enhanced by Triton X-100 (nonionic surfactant). I inferred from these data that the hydrophobic domain of the AWP might lead to an increase in the fluorescence quantum yield of DDAO. However, since the increase in fluorescence intensity was small, the change in fluorescence quantum yield of DDAO in AWP was judged to make a trivial contribution to the fluorescence signal amplification by the AWP-wall.

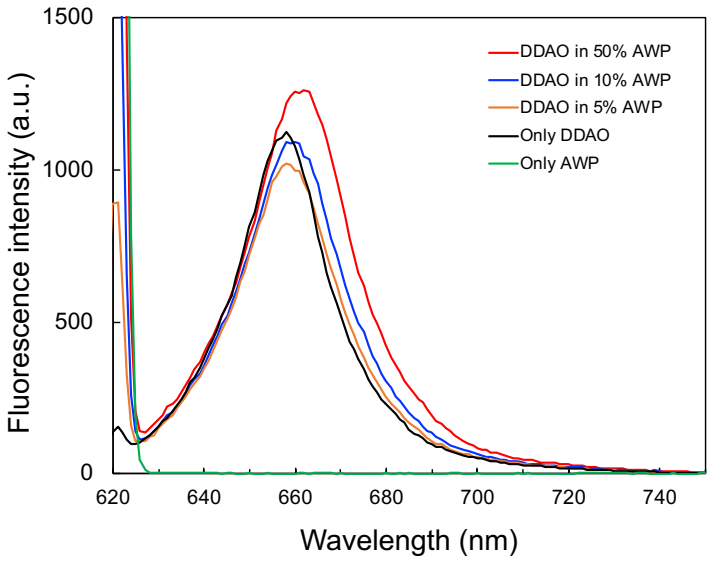


Figure 3.4 Fluorescence emission spectra of 5 μM DDAO in the mixture of Tris-HCl buffer (pH 8.0) and AWP.

To discuss the accumulation of fluorescent molecules in the AWP-wall, I compared the efficiency of fluorescence signal amplification by the AWP-wall with four fluorescent molecule species in addition to DDAO (Figure 3.5). AWP has a peak absorption wavelength at ~310 nm, and the autofluorescence of AWP could be significantly reduced by using long-wavelength excitation light. Therefore, I selected fluorescent molecules (DDAO, Alexa Fluor™ 647, ATTO 647N, Cy5) that emit far-red fluorescence, and Cy3, which has a structure similar to Cy5 and emits greenish yellow fluorescence. The chemical structures of these species are shown in Figure 3.6. Tris-HCl buffer containing each of the fluorescent species individually was introduced into a microchannel having the AWP-wall, and the I_{wall} and $I_{channel}$ were obtained over time. The efficiency of fluorescence signal amplification of the AWP-wall was defined as I_{wall} / $I_{channel}$. I_{wall} / $I_{channel}$ increased over time for all fluorescent molecule species studied, and the fluorescence signal was amplified in the AWP-wall (I_{wall} / $I_{channel}$ > 1) (Figures 3.5 (a), (b)). Because I_{wall} of each species was increased gradually over time, I assumed that these fluorescent molecules were accumulated inside the AWP-wall by diffusion. Additionally, I clarified that the amplification of the fluorescence signal by the AWP-wall was not a phenomenon specific to DDAO, although DDAO showed the highest I_{wall} / $I_{channel}$ at 10 min after injection (Fig. 5 (c)).

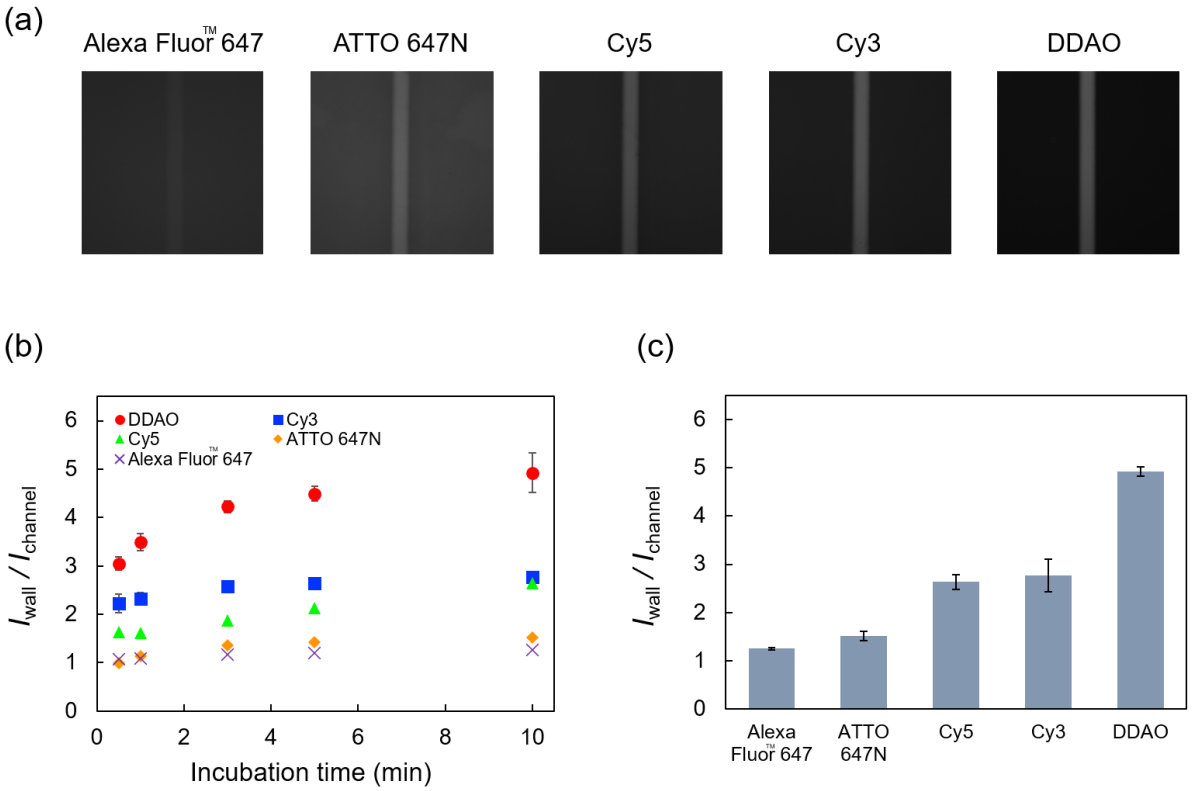


Figure 3.5 Evaluation of the AWP-wall as a fluorescence signal amplifier with five different fluorescent molecules. The concentration of each fluorescent species was 1 μM. (a) Fluorescence images of the AWP-wall after injecting the solution of fluorescent molecules. Incubation time: 10 min. (b) I_{wall} / $I_{channel}$ as a function of time. (c) Comparison of I_{wall} / $I_{channel}$ among fluorescent molecules. Incubation time: 10 min.

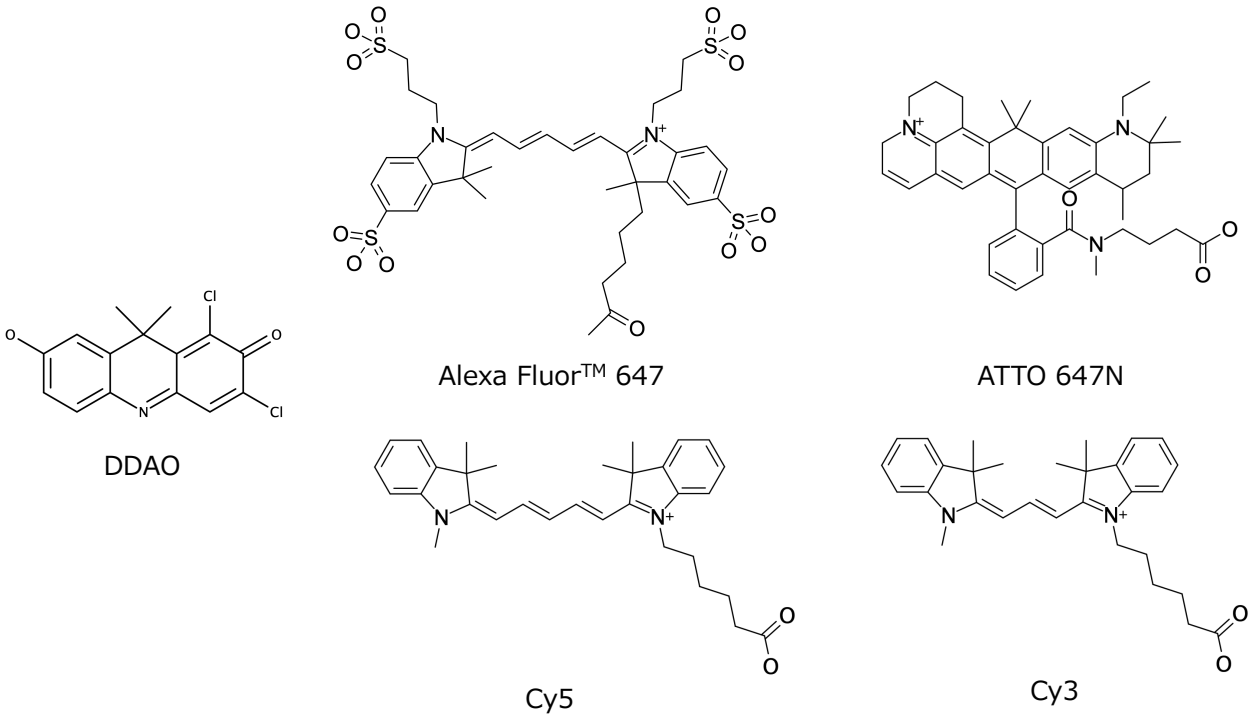


Figure 3.6 Chemical structures of five fluorescent molecules.

Then, I focused on the properties of fluorescent molecules and AWP to discuss their interactions. AWP is a polymer based on poly(vinyl alcohol) (PVA) (Figure 3.7) [21]. Baptista *et al.* [22] presented a molecular dynamics simulation showing that highly hydrophobic molecules interact with PVA through hydrophobic interactions and hydrogen bonds. There is also a possibility that molecular size influences the ability of a molecule to penetrate the AWP-wall. To consider these contribution, I looked at the effects of log *P* and molecular weight of each fluorescent molecule on I_{wall} / $I_{channel}$ and this is shown in Figure 3.8. The DDAO had the highest log *P* and the lowest molecular weight among the fluorescent molecules I considered. Besides, there seemed to be a positive correlation between log *P* (Figure 3.8 (a)) and I_{wall} / $I_{channel}$, and a negative correlation between molecular weight and I_{wall} / $I_{channel}$ (Figure 3.8 (b)). I can deduce that hydrophobicity and low molecular weight enhance the accumulation of fluorescent molecules in the AWP-wall, which leads to the high efficiency of signal amplification. Moreover, Chang *et al.* [23] suggested that the nitrogen atom of the

pyridine moiety showed a strong intermolecular interaction with PVA because of their electrostatic interactions and hydrogen bonding. The nitrogen atom in DDAO may lead to a strong intermolecular interaction with AWP.

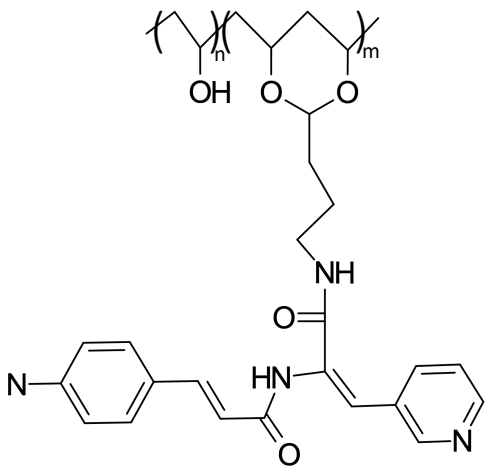


Figure 3.7 Chemical structure of AWP (n:m ≒ 100:1) [21].

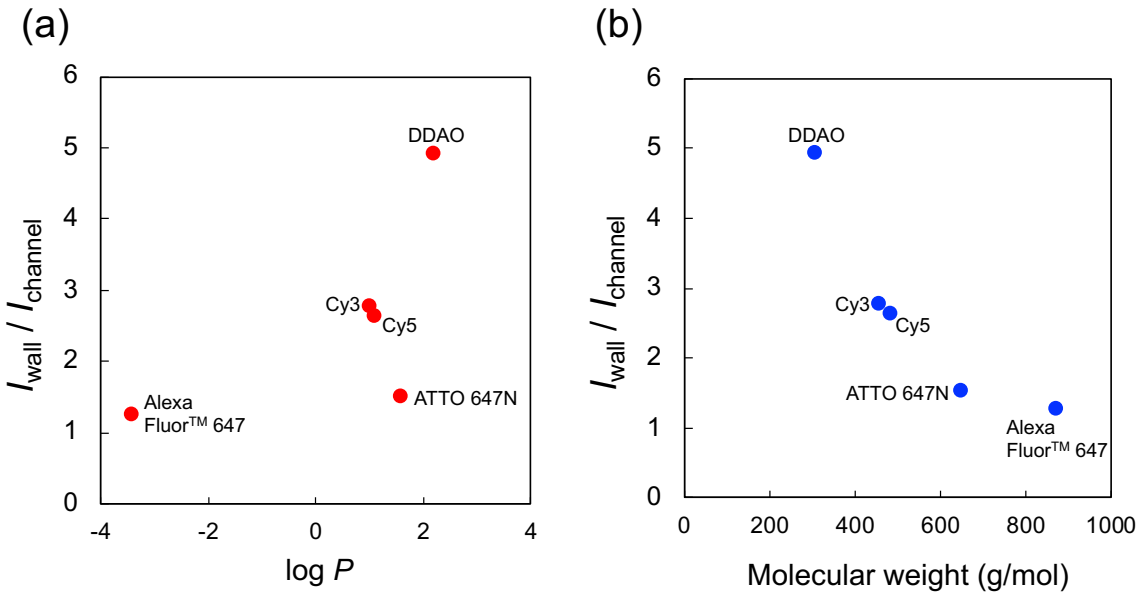


Figure 3.8 Correlations of I_{wall} / $I_{channel}$ with (a) log P and (b) molecular weight of fluorescent molecules.

Lastly, accumulation behavior of fluorescent molecules in AWP was investigated using another platform (Figure 3.9). A sample solution of fluorescent molecules was introduced into a well of a microplate having polymerized AWP on the bottom and the solution was incubated for 2 h. Then, a portion of the supernatant was transferred to an empty well and its fluorescence intensity was measured (Figure 3.9 (a)). By measuring the fluorescence intensity of the supernatant, I was able to ignore the effect of the AWP environment on the fluorescence quantum yield of fluorescent molecules. As indicated in Figure 3.9 (b), the fluorescence intensity of the supernatant after incubation was decreased compared to the control containing all the fluorescent molecules. The amount of change in the fluorescence intensity of DDAO was the highest. These results support the hypothesis that the accumulation of fluorescent molecules in AWP contributes to fluorescence signal amplification by the AWP-wall. I found that the fluorescent molecules were accumulated in AWP even when it was as an AWP-wall in a microplate well. Thus, the proposed method has a good potential for extending its applications to various fields.

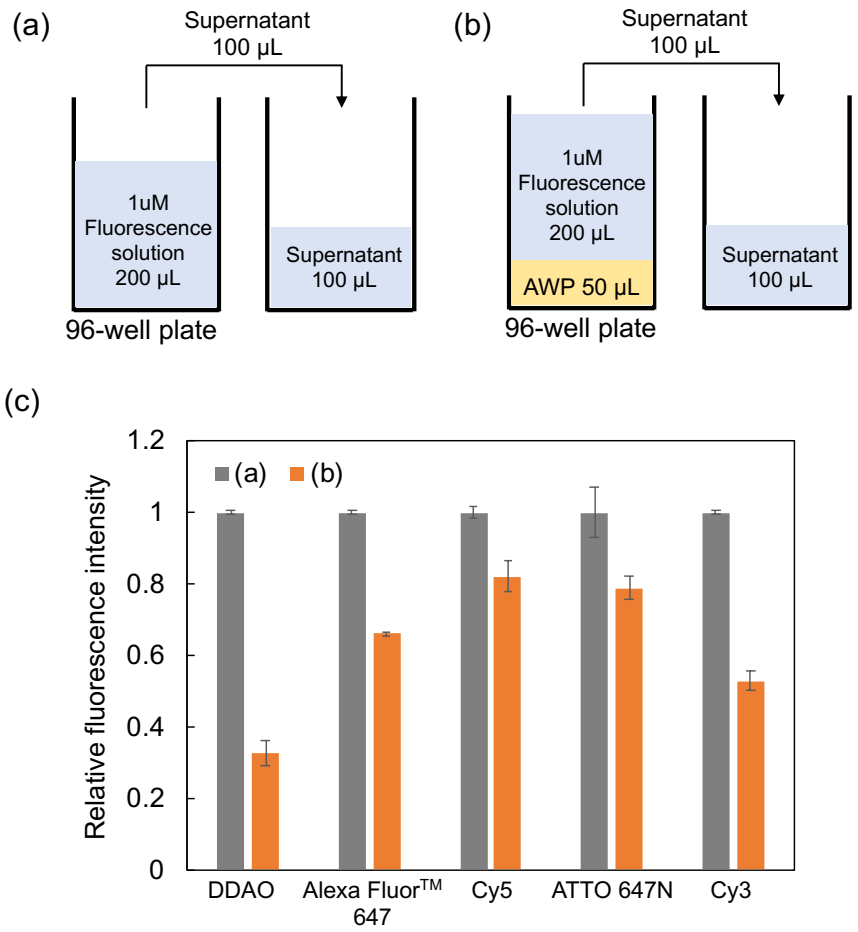


Figure 3.9 Evaluation of transfer of fluorescent molecules to AWP in a microplate. (a),(b) Schematic illustrations of experimental procedure for extraction of fluorescent molecules by the AWP layer: (a) control well and (b) sample well. (c) Relative fluorescence intensity of 100 µL supernatant of fluorescence solution after extraction of AWP for 2 h.

3.4. Conclusions

I determined that the AWP-wall in the microchannel functioned as a fluorescent signal amplifier. Among the five fluorescent molecule species I considered, DDAO showed the highest efficiency of fluorescence signal amplification. The calibration curve of DDAO using the fluorescence intensity inside the AWP-wall had about five times the sensitivity compared to that outside the AWP-wall. The accumulation of fluorescent molecules inside the AWP-wall contributed to the fluorescence signal amplification. Also, the high specific surface area of the AWP-wall enabled rapid accumulation of fluorescent molecules in the AWP-wall.

This method does not require expensive external equipment and complicated operations to concentrate the molecules. Fluorescence signal amplification is accomplished simply by injecting a solution into a microchannel having the AWP-wall. Therefore, I expect this method to be utilized for detecting low abundance analytes. For example, DDAO phosphate and DDAO galactoside are widely used as fluorogenic substrates for enzymatic reactions. Therefore, by combining these substrates with fluorescence signal amplification by the AWP-wall, a highly sensitive detection method can be devised. Moreover, since this method is not limited to use in a microchannel, it has widespread applicability.

3.5 References

[1] Wu, L.; Qu, X. Cancer Biomarker Detection: Recent Achievements and Challenges. *Chem. Soc. Rev.* **2015**, 44, 2963–2997.

[2] Sanjay, S. T.; Fu, G.; Dou, M.; Xu, F.; Liu, R.; Qi, H.; Li, X. Biomarker Detection for Disease Diagnosis Using Cost-Effective Microfluidic Platforms. *Analyst* **2015**, 140, 7062–7081.

[3] Roddam, A. W.; Duffy, M. J.; Hamdy, F. C.; Ward, A. M.; Patnick, J.; Price, C. P.; Rimmer, J.; Sturgeon, C.; White, P.; Allen, N. E. Use of Prostate-Specific Antigen (PSA) Isoforms for the Detection of Prostate Cancer in Men with a PSA Level of 2–10 Ng/Ml: Systematic Review and Meta-Analysis. *Eur. Urol.* **2005**, 48, 386–399.

[4] Grunnet, M.; Sorensen, J. B. Carcinoembryonic Antigen (CEA) as Tumor Marker in Lung Cancer. *Lung Cancer* **2012**, 76, 138–143.

[5] Ikami, M.; Kawakami, A.; Kakuta, M.; Okamoto, Y.; Kaji, N.; Tokeshi, M.; Baba, Y. Immuno-Pillar Chip: A New Platform for Rapid and Easy-to-Use Immunoassay. *Lab Chip* **2010**, 10, 3335–3340.

[6] Han, K. N.; Li, C. A.; Seong, G. H. Microfluidic Chips for Immunoassays. *Annu. Rev. Anal. Chem.* **2013**, 6, 119–141.

[7] Ali, M. A.; Mondal, K.; Jiao, Y.; Oren, S.; Xu, Z.; Sharma, A.; Dong, L. Microfluidic Immuno-Biochip for Detection of Breast Cancer Biomarkers Using Hierarchical Composite of Porous Graphene and Titanium Dioxide Nanofibers. *ACS Appl. Mater. Interfaces* **2016**, 8, 20570–20582.

[8] Barbosa, A. I.; Reis, N. M. A Critical Insight into the Development Pipeline of Microfluidic Immunoassay Devices for the Sensitive Quantitation of Protein Biomarkers at the Point of Care. *Analyst* **2017,** 142, 858–882.

[9] Yamamichi, A.; Kasama, T.; Ohka, F.; Suzuki, H.; Kato, A.; Motomura, K.; Hirano, M.; Ranjit, M.; Chalise, L.; Kurimoto, M.; Kondo, G.; Aoki, K.; Kaji, N.; Tokeshi, M.; Matsubara, T.; Senga, T.; Kaneko, M. K.;

Suzuki, H.; Hara, M.; Wakabayashi, T.; Baba, Y.; Kato, Y.; Natsume, A. An Immuno-Wall Microdevice Exhibits Rapid and Sensitive Detection of IDH1-R132H Mutation Specific to Grade II and III Gliomas. *Sci. Technol. Adv. Mater.* **2016**, 17, 618–625.

[10] Nishiyama, K.; Kasama, T.; Nakamata, S.; Ishikawa, K.; Onoshima, D.; Yukawa, H.; Maeki, M.; Ishida, A.; Tani, H.; Baba, Y.; Tokeshi, M. Ultrasensitive Detection of Disease Biomarkers Using an Immuno-Wall Device with Enzymatic Amplification. *Analyst* **2019**, 144, 4589–4595.

[11] Chávez Ramos, K.; Nishiyama, K.; Maeki, M.; Ishida, A.; Tani, H.; Kasama, T.; Baba, Y.; Tokeshi, M. Rapid, Sensitive, and Selective Detection of H5 Hemagglutinin from Avian Influenza Virus Using an Immunowall Device. *ACS Omega* **2019**, 4, 16683–16688.

[12] Yogo, N.; Hase, T.; Kasama, T.; Nishiyama, K.; Ozawa, N.; Hatta, T.; Shibata, H.; Sato, M.; Komeda, K.; Kawabe, N.; Matsuoka,K.; Chen-Yoshikawa, T. F.; Kaji, N.; Tokeshi, M.; Baba, Y.; Hasegawa, Y. Development of an immuno-wall device for the rapid and sensitive detection of *EGFR* mutations in tumor tissues resected from lung cancer patients. *PloS one* **2020**, 15, e0241422.

[13] Shen, H.; Fang, Q.; Fang, Z.-L. A Microfluidic Chip Based Sequential Injection System with Trapped Droplet Liquid–Liquid Extraction and Chemiluminescence Detection. *Lab Chip* **2006**, 6, 1387–1389.

[14] Berduque, A.; Zazpe, R.; Arrigan, D. W. M. Electrochemical Detection of Dopamine Using Arrays of Liquid–Liquid Micro-Interfaces Created within Micromachined Silicon Membranes. *Anal. Chim. Acta* **2008**, 611, 156–162.

[15] Long, Z.; Liu, D.; Ye, N.; Qin, J.; Lin, B. Integration of Nanoporous Membranes for Sample Filtration/Preconcentration in Microchip Electrophoresis. *Electrophoresis* **2006**, 27, 4927–4934.

[16] Li, F.; Guijt, R. M.; Breadmore, M. C. Nanoporous Membranes for Microfluidic Concentration Prior to Electrophoretic Separation of Proteins in Urine. *Anal. Chem.* **2016**, 88, 8257–8263.

[17] Wainright, A.; Williams, S. J.; Ciambrone, G.; Xue, Q.; Wei, J.; Harris, D. Sample Pre-Concentration by Isotachophoresis in Microfluidic Devices. *J. Chromatogr. A* **2002**, 979, 69–80.

[18] Bottenus, D.; Jubery, T. Z.; Ouyang, Y.; Dong, W.-J.; Dutta, P.; Ivory, C. F. 10 000-Fold Concentration Increase of the Biomarker Cardiac Troponin I in a Reducing Union Microfluidic Chip Using Cationic Isotachophoresis. *Lab Chip* **2011**, 11, 890.

[19] Daina, A.; Michielin, O.; Zoete, V. SwissADME: A Free Web Tool to Evaluate Pharmacokinetics, Drug-Likeness and Medicinal Chemistry Friendliness of Small Molecules. *Sci. Rep.* **2017**, 7, 42717.

[20] Gong, H.; Zhang, B.; Little, G.; Kovar, J.; Chen, H.; Xie, W.; Schutz-Geschwender, A.; Olive, D. M. β-Galactosidase Activity Assay Using Far-Red-Shifted Fluorescent Substrate DDAOG. *Anal. Biochem.* **2009**, 386, 59–64.

[21] Ishizuka, N.; Hashimoto, Y.; Matsuo, Y.; Ijiro, K. Highly Expansive DNA Hydrogel Films Prepared with Photocrosslinkable Poly(Vinyl Alcohol). *Colloids Surfaces A Physicochem. Eng. Asp.* **2006**, 284–285, 440–443.

[22] Baptista, J. G. C.; Rodrigues, S. P. J.; Matsushita, A. F. Y.; Vitorino, C.; Maria, T. M. R.; Burrows, H. D.; Pais, A. A. C. C.; Valente, A. J. M. Does Poly(Vinyl Alcohol) Act as an Amphiphilic Polymer? An Interaction Study with Simvastatin. *J. Mol. Liq.* **2016**, 222, 287–294.

[23] Chang, J. B.; Hwang, J. H.; Park, J. S.; Kim, J. P. The Effect of Dye Structure on the Dyeing and Optical Properties of Dichroic Dyes for PVA Polarizing Film. *Dye. Pigment.* **2011**, 88, 366–371.

CHAPTER 4 Non-competitive Fluorescence Polarization Immunoassay Based on a Fab Fragment for Protein Quantification

4.1 Introduction

Homogeneous immunoassays, such as fluorescence polarization immunoassay (FPIA), cloned enzyme donor immunoassay (CEDIA) and enzyme multiplied immunoassay technique (EMIT) are immunoassays that do not require any bound-free separation or washing operation. In comparison with heterogeneous immunoassays like enzyme-linked immunosorbent assay (ELISA), the assay procedures for homogeneous immunoassays are much simpler and do not require a long analysis time. Among these homogeneous immunoassays, FPIA is one of the most popular homogeneous immunoassays and it is used in many fields, such as therapeutic drug monitoring, food analysis and environmental analysis [1-5]. However, because FPIA is mainly used for measuring small molecules, its applications are limited, and new apparatuses for FPIA are rarely developed. In order to promote the advantages of FPIA, I thought that developing a portable FPIA analyzer which enabled practical applications of FPIA would be desirable. In fact, Nishiyama, Tokeshi *et al.* [6-10] developed a portable FPIA analyzer and have shown various applications such as the detection of mycotoxins and antibodies. However, to date few reports are available on FPIAs for large molecules. If applications can be extended to measure large molecules like proteins, more diverse bio-tests can be performed rapidly and easily owing to the advantages of FPIAs.

FPIA is an analytical method using the degree of fluorescence polarization (*P*), which is a dimensionless number, as a parameter. The *P* value depends on the rotational movement of a fluorescence-labeled molecule [11]. If the whole molecular weight of the fluorescence-labeled molecule become larger after an assay reaction, the rotational movement is suppressed, and an increased *P* value results. As with another homogeneous immunoassay, FPIA does not require separation steps, giving the advantages of simplicity and rapidness [11-13]. In conventional FPIAs, one analyte and another fluorescence-labeled analyte (tracer) bind competitively to an antibody. The higher the difference in molecular weight between the free tracer and the tracer-antibody complex, the larger the signal/blank ratio, which in turn means the sensitivity is much higher. Therefore, it has been difficult to apply competitive FPIAs to large molecules. If FPIAs could be widely applied to large molecules like proteins, the range of applications of FPIAs would be expanded.

In this chapter, I propose a non-competitive FPIA using a fluorescence-labeled Fab fragment for protein quantification. A Fab fragment is the antibody binding region of the whole antibody and it is produced by papain digestion of whole antibody to remove the fragment crystallizable region. Fab fragment has a molecular weight of about 50 kDa. In this proposed assay, the analyte is bound to the fluorescence-labeled Fab fragment and the *P* value is measured after incubation. The relative difference in the molecular weight of the analyte and the analyte-Fab complex becomes larger than that of the IgG antibody (~150 kDa), and a larger difference of the *P* value can be obtained. Urios and Cittanova [14] reported a Fab-based non-competitive FPIA for aldosterone-BSA and IgM antibody quantification. However, to the best of my knowledge, there have been no reported applications of Fab-based non-competitive FPIA to real biological samples and there are only a few discussions about the practical realization of Fab-based non-competitive FPIA. On the other hand, non-competitive assays using aptamers and fluorescence anisotropy as a parameter have been reported [15,16]. These methods used fluorescence-labeled aptamer for non-competitive reaction to an analyte. However, the binding affinity of aptamers changes significantly due to changes in environmental factors such as ion concentration [17,18]. In addition, aptamers are subject to nuclease-mediated degradation in biological samples [19]. These are serious drawbacks for aptamer applications to real biological samples. Fab fragments have relatively good stability and are used in various biosensors [20-22]. Moreover, they can also be easily produced from IgG antibody by papain digestion or expression in *E.coli* [23,24]. Since many IgG antibodies for various targets are easily available, Fab fragments targeting various molecules can also be easily obtained. In principle, using the heavy chain of a camelid antibody (VHH antibody, ~15 kDa), a much lower molecular weight antibody, for non-competitive FPIA gives higher sensitivity [25]. However, the preparation of VHH antibody requires complicated protein engineering approaches, and few VHH antibodies are commercially available. Therefore, Fab fragments are much more practical choice than an aptamer and VHH antibody.

In this study, C-reactive protein (CRP; ~105 kDa) was used as a model analyte for Fab-based non-competitive FPIA. CRP is a non-specific marker of inflammation for many disease processes [26-28]. It naturally exists in ng/ml level in human blood and may increase to hundreds of μg/ml in 72 h following tissue

injury [29]. Some studies of the sensitive detection of CRP by immunoassay have been reported, however, washing procedures and long analysis time were required [30-32]. I tried to apply non-competitive FPIA to the detection of CRP in human serum for point-of-care testing. First, I verified the practicability of Fab-based non-competitive FPIA with CRP standard solution in phosphate buffered saline (PBS). Then, I demonstrated a diagnosis of inflammation based on CRP in human serum as a practical application.

4.2 Experimental

4.2.1 Chemicals

PBS solution (pH 7.4), Blocker™ Casein in PBS, Pierce™ tris(2-carboxyethyl)phosphine hydrochloride (TCEP−HCl) and Alexa Fluor™ 488 C5 maleimide were purchased from Thermo Fisher Scientific, Inc. (USA). Bovine serum albumin (BSA) was purchased from FUJIFILM Wako Pure Chemical Corporation (Japan). Human CRP and human CRP-free serum were purchased from Oriental Yeast Co., Ltd Japan). CRP recombinant Fab monoclonal antibody (engineered with a free cysteine) was purchased from BBI Solutions (UK). Anti-CRP monoclonal IgG antibody was purchased from ProSpec-Tany TechnoGene Ltd (USA). Fluorescein labeling kit-NH_2 and HiLyte Fluor™ 647 Labeling Kit-NH_2 were purchased from Dojindo Molecular Technologies, Inc. (Japan).

4.2.2 Labeling procedure

Labeling of fluorescein and HiLyte Fluor™ 647 to the amino groups of Fab fragment and IgG antibody were conducted following the procedures described in the labeling kit manufacturer's instructions. Labeling of Alexa Fluor™ 488 to the thiol groups of a Fab fragment was conducted as follows. 5 mM TCEP−HCl (2 μL) was added to 1 mg/mL Fab fragment in PBS (168 μL) and incubated for 2 h at 37 °C. Then, 5 mM Alexa Fluor™ 488 C5 maleimide in PBS (4 μL) was added to the mixture and incubated for 2 h at room temperature. Next,

unreacted fluorescent molecules were separated using a modified polyethersulfone membrane (Nanosep 3 K Omega, Pall Corporation, USA). Concentration of fluorescence-labeled Fab fragment was determined based on absorbance at 280 nm acquired with a fluorometer (NanoDrop One, Thermo Fisher Scientific, Inc.).

4.2.3 Assay procedure

For the measurement of CRP in PBS, CRP, fluorescence-labeled Fab fragment and 1% BSA-PBS were added to a microtube. The mixing volume ratio was CRP: fluorescein-labeled Fab fragment: 1% BSA-PBS = 8:1:1. The mixture was incubated for 20 min at room temperature. For the measurement of CRP in CRP-free human serum, the dilution rate of the sample was changed to reduce the effect of the interferences in human serum. Mixing volume ratio was HiLyte Fluor™ 647 labeled Fab fragment: CRP: 0.125 % BSA-PBS = 1:1:8. The mixture was incubated for 10 min at room temperature. Then, 100 μL of the mixture was injected into 96-well black microplates (PROTEOSAVE plates, Sumitomo Bakelite, Japan) and fluorescence polarization was measured with a microplate reader (Infinite 200 PRO, Tecan, Switzerland). When I measured CRP in human serum, the microplate was incubated with Blocker™ Casein in PBS for 3 h before use. The degree of fluorescence polarization was expressed as the amount of change (ΔP). ΔmP is millipolarization units, equivalent to $1000 \times \Delta P$.

4.2.4 Fluorescence analysis of human serum

Fluorescence intensity of human serum was measured with the microplate reader. Fluorescence spectrum of human serum was measured with a fluorescence spectrometer (F-7000, Hitachi High Technologies, Tokyo, Japan).

4.2.5 Portable FP analyzer

I used the previously developed portable FP analyzer for FP measurement [9]. This analyzer made the FP measurement based on the principle of synchronization between the orientation of the liquid crystal molecules and the sampling frequency of a CMOS [6-8]. Thus, *P* value could be obtained as a two-dimensional image. An image of a microdevice captured by the CMOS was processed to produce a *P* image according to the formula in the literature [6] using home-built image processing software. The portable FP analyzer had dimensions of 65 cm (W 35 cm × D 15 cm× H 15 cm) and a weight of 5.5 kg (Figure 4.1 (a)).

4.2.6 Microfluidic device

The basic PDMS microfluidic device was fabricated using the standard soft lithography technique, as described in the previous work [9]. Briefly, the mold was fabricated from negative photoresist SU-8 3050 and a silicon wafer (Sumco Co., Tokyo, Japan). The negative photoresist SU-8 3050 was spin-coated onto a silicon wafer. The PDMS prepolymer with black silicon rubber was poured onto the mold and cured. The cured PDMS was pasted on a glass slide. Figures. 4.1 (b) and (c) show a photograph and a schematic drawing of the microfluidic device. I designed the microfluidic device for this experiment based on the basic device. The microdevice had nine channels arranged in the field of view of the portable FP analyzer, and nine samples could be measured at one time. The width of the channel was 200 μm and the depth is 900 μm. The depth of the microfluidic device was significantly different from the previous device. By employing a channel having a high aspect ratio, it was possible to increase the fluorescence intensity per unit area and reduce specific surface area. These features contributed to highly sensitive measurement. The numbers in Figures. 4.1 (c) denote inlets and outlets, and the solution was injected into the inlet with a pipet (Eppendorf, Hamburg, Germany).

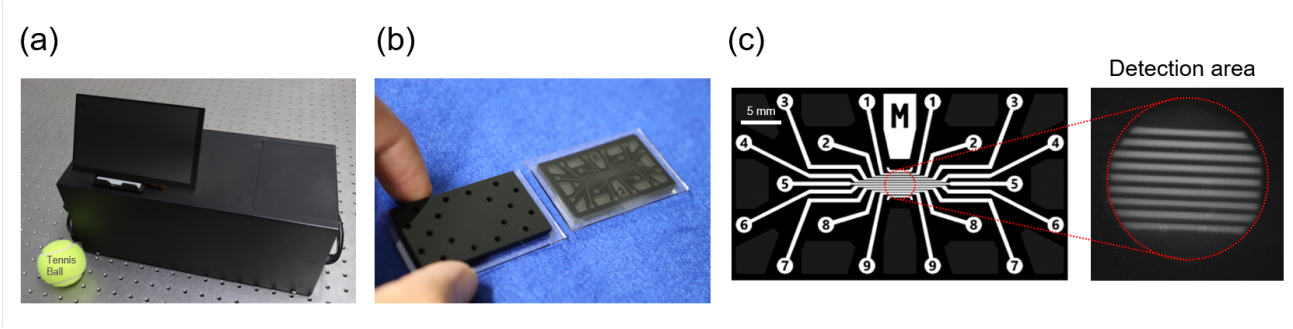


Figure 4.1 (a) Photo of the portable FP analyzer. (b) Photo of the newly designed PDMS microfluidic device. (c) Schematic diagram of the microfluidic device and fluorescence image of the 1 mM fluorescein remaining in the detection area. Each microchannel in the detection area was 200 μm wide and 900 μm deep. Sample volume of each microchannel was ~20 μL.

4.3 Theoretical fluorescence polarization value

Fluorescence polarization (P) was reviewed in the literature [33] and described as follows:

$$\left(\frac{1}{P}-\frac{1}{3}\right)=\left(\frac{1}{P_0}-\frac{1}{3}\right)\left(1+\frac{3\tau}{\rho}\right) \quad (1)$$

where P_0 is the polarization without rotation diffusion, τ is the fluorescent lifetime of the fluorophore, and ρ is the Debye rotational relaxation time. Assuming the fluorophore is a spherical protein, I described ρ as:

$$\rho=\frac{3\eta M_W(V+h)}{RT} \quad (2)$$

where η is the medium viscosity, M_W is the molecular weight, V is the partial specific volume, h is the degree of hydration, R is the gas constant, and T is temperature [13][34]. Therefore, the following equation was obtained by joining equations (1) and (2).

$$P=\frac{M_W}{\frac{1}{P_0}M_W+\frac{(3-P_0)(RT\tau)}{3\eta P_0(V+h)}} \quad (3)$$

Based on equation (3), I calculated $P_{\text{Comp}}-P_{\text{Free}}$. P_{Comp} means the fluorescence polarization of the complex of CRP and fluorescein-labeled antibody. P_{Free} means the fluorescence polarization of free fluorescein-labeled antibody. For the calculation of fluorescein-labeled Fab fragment, I used the values M_W (Comp) = 155,000

g/mol, M_W (Free) = 50,000 g/mol, P_0 = 0.5 [34], T = 298.15 K, η = 0.89 cP [35], V = 0.74 mL/g [34], and h = 0.20 mL/g [34][36].

Fab fragment: $P_{Comp} - P_{Free} = 0.053$

For the calculation of fluorescein-labeled IgG antibody, the molecular weights are M_W (Comp) = 255,000 g/mol, M_W (Free) = 150,000 g/mol.

IgG antibody: $P_{Comp} - P_{Free} = 0.012$

4.4 Results and Discussion

4.4.1 Development of non-competitive FPIA based on a Fab fragment

I provide a proof-of-concept of the one-step non-competitive FPIA using a Fab fragment for protein biomarker quantification. In this proposed assay, fluorescence-labeled Fab fragment was used as a recognition part. Fluorescein, which is often used as a model in theoretical studies of FPIA, was used as a fluorescence label for concept verification [27]. The assay was performed by mixing CRP in PBS with fluorescein-labeled Fab fragment and incubated. In a conventional competitive FPIA, it is necessary to mix an antibody with a tracer and add them to a sample. However, in non-competitive FPIA, the reaction is completed in a one-step mixing of only the fluorescence-labeled antibody. Since the concentration of fluorescein-labeled Fab fragment is constant, the amount of CRP-Fab complex in the mixture is determined according to the concentration of CRP. The CRP-Fab complex has a slower rotational movement than that of free Fab fragment and exhibits a high *P* (Figure 4.2). In non-competitive FPIA, the reaction is completed in one-step mixing of only the fluorescence-labeled antibody with the sample.

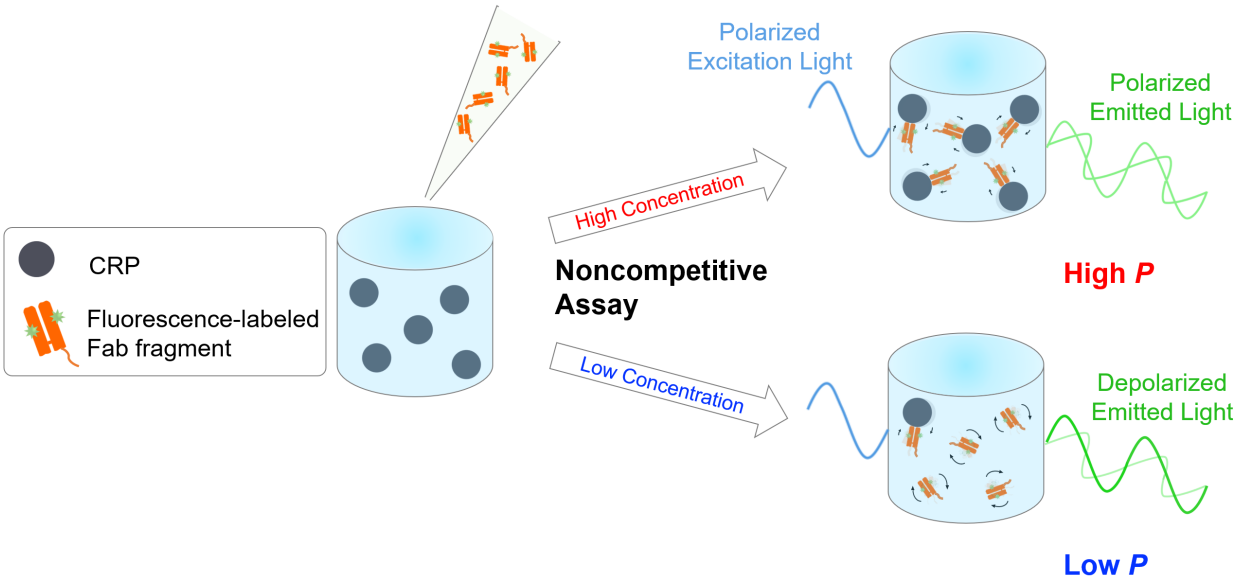


Figure 4.2 Schematic illustration of the non-competitive fluorescence polarization immunoassay using fluorescence-labeled Fab fragment.

In the first experiment, I confirmed the binding ability of fluorescein-labeled Fab fragment to CRP and optimized the Fab fragment concentration. Anti-CRP Fab fragment labeled with fluorescein on amino groups was used. Fluorescein-labeled Fab fragment was mixed with 250 ng/mL of CRP and the change in the *P* value before and after binding of fluorescein-labeled Fab fragment and CRP was measured (Figure 4.3). The bar graph shows the *P* value at each Fab fragment concentration. The *P* value difference before and after adding CRP is indicated by the red dots. The increase in the *P* value was confirmed after adding the CRP at each Fab fragment concentration. The *P* value difference before and after CRP binding reached a plateau at 4 μg/mL. Therefore, I confirmed that even Fab fragment whose amino group was fluorescence-labeled kept its ability to bind to CRP. Also, the *P* value of blank increased with the decrease of tracer concentration. I considered that the ratio of fluorescein-labeled Fab fragment adsorbed on the well to the total amount of that increased at low concentrations. The rotational movement of fluorescein-labeled Fab fragment adsorbed on the wall was suppressed, resulting in a high *P* value. In the second experiment, Fab fragment concentration of 6 μg/mL was used.

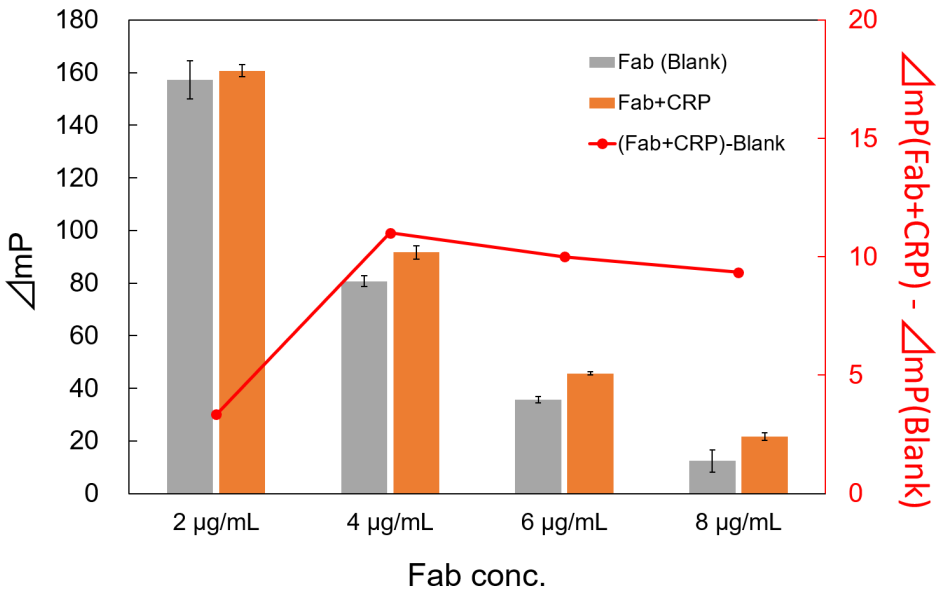


Figure 4.3 Effect of Fab fragment concentration on the *P* value. CRP concentration was 250 ng/mL. The red line indicates the difference in the *P* value between with and without adding CRP.

Next, I prepared calibration curves for CRP in PBS (Figure 4.4). For comparison with Fab-based non-competitive immunoassay, non-competitive FPIA using fluorescein-labeled monoclonal IgG antibody was also conducted. The *P* value increased with the increase of CRP concentration for both Fab fragment and IgG antibody. The difference of the *P* value between the maximum value and the blank sample was $\Delta P_{Max} - \Delta P_{Blank} = 0.043$ for Fab fragment and $\Delta P_{Max} - \Delta P_{Blank} = 0.009$ for IgG antibody. When it is assumed that the fluorescence-labeled molecule is a rigid sphere, the theoretical values of $\Delta P_{Max} - \Delta P_{Blank}$ are 0.053 for Fab fragment and 0.012 for IgG antibody (see the Supporting Information). The ΔP of the experimental results was in good agreement with that of the theoretical value. I experimentally proved that the low molecular weight antibody had an effect on the sensitivity of non-competitive FPIA. The limit of detection (LOD) of CRP in PBS was 207 ng/mL when the fluorescein-labeled Fab fragment was used. However, when using Fab fragment which is a labeled fluorescein at a thiol group that is artificially attached to the end of Fab fragment, ΔP was significantly smaller than the theoretical value (Figure 4.5). Since the Fab fragment is fluorescently labeled at a position far from the

paratope, it is considered that the contribution of the local movement of the fluorescent molecule greatly influences the *P* value [13]. Based on the above results, I concluded that Fab fragment whose amino group is fluorescently labeled is appropriate for non-competitive FPIA targeting protein biomarker.

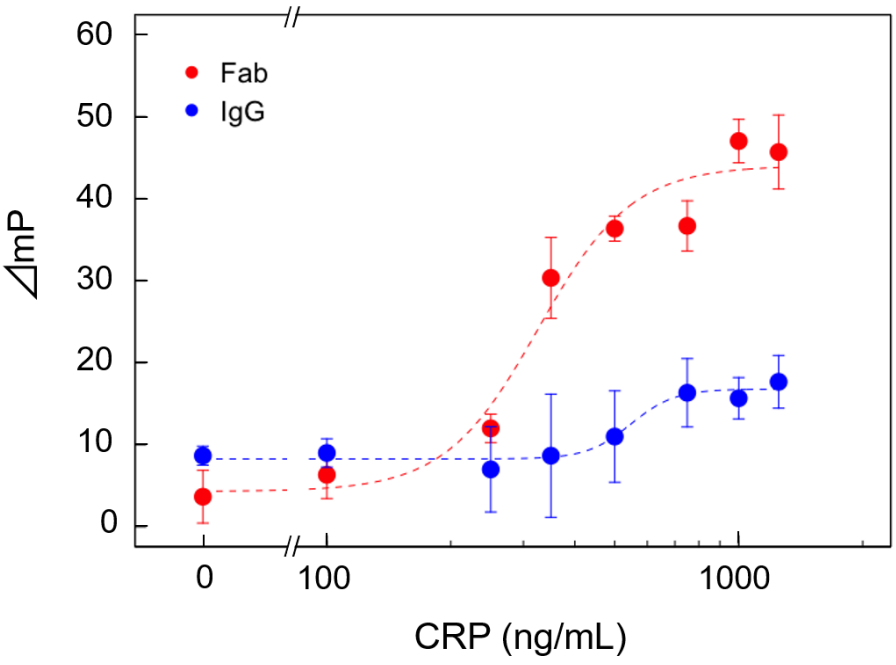


Figure 4.4 Calibration curves for CRP in PBS. Non-competitive FPIAs were conducted with fluorescein-labeled Fab fragment (red) and fluorescein-labeled IgG antibody (blue).

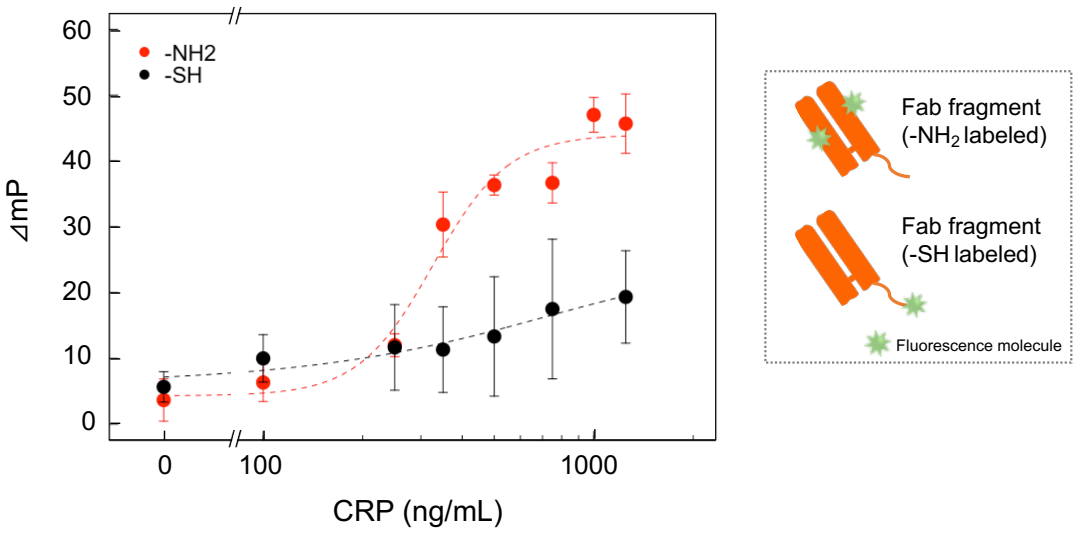


Figure 4.5 Comparison of calibration curves with -NH_2 labeled Fab fragment or -SH labeled Fab fragment.

4.4.2 Application: diagnosis of inflammation based on CRP level in serum

As a practical application of the developed non-competitive FPIA, I conducted the quantification of CRP in human serum for the diagnosis based on the cutoff value of CRP. A common CRP cutoff value for the diagnosis of inflammation is 10 μg/mL [37]. I constructed a highly sensitive non-competitive FPIA for CRP in serum around this cutoff value

Homogeneous immunoassays do not require bound-free separation, and the result could consequently be affected by interferences in a real sample. If the interferences in the real sample emit fluorescence near the fluorescence wavelength of the fluorescent labeling molecule and its concentration deviates, the result is strongly affected by fluorescence interferences. Therefore, the fluorescence spectrum and fluorescence intensity of human serum were measured. Figure 4.6 (a) shows the total fluorescence spectrum and Figure 4.6 (b) shows the total fluorescence intensity of human serum. At an excitation wavelength of 485 nm, human serum showed a much higher fluorescence intensity compared to the intensity at an excitation wavelength of 620 nm. It has been reported that a fluorescent substance having a fluorescence peak wavelength near 500 nm is present in human serum [38]. Thus, using a long-wavelength fluorescent dye as a fluorescent label for Fab fragment can

reduce the effect of autofluorescence of serum. Far-red emitting fluorescent dye (HiLyte Fluor™ 647; ex/em 649/672 nm) was labeled to the amino group of Fab fragment and this was used in a non-competitive FPIA for CRP in serum.

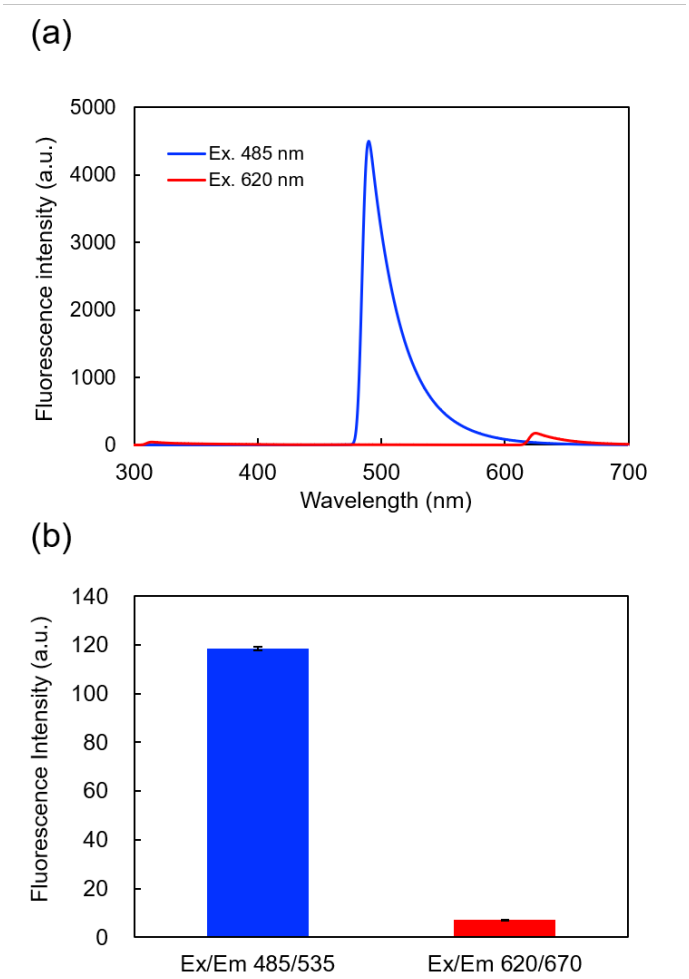


Figure 4.6 (a) Fluorescence spectrum of human serum obtained with a fluorescence spectrometer. (b) Total fluorescence intensity of human serum obtained with a microplate reader.

The incubation time was optimized to achieve a practical and rapid assay. Figure 4.7 shows the relationship between the *P* value and the incubation time after mixing HiLyte Fluor™ 647-labeled Fab fragment with CRP in serum. The *P* value became almost constant at the incubation time of 10 min. In the next experiment, the incubation time was set at 10 min.

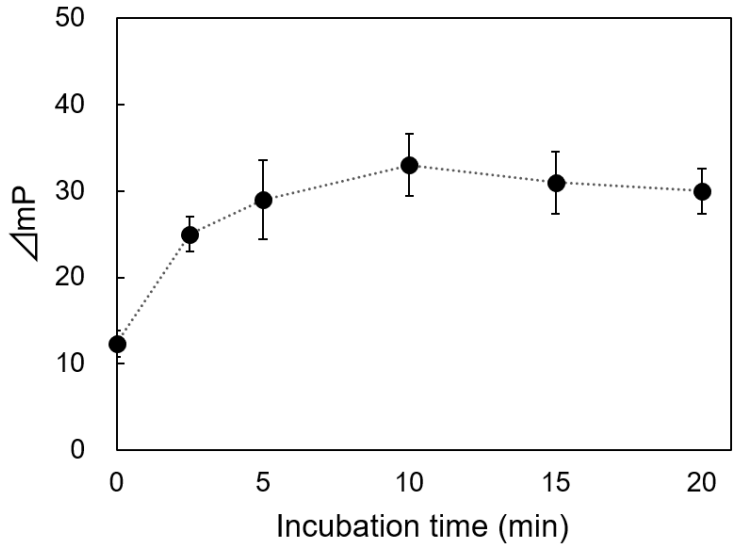


Figure 4.7 The *P* value of the mixture of HiLyte Fluor™ 647- labeled Fab fragment (20 μg/mL) and CRP (10 μg/mL) in human serum as a function of incubation time.

Then, I prepared calibration curves for CRP spiked in CRP-free human serum (Figure 4.8). In order to reduce the effect of the interferences in human serum, I designed the assay protocol in which CRP was diluted 10-fold in the final mixture. In addition, the Fab fragment concentration was adjusted to change the *P* value near the cutoff value. The *P* value was increased with increasing CRP concentration as with CRP in PBS. Thus, analytes in serum can be measured by non-competitive FPIA by selecting optimum fluorescence labels and designing assay protocols. In order to perform highly sensitive measurement near the cutoff value, the calibration curve was prepared by increasing the Fab fragment concentration from 20 μg/mL to 100 μg/mL (Figure 4.8 (b)). As a result, the calibration curves had steep slopes around the cut-off value. An area with a steep calibration curve slope could be easily shifted by adjusting only the Fab fragment concentration. In Figure 4.8 (b), the working range was from ~5 to ~20 μg/mL and average of coefficient of variation was 10.9 %. Furthermore, the calibration curve for CRP in human serum under the cut-off value was also constructed (Figure 4.9). LOD of CRP in human serum was 1.58 μg/mL. This value is sufficient for the diagnosis of inflammation based on CRP.

In addition, the detection of CRP in serum was also accomplished with the portable FP analyzer (Figure 4.10). I demonstrated that non-competitive FPIA enabled diagnosis based on the cutoff value of CRP in serum. In this analytical method, the reaction is completed by simply mixing the fluorescence-labeled Fab fragment with the sample and incubating for 10 min, and no pretreatment is required. This method is very powerful tool as a simple quantification method for protein biomarkers.

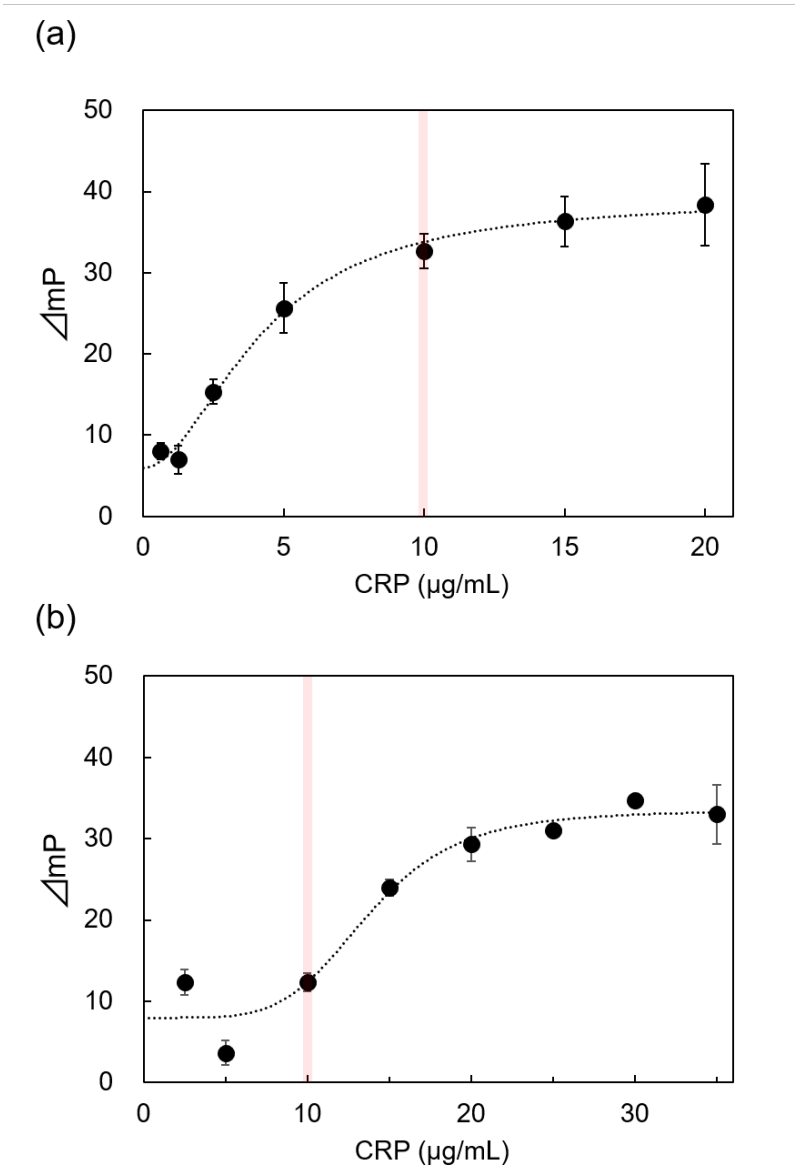


Figure 4.8 Calibration curves for CRP in human serum. HiLyte Fluor™ 647- labeled Fab fragment concentration: (a) 20 μg/mL and (b) 100 μg/mL. The red line indicates the cut-off value of inflammation (CRP: 10 μg/mL).

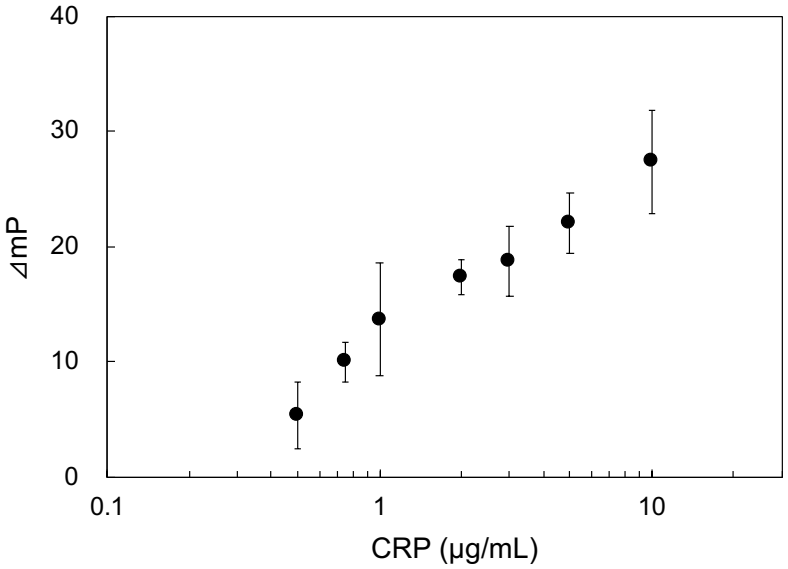


Figure 4.9 Calibration curve for CRP in human serum under the cut-off value. HiLyte Fluor™ 647- labeled Fab fragment concentration: 6 μg/mL.

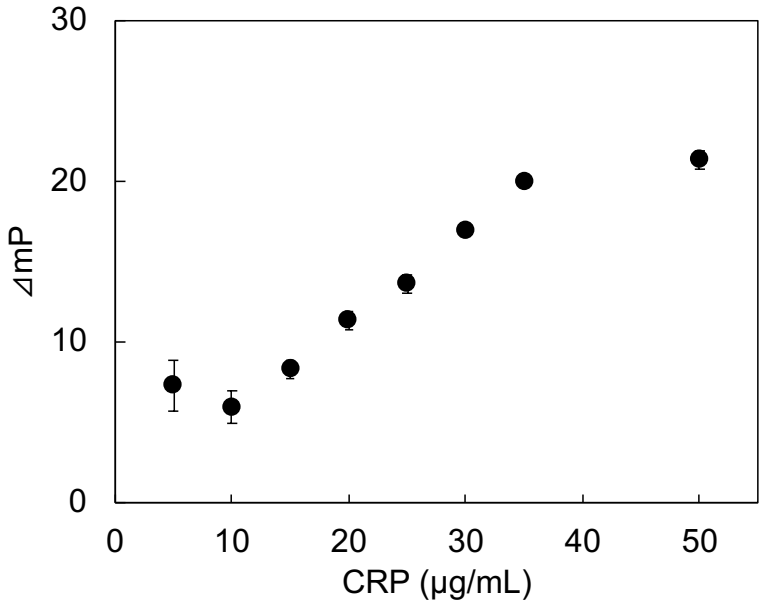


Figure 4.10 Calibration curve for CRP in human with the portable FP analyzer. HiLyte Fluor™ 647- labeled Fab fragment concentration: 100 μg/mL. Mixing volume ratio was HiLyte Fluor™ 647 labeled Fab fragment: CRP: 0.102 % BSA-PBS = 10:10:980.

4.5 Conclusions

In this chapter, I reported a non-competitive FPIA using a fluorescence-labeled Fab fragment. The Fab fragment whose amino group is fluorescently labeled is appropriate for non-competitive FPIA for protein quantification. CRP in human serum was measured without pretreatment by using a far-red emitting fluorescent dye-labeled Fab fragment around the cut-off value of CRP. It can be applied to point-of-care testing of various protein biomarkers by using different fluorescent dyes. A portable FP analyzer that can change the measurement wavelength is now under development. By combining this analyzer with non-competitive FPIA, I expect to realize a rapid and easy-to-use on-site point-of-care testing system for CRP.

4.6 References

[1] Mannaert, E.; Daenens, P. Development of a Fluorescence Polarization Immunoassay for the Routine Detection of N-Desmethylzopiclone in Urine Samples. *Analyst* **1996**, 121, 857.

[2] Xu, Z.-L.; Wang, Q.; Lei, H.-T.; Eremin, S. A.; Shen, Y.-D.; Wang, H.; Beier, R. C.; Yang, J.-Y.; Maksimova, K. A.; Sun, Y.-M. A Simple, Rapid and High-Throughput Fluorescence Polarization Immunoassay for Simultaneous Detection of Organophosphorus Pesticides in Vegetable and Environmental Water Samples. *Anal. Chim. Acta* **2011**, 708, 123–129.

[3] Wang, Q.; Haughey, S. A.; Sun, Y.-M.; Eremin, S. A.; Li, Z.-F.; Liu, H.; Xu, Z.-L.; Shen, Y.-D.; Lei, H.-T. Development of a Fluorescence Polarization Immunoassay for the Detection of Melamine in Milk and Milk Powder. *Anal. Bioanal. Chem.* **2011**, 399, 2275–2284.

[4] Wu, X.-J.; Zhang, J.; Yu, J.-C.; Cao, G.-Y.; Shi, Y.-G.; Zhang, Y.-Y.; Wang, M.-G. Establishment of Norvancomycin Fluorescence Polarization Immunoassay for Therapeutic Drug Monitoring. *J. Antibiot. (Tokyo).* 2012, 65, 35–39.

[5] Porricelli, A. C. R.; Lippolis, V.; Valenzano, S.; Cortese, M.; Suman, M.; Zanardi, S.; Pascale, M. Optimization and Validation of a Fluorescence Polarization Immunoassay for Rapid Detection of T-2 and HT-2 Toxins in Cereals and Cereal-Based Products. *Food Anal. Methods* **2016**, 9, 3310–3318.

[6] Wakao, O.; Fujii, Y.; Maeki, M.; Ishida, A.; Tani, H.; Hibara, A.; Tokeshi, M. Fluorescence Polarization Measurement System Using a Liquid Crystal Layer and an Image Sensor. *Anal. Chem.* **2015**, 87, 9647–9652.

[7] Wakao, O.; Satou, K.; Nakamura, A.; Sumiyoshi, K.; Shirokawa, M.; Mizokuchi, C.; Shiota, K.; Maeki, M.; Ishida, A.; Tani, H.; Shigemura, K.; Hibara, A.; Tokeshi, M. A Compact Fluorescence Polarization Analyzer with High-Transmittance Liquid Crystal Layer. *Rev. Sci. Instrum.* **2018**, 89, 024103.

[8] Wakao, O.; Maeki, M.; Ishida, A.; Tani, H.; Hibara, A.; Tokeshi, M. Sensitive Fluorescent Polarization Immunoassay by Optimizing Synchronization Mismatch Condition. *Sensors Actuators B Chem.* **2019**, 285, 418–422.

[9] Wakao, O.; Satou, K.; Nakamura, A.; Galkina, P. A.; Nishiyama, K.; Sumiyoshi, K.; Kurosawa, F.; Maeki, M.; Ishida, A.; Tani, H.; Proskurnin, M. A.; Shigemura, K.; Hibara, A.; Tokeshi, M. High-Throughput Fluorescence Polarization Immunoassay by Using a Portable Fluorescence Polarization Imaging Analyzer. *Lab Chip* **2019**, 19, 2581–2588.

[10] Nishiyama, K.; Takeda, Y.; Maeki, M.; Ishida, A.; Tani, H.; Shigemura, K.; Hibara, A.; Yonezawa, Y.; Imai, K.; Ogawa, H.; Tokeshi, M. Rapid Detection of Anti-H5 Avian Influenza Virus Antibody by Fluorescence Polarization Immunoassay Using a Portable Fluorescence Polarization Analyzer. *Sensors Actuators B Chem.* **2020**, 316, 128160.

[11] Smith, D. S.; Eremin, S. A. Fluorescence Polarization Immunoassays and Related Methods for Simple, High-Throughput Screening of Small Molecules. *Anal. Bioanal. Chem.* **2008**, 391, 1499–1507.

[12] Maragos, C. Fluorescence Polarization Immunoassay of Mycotoxins: A Review. *Toxins (Basel).* **2009**, 1, 196–207.

[13] Jameson, D. M.; Ross, J. A. Fluorescence Polarization/Anisotropy in Diagnostics and Imaging. *Chem. Rev.* **2010**, 110, 2685–2708.

[14] Urios, P.; Cittanova, N. Adaptation of Fluorescence Polarization Immunoassay to the Assay of Macromolecules. *Anal. Biochem.* **1990**, 185, 308–312.

[15] Zhang, D.; Zhao, Q.; Zhao, B.; Wang, H. Fluorescence Anisotropy Reduction of Allosteric Aptamer for Sensitive and Specific Protein Signaling. *Anal. Chem.* **2012**, 84, 3070–3074.

[16] Zou, M.; Chen, Y.; Xu, X.; Huang, H.; Liu, F.; Li, N. The Homogeneous Fluorescence Anisotropic Sensing of Salivary Lysozyme Using the 6-Carboxyfluorescein-Labeled DNA Aptamer. *Biosens. Bioelectron.* **2012**, 32, 148–154.

[17] Hianik, T.; Ostatná, V.; Sonlajtnerova, M.; Grman, I. Influence of Ionic Strength, PH and Aptamer Configuration for Binding Affinity to Thrombin. *Bioelectrochemistry* **2007**, 70, 127–133.

[18] Lin, P.-H.; Yen, S.-L.; Lin, M.-S.; Chang, Y.; Louis, S. R.; Higuchi, A.; Chen, W.-Y. Microcalorimetrics Studies of the Thermodynamics and Binding Mechanism between L -Tyrosinamide and Aptamer. *J. Phys. Chem. B* **2008**, 112, 6665–6673.

[19] Keefe, A. D.; Pai, S.; Ellington, A. Aptamers as Therapeutics. *Nat. Rev. Drug Discov.* **2010,** 9, 537–550.

[20] Kim, J. P.; Lee, B. Y.; Hong, S.; Sim, S. J. Ultrasensitive Carbon Nanotube-Based Biosensors Using Antibody-Binding Fragments. *Anal. Biochem.* **2008**, 381, 193–198.

[21] Nassef, H. M.; Civit, L.; Fragoso, A.; O'Sullivan, C. K. Amperometric Immunosensor for Detection of Celiac Disease Toxic Gliadin Based on Fab Fragments. *Anal. Chem.* **2009**, 81, 5299–5307.

[22] Crivianu-Gaita, V.; Aamer, M.; Posaratnanathan, R. T.; Romaschin, A.; Thompson, M. Acoustic Wave Biosensor for the Detection of the Breast and Prostate Cancer Metastasis Biomarker Protein PTHrP. *Biosens. Bioelectron.* **2016**, 78, 92–99.

[23] Brezski, R. J.; Jordan, R. E. Cleavage of IgGs by Proteases Associated with Invasive Diseases. *MAbs* **2010**, 2, 212–220.

[24] Kang, H.-J.; Kim, H.-J.; Jung, M.-S.; Han, J.-K.; Cha, S.-H. Optimal Expression of a Fab-Effector Fusion Protein in Escherichia Coli by Removing the Cysteine Residues Responsible for an Interchain Disulfide Bond of a Fab Molecule. *Immunol. Lett.* **2017**, 184, 34–42.

[25] Fukuyama, M.; Nakamura, A.; Nishiyama, K.; Imai, A.; Tokeshi, M.; Shigemura, K.; Hibara, A. Noncompetitive Fluorescence Polarization Immunoassay for Protein Determination. *Anal. Chem.* **2020**, 92, 14393–14397.

[26] Libby, P.; Ridker, P. M. Inflammation and Atherosclerosis: Role of C-Reactive Protein in Risk Assessment. *Am. J. Med.* **2004**, 116, 9–16.

[27] Marnell, L.; Mold, C.; Du Clos, T. W. C-Reactive Protein: Ligands, Receptors and Role in Inflammation. *Clin. Immunol.* **2005**, 117, 104–111.

[28] Allin, K. H.; Bojesen, S. E.; Nordestgaard, B. G. Baseline C-Reactive Protein Is Associated With Incident Cancer and Survival in Patients With Cancer. *J. Clin. Oncol.* **2009**, 27, 2217–2224.

[29] Pandey, A. C-Reactive Protein (CRP) and Its Association with Periodontal Disease: A Brief Review. *J. Clin. Diagnostic Res.* **2014**, 8, ZE21-ZE24.

[30] Hu, C.; Zeimpekis, I.; Sun, K.; Anderson, S.; Ashburn, P.; Morgan, H. Low-Cost Nanoribbon Sensors for Protein Analysis in Human Serum Using a Miniature Bead-Based Enzyme-Linked Immunosorbent Assay. *Anal. Chem.* **2016**, 88, 4872–4878.

[31] Hu, B.; Li, J.; Mou, L.; Liu, Y.; Deng, J.; Qian, W.; Sun, J.; Cha, R.; Jiang, X. An Automated and Portable Microfluidic Chemiluminescence Immunoassay for Quantitative Detection of Biomarkers. *Lab Chip* **2017,** 17, 2225–2234.

[32] Nishiyama, K.; Kasama, T.; Nakamata, S.; Ishikawa, K.; Onoshima, D.; Yukawa, H.; Maeki, M.; Ishida, A.; Tani, H.; Baba, Y.; Tokeshi, M. Ultrasensitive Detection of Disease Biomarkers Using an Immuno-Wall Device with Enzymatic Amplification. *Analyst* **2019**, 144, 4589–4595.

[33] Dandliker, W. .; de Saussure, V. . Fluorescence Polarization in Immunochemistry. *Immunochemistry* **1970,** 7, 799–828.

[34] Jameson, D. M.; Seifried, S. E. Quantification of Protein–Protein Interactions Using Fluorescence Polarization. *Methods* **1999**, 19, 222–233.

[35] Thompson, J. W.; Kaiser, T. J.; Jorgenson, J. W. Viscosity Measurements of Methanol–Water and Acetonitrile–Water Mixtures at Pressures up to 3500bar Using a Novel Capillary Time-of-Flight Viscometer. *J. Chromatogr. A* **2006**, 1134, 201–209.

[36] Szmacinski, H.; Terpetschnig, E.; Lakowicz, J. R. Synthesis and Evaluation of Ru-Complexes as Anisotropy Probes for Protein Hydrodynamics and Immunoassays of High-Molecular-Weight Antigens. *Biophys. Chem.* **1996**, 62 (1–3), 109–120.

[37] U. S. FDA, 2005, Review Criteria for Assessment of C-Reactive Protein (CRP), High Sensitivity C-Reactive Protein (hsCRP) and Cardiac C-Reactive Assays. (Accessed in June 2020) https://www.fda.gov/regulatory-information/search-fda-guidance-documents/review-criteria-assessment-c-reactive-protein-crp-high-sensitivity-c-reactive-protein-hscrp-and-0

[38] Wolfbeis, O. S.; Leiner, M. Mapping of the Total Fluorescence of Human Blood Serum as a New Method for Its Characterization. *Anal. Chim. Acta* **1985**, 167, 203–215.

CHAPTER 5 Application of non-competitive fluorescence polarization immunoassay for antigen and antibody detection of H5 avian influenza virus

5.1 Introduction

Avian influenza is a poultry disease caused by influenza A virus infection. Influenza A virus has many subtypes based on the type of virus surface glycoproteins, hemagglutinin (HA) and neuraminidase (NA). Wild aquatic birds are the primary natural host of influenza A virus, and 16 HAs (H1–H16) and 9 NAs (N1–N9) have been found so far in such birds [1,2]. Avian influenza virus (AIV) usually infects intestinal cells of aquatic birds and does not show pathogenicity; however, it can infect poultry and cause pathogenicity [3,4]. The virus that causes a high mortality when poultry were infected is designated as a highly pathogenic avian influenza virus (HPAIV). To date, some H5 and H7 subtype AIVs have been reported to be HPAIVs [5-8]. H5N1 subtype HPAIV, which appeared after 1996, has been reported not only in poultry but also in humans. The mortality rate for humans infected with H5N1 is reported to exceed 50% [9]. If these HPAIVs have acquired human-to-human infectivity, the deaths of many persons world-wide due to a pandemic become a concern.

Rapid initial response for a suspected infection and continuous surveillance are indispensable to prevent poultry epidemics of HPAIV and further human threats [10,11]. When a diagnosis is performed at the site of a disease outbreak, a rapid, simple and accurate antigen detection method is required. The detection of viral nucleic acid by a polymerase chain reaction (PCR) is used as a gold standard method for the diagnosis of viral infections [12-14]. PCR testing has good sensitivity and specificity and is suitable for definitive diagnosis. However, PCR testing requires complicated procedures and long analysis times, conditions which are not suitable for an initial diagnosis. On the other hand, simple analytical methods for detecting antigens and antibodies by lateral flow immunoassay (LFIA) have been developed [15-18]. Typical LFIA devices with visual observation do not have high accuracy and sensitivity. In order to obtain high sensitivity with LFIA devices, expensive materials such as metal nanoparticles and quantum dots, and read-out equipment are often required for higher sensitivity. However, these methods compromise the simplicity and inexpensiveness of LFIA.

In the process from a disease occurrence to its cleanup and under a usual surveillance system, antibody detection to check for previous infections also plays an important role. Even in poultry that do not currently

have the virus, the history of past infection can be determined by detecting antibodies. This is essential for investigating the routes of transmission of infectious diseases. As a recent example, antibody tests for severe acute respiratory syndrome coronavirus 2 (SARS-CoV-2) have received broad attention to prevent the spread of the novel coronavirus disease (COVID-19) [19,20]. Although some antibody tests, such as the agar gel immunodiffusion test, hemagglutination inhibition test and enzyme-linked immunosorbent assay are used for the detection of anti-AIV antibody [21-25], these methods require complicated operations and a long reaction time. Therefore, it is impractical to use these methods outside the laboratory. If the method is developed that can rapidly and easily provide antibody test results outside the laboratory, field applications become possible and the surveillance system using the antibody test can be significantly strengthened.

In this chapter, I developed a system that selectively detected H5-AIV and anti-H5-AIV antibody using non-competitive FPIA (NC-FPIA) with a portable FPIA analyzer. I prepared a fluorescein-labeled Fab fragment (F-Fab) for the detection of H5-AIV and fluorescein-labeled H5 subtype HA glycoprotein for the detection of anti-H5-AIV antibody in serum. For the detection of H5-AIV, I prepared a fluorescein-labeled Fab fragment (F-Fab). After the F-Fab was reacted with H5-HA on the H5-AIV surface, the *P* value was measured with a portable FPIA analyzer. For the detection of anti-H5-AIV antibody, the *P* value of the mixture of an anti-AIV serum and fluorescein-labeled H5 subtype HA glycoprotein was measured. If NC-FPIA can be applied to virus and its antibody detection, it will greatly contribute to speeding up the diagnosis of viral infectious diseases. Furthermore, unlike ELISA, FPIA has the advantage of being easy to apply to various animal species because FPIA does not require a suitable secondary antibody for each animal species. As far as I know, this is the first reported detection of a virus by FPIA.

5.2 Experimental

5.2.1 Materials

Phosphate-buffered saline (PBS; pH 7.4) and Micro BCA Protein Assay Kit were purchased from Thermo Fisher Scientific, Inc. (USA). The Sylgard 184 silicone elastomer kit for polydimethylsiloxane (PDMS) microdevice fabrication was purchased from Dow Corning Toray Co., Ltd. (Japan). The PDMS included black silicon rubber to decrease the background signal of fluorescence. A negative photoresist (SU-8 3050) for PDMS microdevice fabrication was purchased from Nippon Kayaku Co., Ltd. (Japan). Isogen-LS was purchased from Nippon Gene (Japan). SuperScript III Reverse Transcriptase was purchased from Invitrogen (USA). TaKaRa Ex Taq was purchased from TaKaRa (Japan). Expression vector pET-32b and Rosetta-gamiTM 2 (DE3) pLysS were purchased from Novagen (USA). Isopropyl-β-d-thiogalactopyranoside was purchased from Wako Pure Chemical Industries (Osaka, Japan). Nickel–nitrilotriacetic acid (Ni–NTA) agarose was purchased from Qiagen (Germany). Bovine serum albumin (BSA) was purchased from FUJIFILM Wako Pure Chemical Corporation (Japan). H5N1 hemagglutinin polyclonal antibody (anti-H5-HA rabbit IgG polyclonal antibody) was purchased from Bioss Antibodies (USA). Fluorescein labeling kit-NH_2 was purchased from Dojindo Molecular Technologies, Inc. (Japan) for labeling of Fab fragment. Lightning-Link® Rapid Fluorescein was purchased from Innova Biosciences Co., Ltd. (UK) for labeling of recombinant H5 subtype AIV HA (H5-rHA).

5.2.2 Preparation of purified H5N3 AIV

The purification of H5N3 subtype AIV (A/duck/Hong Kong/820/1980) and H1N1 subtype influenza A virus (A/Puerto Rico/8/34) was performed as previously described [26]. Shimane strain and Hong Kong strain were kindly provided by Dr. Toshihiro Ito (Tottori University, Japan) and Dr. Yoshihiro Sakoda (Hokkaido University, Japan), respectively. A/Puerto Rico/8/34 strain was purchased from ATCC (Manassas, VA: Catalog No. VR-95TM). The concentration of H5-rHA and purified H5N3 and H1N1 viruses were measured by the Micro BCA Protein Assay Kit.

5.2.3 Preparation of F-Fab

Anti-H5-HA Fab fragment was purchased from Hokudo Co., Ltd (Japan). Fab fragment was produced by the papain digest of commercial anti-H5-HA rabbit IgG polyclonal antibody (Bioss antibodies). Labeling of fluorescein on the amino groups of the Fab fragment was conducted following the procedures described in the manufacturer's instructions of the fluorescein labeling kit-NH_2.

5.2.4 Preparation of Fluorescein-labeled antigen

As an antigen for the FPIA, recombinant H5 subtype AIV HA (H5-rHA) was produced using the bacterial expression system as Horie *et al.* [27] previously described with slight modifications. Briefly, viral RNA was extracted from H5N3 subtype AIV (A/whistling swan/Shimane/499/1983) [28]. The viral RNA was extracted from the virus with Isogen-LS, and then reverse transcribed into cDNA by using SuperScript III Reverse Transcriptase. For amplification of the partial HA gene (aa 284–425), PCR was performed using the TaKaRa Ex Taq and the following primers: 5'-GGCCATGGAACTGGAGTATGGTAACTGT-3' and 5'-GGCCATGGCCATTTTCTTATTTAAATT-3', which include restriction enzyme site sequences (underlined). The PCR cycle included an initial cycle at 94 ℃ for 1 min, then 30 cycles at 94 ℃ for 20 s, 58 ℃ for 30 s, and 72℃ for 2 min, and a final extension at 72℃ for 7 min. The PCR product was ligated into the expression vector pET-32b. The expression vector prepared was used to transform the Rosetta-gamiTM 2 (DE3) pLysS, and isopropyl-β-d-thiogalactopyranoside was used to induce the expression of the partial HA gene. The protein extracted from the bacteria was purified using nickel–nitrilotriacetic acid (Ni–NTA) agarose. The recombinant protein obtained was concentrated using an ultrafiltration membrane, and then dialyzed against PBS. The recombinant protein was identified by Western blotting using anti-H5 mouse serum, and its concentration was measured by the Micro BCA Protein Assay Kit. The resultant H5-rHA was labeled using the Lightning-Link Fluorescein Conjugation Kit.

5.2.5 Anti-AIV sera

The goat antisera against H1–H15 subtypes and the chicken antiserum against H16 subtype AIV were kindly provided by Dr. Yoshihiro Sakoda (Hokkaido University, Japan). The immunogen of each serum is shown in Table 5.1.

Table 5.1 Immunogens of goat anti-AIV sera.

Serum name	Strain name (subtype) of immunogen AIV	GenBank Accession number
H1	A/swine/Hokkaido/1/1981 (H1N1)	HA gene: AB434392
H2	A/duck/Hong Kong/278/1978 (H2N9)	HA gene: AB292785
H3	A/duck/Hokkaido/5/1977 (H3N2)	HA gene: AB277754
H4	A/duck/Czechoslovakia/1956 (H4N6)	HA gene: GU052381
H5	A/duck/Hong Kong/820/1980 (H5N3)	HA gene: LC042027
H6	A/shearwater/Australia/1/1972 (H6N5)	HA gene: AB278600
H7	A/duck/Hong Kong/301/1978 (H7N2)	HA gene: AB302789
H8	A/turkey/Ontario/6118/1967 (H8N4)	HA gene: GU053171
H9	A/duck/Hong Kong/448/1978 (H9N2)	HA gene (partial): AB080224
H10	A/chicken/Germany/N/1949 (H10N7)	HA gene: GQ176136
H11	A/duck/England/1/1956 (H11N6)	HA gene: GU052203
H12	A/duck/Alberta/60/1976 (H12N5)	HA gene: CY130078
H13	A/gull/Maryland/704/1977 (H13N6)	HA gene: CY130086
H14	A/mallard/Astrakhan/263/1982 (H14N5)	HA gene: CY130094
H15	A/duck/Australia/341/1983 (H15N8)	HA gene: AB295613
H16	A/black-headed gull/Sweden/5/1999 (H16N3)	HA gene: AY684891

5.2.6 Potable FP analyzer

The portable FP analyzer and microfluidic device were same as these described in Chapter 4.

5.2.7 Measurement procedure of H5N3 AIV

NC-FPIA was demonstrated using a portable FPIA analyzer with a microfluidic device (Fig. S1) [29]. Antigen (purified virus or H5-rHA) in PBS, 80 ng/mL F-Fab and 1% BSA in PBS were added to a microtube. The mixing volume ratio was antigen: F-Fab: 1% BSA-PBS = 8:1:1. The mixture was incubated at room temperature for 15 min. Then, 20 μL of the mixture was injected into the microfluidic device and the *P* value was measured with the portable FP analyzer.

5.2.8 Measurement procedure of antibody

Anti-AIV serum diluted in a prescribed ratio and 640 ng/mL fluorescein-labeled H5-rHA were mixed at a volume ratio of 1:1. The mixture was incubated at room temperature for 15 min. Then, 20 μL of the mixture was injected into the microfluidic device and *P* value was measured with the portable FP analyzer. The FP analyzer acquired P images in the detection area. The *P* value measured was determined by reading out the luminance on the P image in the detection area of the microdevice.

5.3 Results and Discussion

5.3.1 Virus detection

I constructed a NC-FPIA with a portable FPIA analyzer for virus detection. Unlike conventional competitive FPIA, only fluorescence-labeled Fab is used as the reagent. F-Fab was added to a virus sample and the *P* value was measured after incubation (Figure 5.1). If I apply conventional competitive FPIA to a virus, antigens that competitively react with the antibody is needed as a tracer. The smaller the molecular weight of the tracer is, the greater the difference in the *P* value before and after binding to the antibody is, resulting in high sensitivity. Therefore, it is desirable to use only a part of the virus like a membrane protein as a tracer. However, it is difficult to react a small tracer and a virus to the antibody competitively because the diffusion

coefficient in the solution greatly differs between the small tracer and the virus particle. In this proposed NC-FPIA, only F-Fab was used as a reagent. When a F-Fab is bound to a virus, the *P* value becomes high due to the much slower rotational motion of the virus-Fab complex. High detection sensitivity can be achieved by using a Fab fragment (~50 kDa) instead of the commonly used IgG antibody (~150 kDa) (Chapter 4).

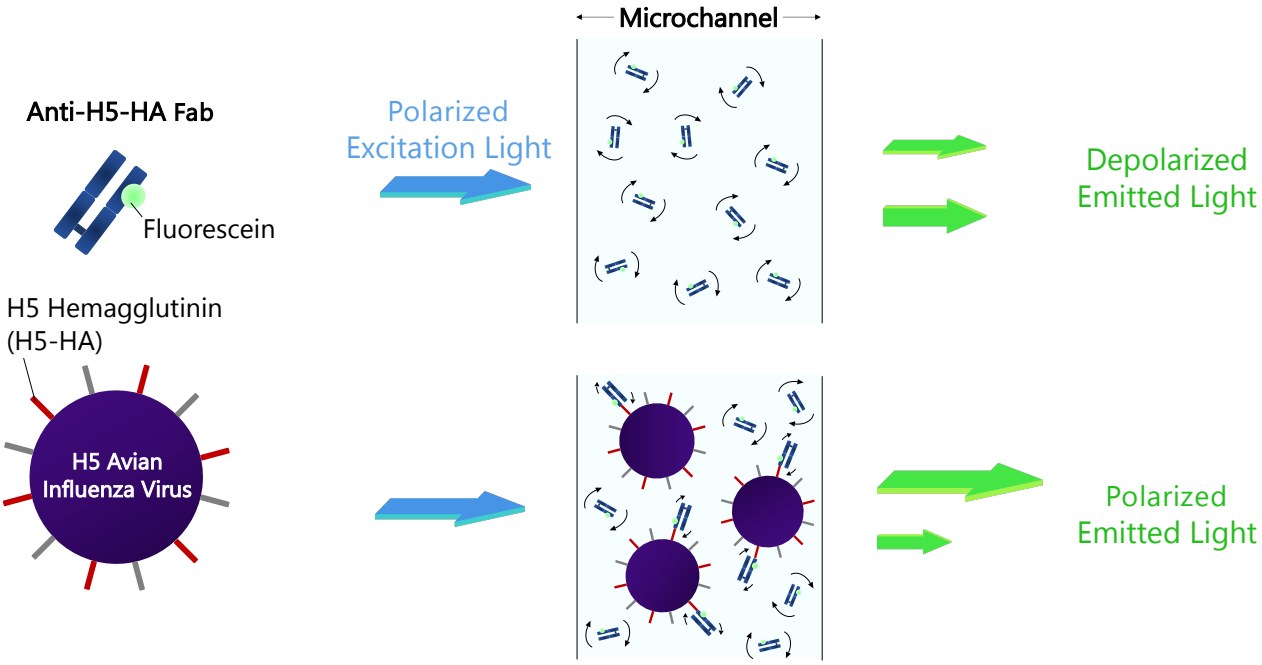


Figure 5.1 Schematic illustration of the NC-FPIA using F-Fab for H5-AIV quantification.

I prepared a calibration curve for the purified H5N3 AIV (Figure 5.2). The *P* value increased with increasing virus concentration, and the detection limit was 2.8 μg/mL. The change of the *P* value was $\Delta mP_{max} - \Delta mP_{blank}$ = 13.0 mP. I clarified that the Fab-based NC-FPIA can detect viruses as well as protein targets with equivalent sensitivity. It is possible to change the measurable concentration range by changing of the F-Fab concentration or using a Fab fragment with different affinity to H5-HA. Then, I evaluated the selectivity of F-Fab for H5N3 AIV.

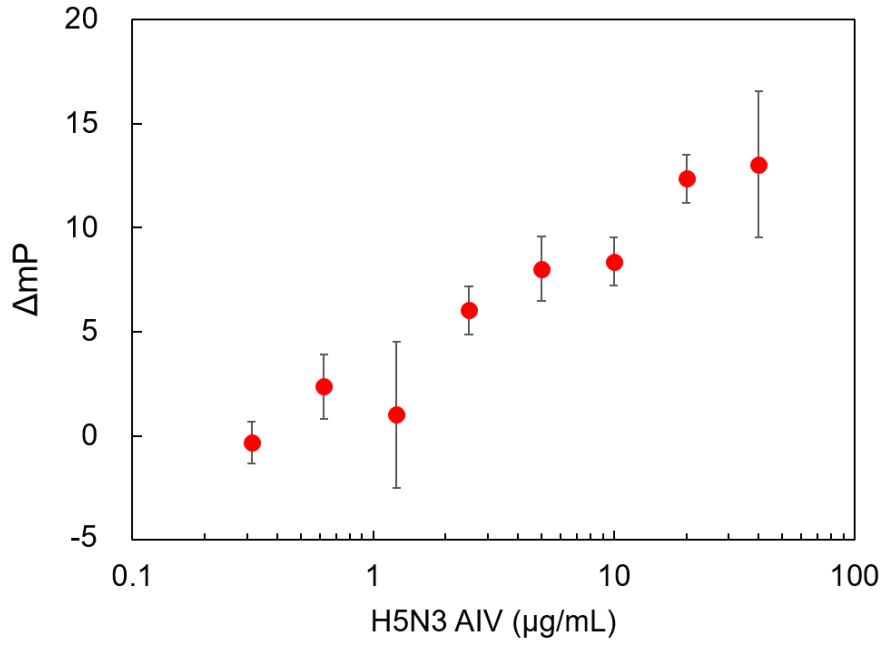


Figure 5.2 Calibration curve for the purified H5N3 AIV in PBS. F-Fab concentration: 80 ng/mL. ΔmP = 1000 × ($P_{sample} - P_{blank}$).

Figure 5.3 shows the results of the selectivity test for H5N3 AIV using the purified H1N1 virus as a negative control. The *P* value after reaction between F-Fab and H5N3 AIV was significantly higher than that of blank and H1N1 virus. In addition, it was confirmed that F-Fab had the high affinity for H5-rHA (Figure 5.4). These results indicated that F-Fab had high selectively to H5N3 AIV. To achieve the detection of H5-AIV with much higher sensitivity and selectively, using the Fab fragment which has a higher selectivity and affinity for H5-HA is ideal. However, the present results are promising in that Fab-based NC-FPIA has a greater possibility for achieving the rapid on-site diagnosis of viral infectious diseases.

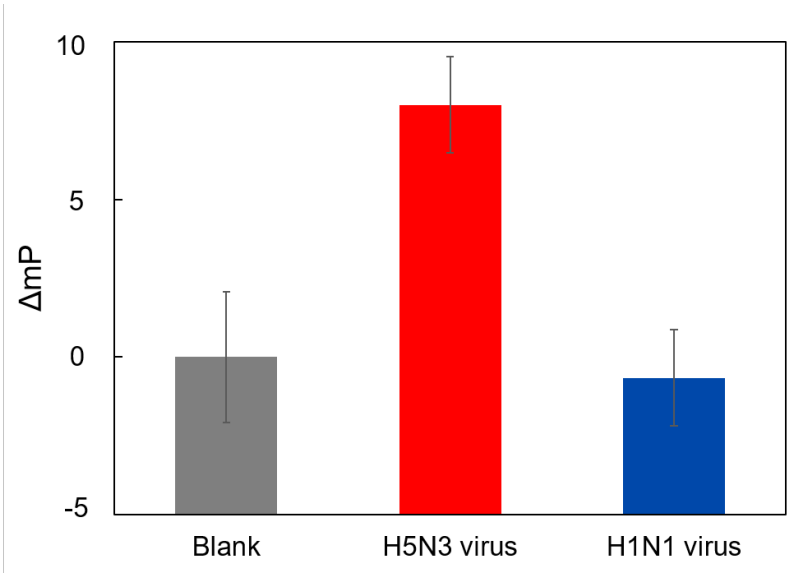


Figure 5.3 Selectivity of the F-Fab for NC-FPIA of H5N3 virus. H1N1 virus was used as a negative control. Concentrations of H5N3 virus and H1N1 virus were each 5 μg/mL. $\Delta mP = 1000 \times (P_{\text{sample}} - P_{\text{blank}})$.

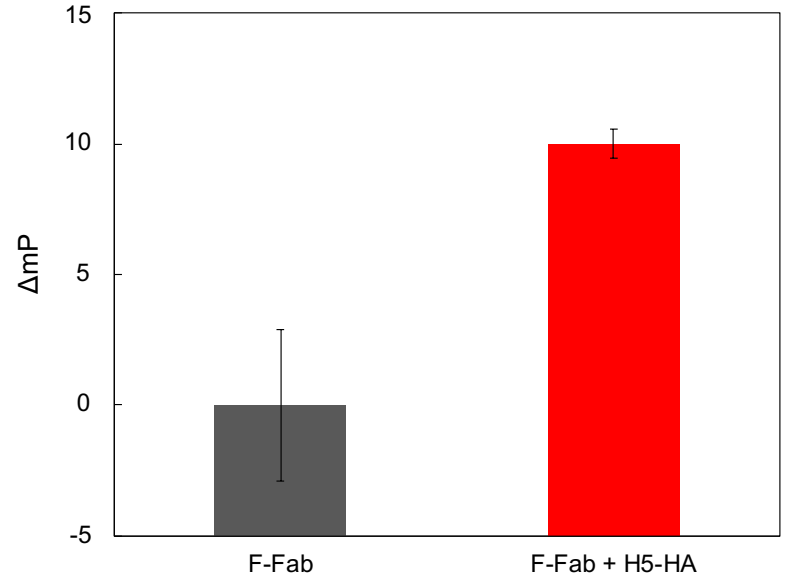


Figure 5.4 Evaluation of the binding ability of F-Fab to H5-rHA. 80 ng/mL F-Fab and 20 μg/mL H5-rHA were used. $\Delta mP = 1000 \times (P_{\text{sample}} - P_{\text{F-Fab}})$.

From the above results, I demonstrated that AIV can be detected by NC-FPIA with an incubation time of 15 min by using a Fab fragment that selectively binds to a protein on the virus surface. Also, since a portable

FPIA device is used for measurement, the sample volume required for one assay is 20 μL or less. By preparing a suitable fluorescently labeled-Fab fragment, this method can be applied to various viral infectious diseases like COVID-19.

5.3.2 Antibody detection

A free fluorescence-labeled antigen emits random fluorescence when excited by polarized light and it gives a low *P* value. When a fluorescence-labeled antigen is bound to an antibody, *P* value is high due to the much slower Brownian motion of the antibody-H5-rHA complex [30-31]. Figure 5.5 shows the schematic illustration of FPIA in this work. When anti-H5 antibody in serum binds to a fluorescein-labeled H5-rHA, *P* value becomes high. Therefore, anti-H5-AIV serum containing a large amount of anti-H5 HA antibodies shows a higher *P* value than that of the antibody-negative serum.

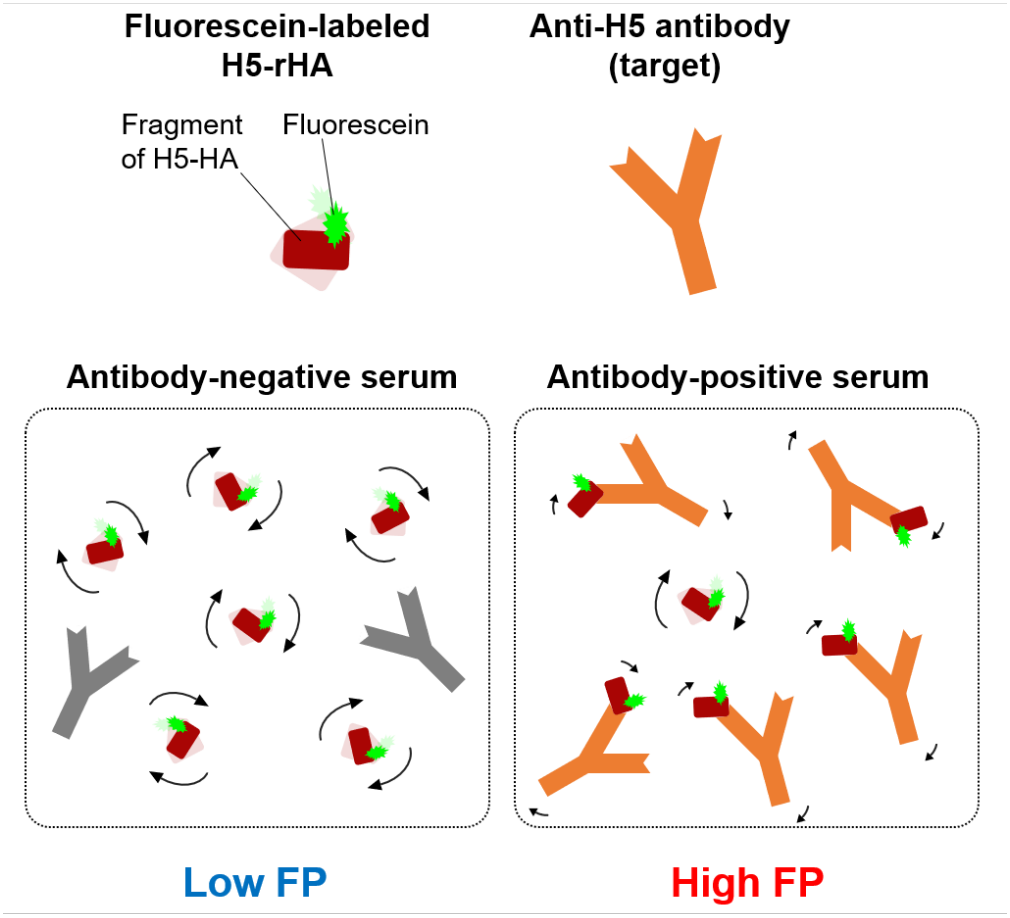


Figure 5.5 Schematic illustration of the fluorescence polarization immunoassay for antibody detection.

Figure 5.6 shows the measured *P* value results after mixing fluorescein-labeled H5-rHA and anti-H5-AIV serum diluted with PBS. P value increased as the serum dilution rate decreased (increased concentration). The more antibodies the serum had, the greater the number of antigen-antibody complexes that were formed in the excess amount of fluorescein-labeled H5-rHA. Increasing *P* value with increasing concentration of serum meant that antigen-antibody complexes successfully formed. Therefore, I concluded that this fluorescein-labeled H5-rHA could be used for detection of anti-H5 antibody in serum. The limit of detection was about 20-fold dilution. The microdevice required 20 μL of solution per one channel. Since serum and fluorescein-labeled H5-rHA were mixed at a volume ratio of 1 : 1, the required serum volume for an analysis was 10 μL. When a serum with 5-fold dilution was used for the analysis, the required volume of the original serum was 2 μL. It would be

sufficiently small for application to on-site diagnosis and surveillance. Therefore, 5-fold dilution of antiserum was used in the next experiment.

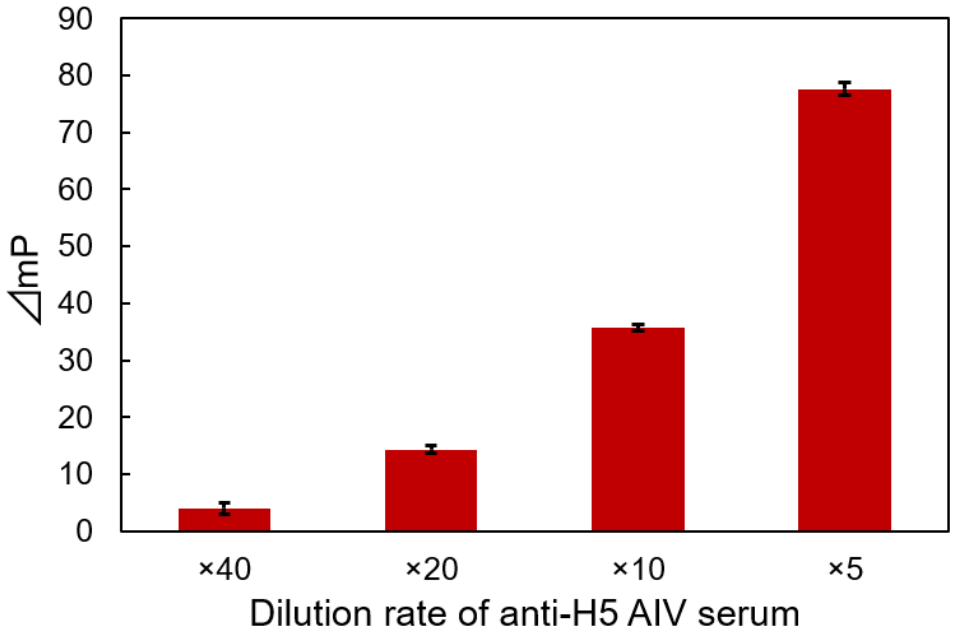


Figure 5.6 Fluorescence polarization as a function of dilution rate of anti-H5 serum.

Next, I verified whether this system could selectively detect anti-H5-AIV serum in anti-H1–H16 AIV sera. Figure 5.7 shows the *P* value obtained with anti-H1–H16 sera. The cutoff value for positive anti-H5-AIV antibody was defined as the average + 3SDs. Anti-H5 serum showed the highest *P* value among all anti-AIV sera and all other antisera except anti-H5 was below the cut-off value. Therefore, I showed that there was no false positive result with other anti-subtype sera. The incubation time was 15 min (total analysis time was within 20 min), which was significantly shorter than the time needed by conventional ELISA-based devices. These findings showed that this FPIA system selectively detected the anti-H5-AIV serum.

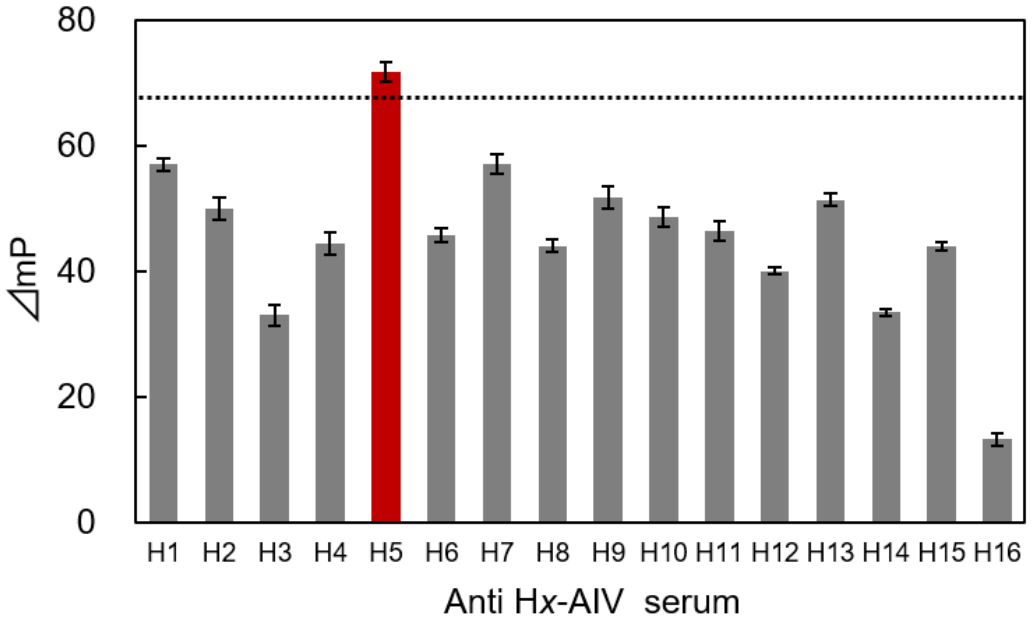


Figure 5.7 Fluorescence polarization obtained with anti H1-H16 avian influenza virus sera ($n = 3$). The dashed line represents the cut-off value.

5.4 Conclusions

I developed the rapid and easy-to-use system for the FPIA detection of H5N3 AIV and anti-H5-AIV serum. The reaction is completed by simply mixing the reagent with the sample. Analysis time was within 20 min and required sample volume was only 2 μL. The portable FP analyzer with the microfluidic device makes it possible to conduct on-site analysis. Further study on blocking of protein adsorption to PDMS devices may lead to improved sensitivity and selectivity of a detection. By preparing appropriate fluorescence-labeled Fab and fluorescence-labeled antigen, this system can be applied to antigen and antibody detection for other viruses such as SARS-CoV-2. In the future, I plan to conduct experiments using real samples acquired in the field.

5.5 References

[1] Fouchier, R. A. M.; Munster, V.; Wallensten, A.; Bestebroer, T. M.; Herfst, S.; Smith, D.; Rimmelzwaan, G. F.; Olsen, B.; Osterhaus, A. D. M. E. Characterization of a Novel Influenza A Virus Hemagglutinin Subtype (H16) Obtained from Black-Headed Gulls. *J. Virol.* **2005**, 79, 2814–2822.

[2] Watanabe, Y.; Ibrahim, M. S.; Suzuki, Y.; Ikuta, K. The Changing Nature of Avian Influenza A Virus (H5N1). *Trends Microbiol.* **2012**, 20, 11–20.

[3] Ligon, B. L. Avian Influenza Virus H5N1: A Review of Its History and Information Regarding Its Potential to Cause the Next Pandemic. Semin. Pediatr. *Infect. Dis.* **2005**, 16, 326–335.

[4] Webster, R. G.; Bean, W. J.; Gorman, O. T.; Chambers, T. M.; Kawaoka, Y. Evolution and Ecology of Influenza A Viruses. *Microbiol. Rev.* **1992**, 56, 152–179.

[5] Liu, J.; Xiao, H.; Lei, F.; Zhu, Q.; Qin, K.; Zhang, X.-W.; Zhang, X.-L.; Zhao, D.; Wang, G.; Feng, Y.; Ma, J.; Liu, W.; Wang, J.; Gao, G. F. Highly Pathogenic H5N1 Influenza Virus Infection in Migratory Birds. *Science* **2005**, 309, 1206.

[6] Alexander, D. J. A Review of Avian Influenza in Different Bird Species. *Vet. Microbiol.* **2000**, 74, 3–13.

[7] Gambotto, A.; Barratt-Boyes, S. M.; de Jong, M. D.; Neumann, G.; Kawaoka, Y. Human Infection with Highly Pathogenic H5N1 Influenza Virus. *Lancet* **2008**, 371, 1464–1475.

[8] Avian Influenza Portal http://www.oie.int/en/animal-health-in-the-world/web-portal-on-avian-influenza/ (accessed 15 November 2019)

[9] Cumulative number of confirmed human cases of avian influenza A(H5N1) reported to WHO https://www.who.int/influenza/human_animal_interface/H5N1_cumulative_table_archives/en/ (accessed 15 November 2019)

[10] Tsuda, Y.; Sakoda, Y.; Sakabe, S.; Mochizuki, T.; Namba, Y.; Kida, H. Development of an Immunochromatographic Kit for Rapid Diagnosis of H5 Avian Influenza Virus Infection. *Microbiol. Immunol.* **2007**, 51, 903–907.

[11] Bui, V. N.; Ogawa, H.; Ngo, L. H.; Baatartsogt, T.; Abao, L. N. B.; Tamaki, S.; Saito, K.; Watanabe, Y.; Runstadler, J.; Imai, K. H5N1 Highly Pathogenic Avian Influenza Virus Isolated from Conjunctiva of a Whooper Swan with Neurological Signs. *Arch. Virol.* **2013**, 158, 451–455.

[12] Li, Z.; Yi, Y.; Luo, X.; Xiong, N.; Liu, Y.; Li, S.; Sun, R.; Wang, Y.; Hu, B.; Chen, W.; Zhang, Y.; Wang, J.; Huang, B.; Lin, Y.; Yang, J.; Cai, W.; Wang, X.; Cheng, J.; Chen, Z.; Sun, K.; Pan, W.; Zhan, Z.; Chen, L.; Ye, F. Development and Clinical Application of a Rapid IgM-IgG Combined Antibody Test for SARS-CoV-2 Infection Diagnosis. *J. Med. Virol.* **2020**, 92, 1518–1524.

[13] Spackman, E.; Senne, D. A.; Myers, T. J.; Bulaga, L. L.; Garber, L. P.; Perdue, M. L.; Lohman, K.; Daum, L. T.; Suarez, D. L. Development of a Real-Time Reverse Transcriptase PCR Assay for Type A Influenza Virus and the Avian H5 and H7 Hemagglutinin Subtypes. *J. Clin. Microbiol.* **2002**, 40, 3256–3260.

[14] Gurukumar, K. R.; Priyadarshini, D.; Patil, J. A.; Bhagat, A.; Singh, A.; Shah, P. S.; Cecilia, D. Development of Real Time PCR for Detection and Quantitation of Dengue Viruses. *Virol. J.* **2009**, 6, 10.

[15] Grant, B. D.; Anderson, C. E.; Williford, J. R.; Alonzo, L. F.; Glukhova, V. A.; Boyle, D. S.; Weigl, B. H.; Nichols, K. P. SARS-CoV-2 Coronavirus Nucleocapsid Antigen-Detecting Half-Strip Lateral Flow Assay Toward the Development of Point of Care Tests Using Commercially Available Reagents. *Anal. Chem.* **2020**, 92, 11305–11309.

[16] Chen, Z.; Zhang, Z.; Zhai, X.; Li, Y.; Lin, L.; Zhao, H.; Bian, L.; Li, P.; Yu, L.; Wu, Y.; Lin, G. Rapid and Sensitive Detection of Anti-SARS-CoV-2 IgG, Using Lanthanide-Doped Nanoparticles-Based Lateral Flow Immunoassay. *Anal. Chem.* **2020**, 92, 7226–7231.

[17] Li, X.; Lu, D.; Sheng, Z.; Chen, K.; Guo, X.; Jin, M.; Han, H. A Fast and Sensitive Immunoassay of Avian Influenza Virus Based on Label-Free Quantum Dot Probe and Lateral Flow Test Strip. *Talanta* **2012,** 100, 1–6.

[18] Cui, S.; Chen, C.; Tong, G. A Simple and Rapid Immunochromatographic Strip Test for Monitoring Antibodies to H5 Subtype Avian Influenza Virus. *J. Virol. Methods* **2008**, 152, 102–105.

[19] Petherick, A. Developing Antibody Tests for SARS-CoV-2. *Lancet* **2020**, 395, 1101–1102.

[20] Li, Z.; Yi, Y.; Luo, X.; Xiong, N.; Liu, Y.; Li, S.; Sun, R.; Wang, Y.; Hu, B.; Chen, W.; Zhang, Y.; Wang, J.; Huang, B.; Lin, Y.; Yang, J.; Cai, W.; Wang, X.; Cheng, J.; Chen, Z.; Sun, K.; Pan, W.; Zhan, Z.; Chen, L.; Ye, F. Development and Clinical Application of a Rapid IgM-IgG Combined Antibody Test for SARS-CoV-2 Infection Diagnosis. *J. Med. Virol.* **2020,** 92, 1518–1524.

[21] Chávez Ramos, K.; Nishiyama, K.; Maeki, M.; Ishida, A.; Tani, H.; Kasama, T.; Baba, Y.; Tokeshi, M. Rapid, Sensitive, and Selective Detection of H5 Hemagglutinin from Avian Influenza Virus Using an Immunowall Device. *ACS Omega* **2019**, 4, 16683–16688.

[22] Ohtsuka, K.; Endo, H.; Morimoto, K.; Vuuong, B. N.; Ogawa, H.; Imai, K.; Takenaka, S. Detection of an Antibody to Avian Influenza Virus by an Electrochemical Immunoassay (EELISA). *Anal. Sci.* **2008**, 24, 1619–1622.

[23] Moreno, A.; Lelli, D.; Brocchi, E.; Sozzi, E.; Vinco, L. J.; Grilli, G.; Cordioli, P. Monoclonal Antibody-Based ELISA for Detection of Antibodies against H5 Avian Influenza Viruses. *J. Virol. Methods* **2013**, 187, 424–430.

[24] WHO manual on animal influenza diagnosis and surveillance http://www.wpro.who.int/emerging_diseases/documents/docs/manualonanimalaidiagnosisandsurveillance.pdf#search=%27WHO+diagnosis+of+animal+influenza%27 (accessed 15 November 2019)

[25] Manual of diagnostic tests and vaccines for terrestrial animals 2019, Chapter 3.3.4. Avian influenza (infection with avian influenza viruses). https://www.oie.int/fileadmin/Home/eng/Health_standards/tahm/3.03.04_AI.pdf (accessed 15 November 2019)

[26] Imai, K.; Ogawa, H.; Bui, V. N.; Inoue, H.; Fukuda, J.; Ohba, M.; Yamamoto, Y.; Nakamura, K. Inactivation of High and Low Pathogenic Avian Influenza Virus H5 Subtypes by Copper Ions Incorporated in Zeolite-Textile Materials. *Antiviral Res.* **2012**, 93, 225–233.

[27] Horie, M.; Ogawa, H.; Yamada, K.; Hara, A.; Bui, V. N.; Awad, S. S.; Yoshikawa, R.; Mase, M.; Tsukamoto, K.; Yamaguchi, S.; Nakamura, K.; Imai, K. A Latex Agglutination Test Using a Recombinant Nucleoprotein for Detection of Antibodies against Avian Influenza Virus. *J. Virol. Methods* **2009**, 161, 259–264.

[28] Otsuki, K.; Takemoto, O.; Fujimoto, R.; Yamazaki, K.; Kubota, T.; Hosaki, H.; Mitani, T.; Kawaoka, Y.; Tsubokura, M. Isolation of H5 Influenza Viruses from Whistling Swans in Western Japan in November 1983. *Acta Virol.* **1984**, 28, 524.

[29] Wakao, O.; Satou, K.; Nakamura, A.; Galkina, P. A.; Nishiyama, K.; Sumiyoshi, K.; Kurosawa, F.; Maeki, M.; Ishida, A.; Tani, H.; Proskurnin, M. A.; Shigemura, K.; Hibara, A.; Tokeshi, M. High-Throughput Fluorescence Polarization Immunoassay by Using a Portable Fluorescence Polarization Imaging Analyzer. *Lab Chip* **2019**, 19, 2581–2588.

[30] Smith, D. S.; Eremin, S. A. Fluorescence Polarization Immunoassays and Related Methods for Simple, High-Throughput Screening of Small Molecules. *Anal. Bioanal. Chem.* **2008**, 391, 1499–1507.

[31] Jameson, D. M.; Ross, J. A. Fluorescence Polarization/Anisotropy in Diagnostics and Imaging. *Chem. Rev.* **2010**, 110, 2685–2708.

CHAPTER 6 Conclusion and Future Prospects

Analytical systems based on immunoassays and microfluidic devices for the quantification of biomolecules were developed in the present research and are described in this thesis.

Chapter 2 described the development of an ultrasensitive immunoassay system that uses an immuno-wall device; an enzymatic amplification reaction was also developed. The ultrasensitive detection of a trace biomarker was achieved using an alkaline phosphatase label, with the signal provided by an enzymatic reaction with a fluorogenic substrate in a microchannel. The highest signal/background ratio was obtained using DDAO phosphate. To evaluate device performance, human C-reactive protein (CRP) was detected as a model biomarker. The detection limit (LOD) of CRP in phosphate-buffered saline was determined to be 2.5 pg/mL with a sample volume of 0.25 μL. This LOD is approximately three orders of magnitude lower than that obtained with the fluorescent-dye-labeled (DyLight 650-labeled) antibody. In addition, the present device provided a wide (0.0025–10 ng/mL) detection range for CRP. Since the LOD of CRP obtained by the conventional immuno-wall device using the fluorescence-labeled antibody was 1.7 ng/mL, the application of the enzyme immunoassay succeeded in significantly improving measurement sensitivity.

Chapter 3 investigated a simple method for fluorescence-signal amplification that uses the AWP structure in a microchannel. When a solution of fluorescent molecules was introduced into the microchannel with the AWP-wall, they accumulated inside the AWP-wall by diffusion. Consequently, the fluorescence intensity inside the AWP-wall was locally higher. Among the fluorescent molecules considered in this chapter, DDAO showed the highest efficiency during fluorescence-signal amplification. A calibration curve for DDAO based on the fluorescence intensity inside the AWP-wall was prepared, which revealed a five-fold greater sensitivity than that observed for the microchannel devoid of the AWP-wall. This method easily improves fluorescence detection sensitivity. Furthermore, because this method is not limited only to microchannel use, it is expected to be applicable to a variety of fields.

Chapter 4 described the development of NC-FPIA for the quantification of large molecules using a fluorescently labeled Fab fragment. Most conventional FPIAs are homogeneous and competitive immunoassays.

The Fab fragment, with a fluorescently labeled amino group, is appropriate for protein quantification using non-competitive FPIA. The Fab-based NC-FPIA was validated using CRP as a model substance, with the quantitative analysis of CRP in phosphate-buffered saline (PBS) successfully demonstrated to a LOD of 207 ng/mL. Moreover, using a far-red emitting fluorescent dye (HiLyte Fluor™647) as a fluorescent compound for labeling the Fab fragment, CRP in human serum was able to be determined in 10 min without sample pretreatment, with a CRP cut-off value of 10 μg/mL. The LOD of CRP in human serum was determined to be 1.58 μg/mL. Using the developed method, the reaction was complete through simple one-step mixing with only one type of reagent for the fluorescence labeling of the Fab fragment, and no washing was required. The total measurement time was about 15 min, which is equivalent to those of qualitative measurement methods, such as the lateral flow method. Therefore, the protein was rapidly quantified using a greatly simplified procedure.

Chapter 5 described the development of an analytical system for the selective detection of H5-AIV and anti-H5-AIV antibodies using NC-FPIA with a portable FPIA analyzer. NC-FPIA, which is a separation-free immunoassay, was used to detect H5-AIV, along with a fluorescein-labeled Fab fragment that binds to H5 hemagglutinin. H5-AIV was successfully detected using an incubation time of 15 min with a portable FPIA analyzer. To detect the anti-H5-AIV antibody, a fragment of recombinant H5 subtype AIV hemagglutinin was produced and labeled with fluorescein and used as a labeled antigen for NC-FPIA. FP was found to increase proportionately with the concentration of the anti-H5-AIV antibody (serum) and was significantly higher than that obtained with other sera. The selective detection of anti-H5 subtype AIV antibody was confirmed. An analysis time of less that 20 min and a sample volume of less than 20 μL was used to detect each antibody.

Table 6.1 compares the performance of the two analytical systems reported in Chapters 2 and 4. Both of these systems detect using fluorescence signals. The two developed immunoassay systems can perform highly sensitive measurements easily and rapidly. In the future, both the fluorescence-intensity and fluorescence-polarization detection systems will be integrated in a single detector. The appropriate immunoassay device will be used depending on the application. The analytical system using the immuno-wall device described in Chapter 2 ultrasensitively detected small amounts of samples and is expected to be used to

detect trace biomarkers in early diagnosis applications. Our research group has been working on applying the immuno-wall to gene mutation testing for the epidermal growth factor receptor and anaplastic lymphoma kinase lung cancer markers; it is also expected to be used in applications that require quick and convenient diagnoses, such as intraoperative rapid pathological diagnosis. A portable fluorescence detection device is also being currently developed and is expected to realize an analytical system that meets all of the requirements of PONT. Since the AWP-based fluorescence-signal amplification method introduced in Chapter 3 is a very simple and versatile technology, it is expected to be applied in various fields, including microanalysis. The NC-FPIA analytical system for protein detection introduced in Chapters 4 and 5 is rapid and easy to operate; it is ideal for rapid first screening applications in the field when used with the portable FP analyzer developed in this thesis. Although it does not have the same detection sensitivity as the immuno-wall, CRP, as a model diagnosis biomarker, could be detected near the cutoff value. In addition, the antigen and antibody tests for diagnosing viral infections described in Chapter 5 can be performed quickly using the same platform. Recently, the COVID-19 pandemic has resulted in a strong demand for a rapid method for diagnosing viral infections, and such an analytical tool would be very powerful. In addition, the developed appropriate fluorescently labeled Fabs and fluorescently labeled antigens can be used to detect various viral infectious diseases. I am convinced that the two analytical systems developed herein will innovate the PONT field in the future.

Table 6.1 Comparing the analytical performance of the immuno-wall device and NC-FPIA for CRP in PBS

	Immuno-wall device	**NC-FPIA**
Type of immunoassay	ELISA (Heterogeneous Immunoasssay)	FPIA (Homogeneous Immunoasssay)
Sample volume	0.25 μL	16 μL
Number of reagents	3	1
Number of washing steps	3	0
Total incubation time	46 min	10 min
Meaurement range	0.0025–10 ng/mL	207-1000 ng/mL
Limit of detection	2.5 pg/mL	207 ng/mL

List of Publications

Reviewed Papers

[1] **Keine Nishiyama**, Kanako Sugimura, Noritada Kaji, Manabu Tokeshi, Yoshinobu Baba, "Development of a Microdevice for Facile Analysis of Theophylline in Whole Blood by a Cloned Enzyme Donor Immunoassay", *Lab on a Chip*, 19, 233-240 (2019). - This paper was selected as a back cover picture of Lab on a Chip.

[2] **Keine Nishiyama**, Koki Hoshikawa, Masatoshi Maeki, Akihiko Ishida, Hirofumi Tani, Manabu Tokeshi, "A Concentric Ring Electrode for a Wall-jet Cell in a Microfluidic Device", *Electroanalysis*, 31, 1736-1743 (2019). - This paper was selected as a front cover picture of Electroanalysis.

[3] **Keine Nishiyama**, Toshihiro Kasama, Seiya Nakamata, Koya Ishikawa, Daisuke Onoshima, Hiroshi Yukawa, Masatoshi Maeki, Akihiko Ishida, Hirofumi Tani, Yoshinobu Baba, Manabu Tokeshi, "Ultrasensitive Detection of Disease Biomarkers Using an Immuno-wall Device with Enzymatic Amplification", *Analyst*, 144, 4589-4595 (2019).

[4] Osamu Wakao, Ken Satou, Ayano Nakamura, Polina Galkina, **Keine Nishiyama**, Ken Sumiyoshi, Fumio Kurosawa, Masatoshi Maeki, Akihiko Ishida, Hirofumi Tani, Mikhail A. Proskurnin, Koji Shigemura, Akihide Hibara, Manabu Tokeshi, "High-Throughput Fluorescence Polarization Immunoassay by Using a Portable Fluorescence Polarization Imaging Analyzer", *Lab on a Chip*, 19, 2581-2588 (2019).

[5] Kenia Chávez Ramos, **Keine Nishiyama (equal contribution to 1st author)**, Masatoshi Maeki, Akihiko Ishida, Hirofumi Tani, Toshihiro Kasama, Yoshinobu Baba, Manabu Tokeshi, "Rapid, Sensitive and Selective Detection of H5 Hemagglutinin from Avian Influenza Virus Using an Immuno-Wall Device", *ACS Omega*, 4, 16683-16688 (2019).

[6] **Keine Nishiyama**, Yohei Takeda, Masatoshi Maeki, Akihiko Ishida, Hirofumi Tani, Koji Shigemura, Akihide Hibara, Yutaka Yonezawa, Kunitoshi Imai, Haruko Ogawa, Manabu Tokeshi, "Rapid Detection of Anti-HS Avian Influenza Virus Antibody by Fluorescence Polarization Immunoassay Using a Portable Fluorescence Polarization Analyzer", *Sensors and Actuators B: Chemical*, 316, 128160 (2020). - This paper was selected as a highlighted article of Sensors and Actuators B: Chemical.

[7] Mao Fukuyama, Ayano Nakamura, **Keine Nishiyama**, Ayuko Imai, Manabu Tokeshi, Koji Shigemura, Akihide Hibara, "Noncompetitive Fluorescence Polarization Immunoassay for Protein Determination", *Analytical Chemistry*, 92, 14393-14397, (2020).

[8] Naoyuki Yogo, Tetsunari Hase, Toshihiro Kasama, **Keine Nishiyama**, Naoya Ozawa, Takahiro Hatta, Hirofumi Shibata, Mitsuo Sato, Kazuki Komeda, Nozomi Kawabe, Kohei Matsuoka, Toyofumi Fengshi Chen-Yoshikawa, Noritada Kaji, Manabu Tokeshi, Yoshinobu Baba, Yoshinori Hasegawa, "Development of an Immuno-Wall Device for the Rapid and Sensitive Detection of EGFR Mutations in Tumor Tissues Resected from Lung Cancer Patients", *PLoS ONE*, 15, e0241422 (2020).

[9] **Keine Nishiyama**, Mao Fukuyama, Masatoshi Maeki, Akihiko Ishida, Hirofumi Tani, Akihide Hibara, Manabu Tokeshi, "One-Step Non-Competitive Fluorescence Polarization Immunoassay Based on a Fab Fragment for C-Reactive Protein Quantification", *Sensors and Actuators B: Chemical*, 326, 128982 (2021).

[10] **Keine Nishiyama**, Yohei Takeda, Kazuki Takahashi, Mao Fukuyama, Masatoshi Maeki, Akihiko Ishida, Hirofumi Tani, Koji Shigemura, Akihide Hibara, Haruko Ogawa, Manabu Tokeshi, "Non-Competitive Fluorescence Polarization Immunoassay for Detection of H5 Avian Influenza Virus Using a Portable Analyzer", *Analytical and Bioanalytical Chemistry*, in press, DOI: 10.1007/s00216-021-03193-y.

[11] **Keine Nishiyama**, Masatoshi Maeki, Akihiko Ishida, Hirofumi Tani, Hideaki Hisamoto, Manabu Tokeshi, "Simple Approach for Fluorescence Signal Amplification Utilizing a Poly(vinyl alcohol)-Based Polymer Structure in a Microchannel", *ACS Omega*, accepted.

[12] **Keine Nishiyama**, Kazuki Takahashi, Mao Fukuyama, Masatoshi Maeki, Akihiko Ishida, Hirofumi Tani, Koji Shigemura, Akihide Hibara, Manabu Tokeshi, "Facile and Rapid Detection of SARS-CoV-2 Antibody Based on a Noncompetitive Fluorescence Polarization Immunoassay in Patient Samples", submitted.

[13] **Keine Nishiyama**, Ryohei Mizukami, Shizuka Kuki, Akihiko Ishida, Junji Chida, Hiroshi Kido, Masatoshi Maeki, Hirofumi Tani, Manabu Tokeshi, "Electrochemical Sensor for Blood ATP and Lactate for the Rapid and Straightforward Evaluation of Illness Severity", submitted.

Reviewed International Conference Papers

[1] **Keine Nishiyama**, Toshihiro Kasama, Masatoshi Maeki, Akihiko Ishida, Hirofumi Tani, Manabu Tokeshi, "Development of Immuno-Wall Device for Biomarker Detection in Clinical Diagnosis", *Proceedings of Microprocesses and Nanotechnology Conference 2018 (MNC2018)*, 1, 16C-10-4 (2018).

[2] **Keine Nishiyama**, Toshihiro Kasama, Masatoshi Maeki, Akihiko Ishida, Hirofumi Tani, Manabu Tokeshi, "Immuno-Wall Device for Highly Sensitive Detection of Disease Markers", *Proceedings of the 12th IEEE International Conference on Nano/Molecular Medicine and Engineering (IEEE-NANOMED 2018)*, 1, 51-52 (2018).

[3] **Keine Nishiyama**, Toshihiro Kasama, Masatoshi Maeki, Akihiko Ishida, Hirofumi Tani, Yoshinobu Baba, Manabu Tokeshi, "Fluorescence Signal Amplification for Sensitive Enzyme Immunoassay Utilizing an Immuno-Wall", *Proceedings of the Micro Total Analysis System 2019 (μTAS 2019)*, 1, 689-690 (2019).

[4] **Keine Nishiyama**, Yohei Takeda, Masatoshi Maeki, Akihiko Ishida, Hirofumi Tani, Koji Shigemura, Akihide Hibara, Haruko Ogawa, Manabu Tokeshi, "Detection of Avian Influenza Virus and Its Antibody by Fluorescence Polarization Immunoassay", *Proceedings of the Micro Total Analysis System 2020 (μTAS 2020)*, 1, 1226-1227 (2020).

Commentaries

[1] **Keine Nishiyama**, Manabu Tokeshi, “Development of a Microfluidic Device using CEDIA for Simple Measurement of Theophylline in Blood”, *Biomedcircuus.com*, http://biomedcircus.com/paper_03_55.html (2019).

[2] **Keine Nishiyama**, Niko Kimura, Masatoshi Maeki, Manabu Tokeshi, “Microfluidic Device: As a Tool of Pharmaceutical Research and Development”, *Journal of pharmaceutical science and technology, Japan*, 79, 124-129 (2019).

[3] **Keine Nishiyama**, Akihide Hibara, Manabu Tokeshi, “Rapid Antibody Test by Fluorescence Polarization Immunoassay”, *Chemistry and Micro-Nano Systems*, 19 (2), 13-15 (2020).

Acknowledgement

This thesis is the result of the author's research in the Laboratory of Bioanalytical Chemistry, Graduate School of Engineering, Hokkaido University.

First of all, I would like to express my sincerest respect and gratitude to my supervisor, Professor Manabu Tokeshi of the Division of Applied Chemistry, Faculty of Engineering, Hokkaido University, for his guidance and wisdom, meaningful advice, and continuous support. He warmly accepted me as a Ph.D. student and provided encouragement in the face of many challenges; without his encouragement and persistent help, this thesis would not have been possible. I would like to acknowledge Associate Professor Hirofumi Tani, Assistant Professor Akihiko Ishida, and Assistant Professor Masatoshi Maeki for valuable discussions, advice, and assistance. Very special thanks go out to Prof. Ishida for help in relation to two research papers from my undergraduate and master research.

I would like to acknowledge Professor Toshifumi Satoh and Associate Professor Hirofumi Tani of the Faculty of Engineering, Hokkaido University, and Professor Kazuki Sada of the Faculty of Science, Hokkaido University, for accepting the responsibilities as my official co-supervisors.

I must acknowledge Professor Yoshinobu Baba (Nagoya University) and Assistant Professor Toshihiro Kasama (The University of Tokyo). Prof. Kasama provided me with valuable advice and perspectives in relation to the immuno-wall device. Owing to his kind support, my research on the immuno-wall device began smoothly. I also thank Mr. Seiya Nakamata for experimental advice on the fabrication of the immuno-wall device.

I would like to acknowledge Professor Hideaki Hisamoto (Osaka Prefecture University) who provided helpful advice on research into fluorescence-signal amplification by the AWP-wall.

For their prior research into the portable FP analyzer, I acknowledge Professor Akihide Hibara (Tohoku Univeristy) and Assistant Professor Mao Fukuyama (Tohoku University), who provided precious

technical advice about FPIA in the team meeting. Their discussions always stimulate my scientific curiosity. I also thank Dr. Osamu Wakao, who had previously developed the portable FP analyzer. I would like to express my appreciation to Mr. Koji Shigemura's team at Tianma Japan, Ltd., for developing the portable FP analyzer and for providing material support.

I would like to acknowledge Professor Haruko Ogawa (Obihiro University of Agriculture and Veterinary Medicine) and Assistant Professor Yohei Takeda (Obihiro University of Agriculture and Veterinary Medicine) who kindly provided me with valuable virus samples and reagents for FPIA, as well as providing helpful advice.

I would like to acknowledge the Grant-in-Aid of the Japan Society for the Promotion of Science Fellows and acknowledge the support of the JST-SENTAN program.

As a Ph.D. student, I attended many academic conferences and meetings. I wish to thank all professors, students, and participants. Especially, I deeply thank Professor Noritada Kaji (Kyusyu University) and Professor Shoji Takeuchi (The University of Tokyo) for valuable discussions.

I would like to thank all of my lab mates. Takeshi Komatsu and Niko Kimura have worked hard together with me as a Ph.D. candidate. Kazuki Takahashi supported my experiment on FPIA. In addition, I would like to express my gratitude to Dr. Kenia Chávez Ramos (National Autonomous University of Mexico) and Ms. Polina A. Galkina (Moscow State University), who supported my experiment during the internship period. I would also like to thank our lab secretary, Kokoro Haruki-San; she supported my project management and provided many life-related suggestions.

I would like to thank Starbucks Coffee Japan as my third place. A cup of coffee and warm hospitality of baristas always encouraged me to write papers.

Finally, I would like to thank my family for providing me with the opportunity to study as a Ph.D. student; they have always supported me.